**POLISH
MARITIME
RESEARCH**

in internet
www.bg.pg.gda.pl/pmr/pmr.php

POLISH MARITIME RESEARCH
No 1(72)   2012   Vol 19

CONTENTS

Editorial

POLISH MARITIME RESEARCH is a scientific journal of worldwide circulation. The journal appears as a quarterly four times a year. The first issue of it was published in September 1994. Its main aim is to present original, innovative scientific ideas and Research & Development achievements in the field of :

Engineering, **Computing & Technology**, **Mechanical Engineering**,

which could find applications in the broad domain of maritime economy. Hence there are published papers which concern methods of the designing, manufacturing and operating processes of such technical objects and devices as : ships, port equipment, ocean engineering units, underwater vehicles and equipment as well as harbour facilities, with accounting for marine environment protection.

The Editors of POLISH MARITIME RESEARCH make also efforts to present problems dealing with education of engineers and scientific and teaching personnel. As a rule, the basic papers are supplemented by information on conferences , important scientific events as well as cooperation in carrying out international scientific research projects.

Scientific Board

An integrated hydraulic drive system of a novel device for launching lifeboats from large passenger ships

Czesław Dymarski, Prof.
Gdańsk University of Technology

ABSTRACT

This paper presents a continuation of the projects [5, 6] dealing with the novel concepts of evacuating people from large passenger ships. A novel integrated drive and control system for chain lift with lifeboats fastened on it as well as for stern port- ramp, is presented. Additional novel elements is the application of the stern port - ramp fitted with a buoyancy element, and its increased capability of automatic adjusting its operational deflection in the case of a large forward trim of ship. It increases safety and comfort of evacuation in the difficult conditions, but to obtain it a more complex drive and control system has been required to be designed.

Keywords: ship deck equipment; ship evacuating systems; life saving appliances systems;
lifeboat chain lift; hydraulic drive and control system

INTRODUCTION

Contemporary large passenger ships are able to take onboard even six and half thousand of people [8]. One of the most complex problems the designers and ship owners of such ships face is to ensure safety in the case of a fire or danger of ship sinking resulting in necessity of fast abandoning the ship by such a large number of people especially in heavy weather conditions. For this aim have been used so far life boats and rafts located in series along both ship sides, placed on special davits on evacuation deck as shown in Fig. 1 presenting the *Queen Mary 2*, one of the largest and most modern passenger ships.

According to the requirements in force the davits are to ensure putting the life boats overboard with the use of gravity forces or stored energy in the conditions of ship's heel up to 20° and trim up to 10°and then embarking people on them and lowering the boats to water.

To the group of davits which lean out overboard together with life boats by using gravity forces the following belong:
- the quadrant davits shown in Fig. 2, which have been used most often so far on large passenger ships,
- the gravity roller track – quadrant davit shown in Fig. 3, used less often in present because of a greater space needed to accommodate them,
- the quadrant davits shown in Fig. 4, applicable rather to smaller ships.

Fig. 1. The passenger ship Queen Mary 2 with visible life boats placed on ship sides [7]
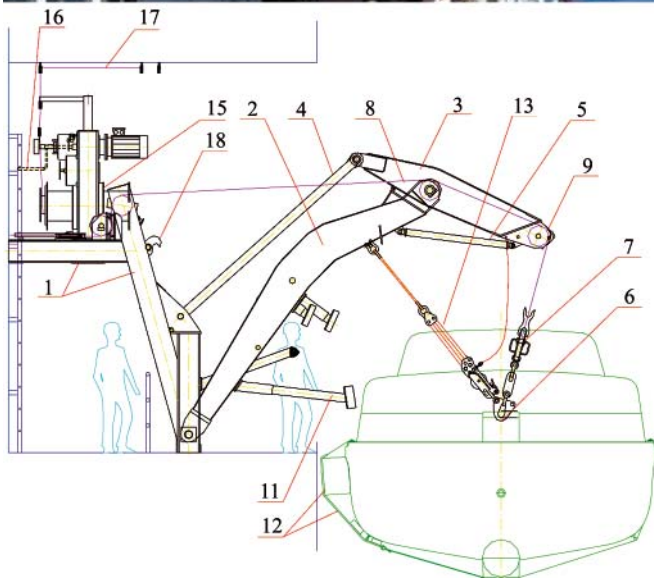
Fig. 2. The life boat quadrant davits. Up – a photo of the davits in voyage position; down - in the position along ship side for embarking the people on the lifeboats from evacuation deck

To the group of the davits which require some energy for putting them overboard the following belong:
- the telescopic davits shown in Fig. 5, which accommodate relatively smallest space and hence are often and often applied on the newest passenger ships,
- the quadrant davits fitted with a leaning mechanism driven by hydraulic cylinder,
- the pivot davits used mainly on small rescue boats.

During evacuation of people from an endangered ship equipped with the above mentioned devices the following operations are required to be performed:
- to remove the protection of fastening devices of boats and davits, used during voyage,
- to put overboard the davits together with the boat hanging on them and lowering the boat to the level of evacuation deck,
- to draw-up and fix the boat on the level of evacuation deck,
- to embark the people on the boat, take the seats and fasten the belts by them,
- to free the boat out of the ship side, steady lower the boat onto water and release hooks and lines after launching,
- to start the engine and sail the boat away from the ship.
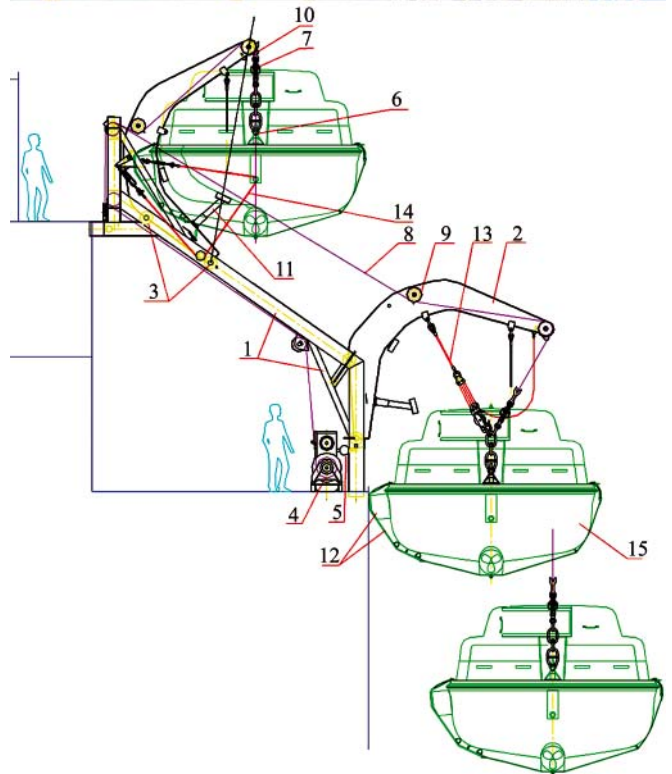
Fig. 3. The gravity roller track – quadrant davits in various positions during trial evacuation of people from ship.

Because of a limited space some of the above mentioned operations especially those connected with boat movement cannot be performed simultaneously by neighbouring devices that highly increases duration of evacuation time. It should be mentioned that the most difficult are the last three operations especially in the rough sea conditions.

In this paper is presented a novel concept of evacuating the people from a large passenger ship, elaborated in the Faculty of Ocean Engineering and Ship Technology, Gdansk University of Technology, within the frame of the European project SAFECRAFTS. The concept covers a design solution of the novel device already presented in the publications [5, 6], as well as an original drive and control system for two basic devices of the system, namely the stern ramp and the chain lift on which life boats are fastened.

Fig. 4. The life boat davits during and after installation
of them on a sailing passenger ship.

Fig. 5. Photos of the life boat davit fitted with a telescopic mechanism for
putting the boats overboard. Left - in voyage position; right – in overboard
position.

Depth (from keel to funnel) – 72 m
Mass displacement – 150 000 t
Maximum speed – ~30 knots
Installed power – 115.4 MW
Drive – 4 pod propellers of 21.5 MW
power each, including two
azimutal ones
Number of passengers
and crew members – 2620 + 1253 = 3873 persons.

DESIGN CONCEPT AND PRINCIPLE OF OPERATION OF THE DEVICE

The designed evacuation system presented in Fig. 6 consists of two independent devices located aft, outside valuable, useful space of the ship. Each of the devices covers a port - ramp and four mechanically mutually coupled chain lifts placed in a special casing, two of them on each side walls.

In the lower part of the casing a slipway equipped with rollers is placed. The casing is open from the aft side. Only the lower, rear part of the casing can be closed with the use of a simple port - ramp fitted, on its inner side, with a frame with rollers, which can form, after opening the ramp, an extension of the slipway reaching below water level.

On the lift chains are fastened suitably spaced catches on which closed life boats are placed. During voyage the port - ramp and chain lifts are blocked mechanically. Also, the boats are blocked in their positions on the lift catches by using the so called slip hooks which, apart from a typical releasing mechanism, are fitted also with a hydrostatic

AIMS AND MAIN ASSUMPTIONS OF THE ELABORATED CONCEPT OF THE DEVICE

The main aim and assumption of the project was to elaborate a novel method and device capable of evacuating people from an endangered passenger ship in heavy sea conditions, in a safe and more comfortable way than that has been used so far, and simultaneously within a shorter time.

The conceptual design was elaborated to be applicable to ships similar to the *Queen Mary 2*, the most representative for the group of ships of the kind, and because of availability of its technical data.

The main technical and operational parameters of the ship are the following:

Length – 345 m
Breadth – 41 m
Draught – 10 m

Fig. 6. *General concept of the device for evacuating the people:* ***a)*** *Side view of the ship with the installed device;* ***b)*** *rear view of the ship with visible elements of the drive system;* ***c)*** *cross-section of the casing with chain lifts and boats and visible mechanism for opening the port-ramp;* ***d)*** *top view of the boat placed on the lift in the casing, with visible elements of seating of the boat on the lift.*

release. Owing to that in the case of sinkage of the ship the boats are automatically released.

Because of the shape and location of the casing, eight life boats are used in each casing for a ship like the QM2. The number of boats is limited by the ship's depth and spacing to be kept between successive boats. The boats are large enough to accommodate 120 or 150 persons. The spacing between boats must be such as to avoid collisions during evacuation.

Specificity of the presented concept consists in that it makes it possible to simultaneously evacuate all the people onboard and start remotely the operation also from inside the boats.

The evacuation process initiated this way is automatically continued until the last boat is launched.

When the first boat is settled on the slipway in order to drive down on rollers in uniformly accelerated motion the next boat located on the chain lift approaches it. For this reason it is very important to keep suitable spacing between the boats placed on the lift.

A favourable feature of the solution in question is that persons embark the boat when it is stiffly connected with ship's hull. This way, in the presented solution, the problem of movement of the boat against the ship, which usually occurs in the case of embarking the boat hanging already along ship side, was eliminated. Owing to this, people are not exposed to stress and fear which is a typical reaction to the sight of rough sea in the gap between the boat and ship side during embarkation on the boats launched in the traditional way by means of side boat davits. There are no impacts of the boat against ship side, to which the boat and passengers inside are usually exposed during lowering the life boats hanging on lines along side of the ship rolling in waves, especially in heavy weather conditions. In the discussed solution the process of lowering and launching the boats is fully controlled and free from any sudden acceleration and panting against water surface as it is the case during evacuation with the use of systems based on free-fall lifeboats. Life boat engine is started up already during the boat's going down along the slipway. As the boat moves during launching in opposite direction relative to the ship, hence, floating already in water, it continues the motion and sails away from the endangered ship. The above mentioned features are of special importance for older and handicapped persons for which both stress and sudden accelerations could be dangerous.

Structure of the boats used in the presented solution contains some features of both the free-fall boats and life boats lowered with the use of side davits. Like free-fall boats, they have appropriately formed sides adjusted to going down on rollers. Because of their launching mode which produces much smaller dynamic loads they do not need to be as much resistant to loads as the free-fall boats. Their proportions are similar to those of free-fall boats, namely, they are more slender and longer than the side life boats. This makes it possible to save a part of expensive, usable space of ship. The launching mode consists in lowering the boats at a controlled speed by using the chain mechanism. The motion takes place under action of gravity forces and its speed is limited by means of a two-way flow controller installed in the hydraulic lift system, or a centrifugal brake. The boats are horizontally placed on the lift both during ship voyage and lowering process. Reaching the lower part of the casing the boat, while settling on the rollers fastened to the frame inclined by15° against the deck level, releases itself from the chain lift. In the initial, fore part of the slipway three rollers are installed very close to each other to provide a greater comfort during the transient phase of evacuation when the boat changes its angular position. The boat travels its final path along the slipway inside the ship hull and next along the stern ramp, developing uniformly accelerated motion and freely going down on the rollers, and it finally enters the water at a relatively small slope angle. This highly moderates dynamics of its contact with water and lowers accelerations acting on the boat and people inside.

In the proposed solution a simple port - ramp was used. It consists of a main segment built of steel plating and a buoyancy element in its rear part, as well as a number of stiffeners and frames which provide sufficient stiffness and strength of the ramp in heavy sea conditions. On the inner side of the ramp there is a metal frame made of square cross-section pipes to which rollers are fixed so that after opening the ramp the structure serves as an extension of the slipways, along which the boats can go down to water. Weight of the port-ramp is greater than its full buoyancy that means that its position as the extension of the slipway, will be maintained also in the case of ship's trim astern and its full immersion. The solution is favourable as on the one hand the limited buoyancy of the ramp decreases loading exerted to the drive system and on the other hand it does not cause dynamic displacements of the ramp against ship's hull in the case of evacuation at rough sea.

The drive system of the ramp is untypical as it makes it possible to automatic increasing its deflection angle in the case of a large ship trim forward when the end of the opened ramp is above water level.

Deflection process of the port- ramp is realized by means of two identical line hoisting winches, or one double-drum winch, and double pulley block system on both sides of the ramp. The upper pulley block of each line pulley block system of the ramp lowering system is hung on ship's hull through a hydraulic cylinder whose working chamber is connected with a gas-hydraulic accumulator. Geometrical parameters of the hydraulic cylinder and charging pressure of the accumulator were so selected as to obtain the force exerted to the piston rod of the cylinder - due to the total weight of the ramp in air and the boat including people - greater than the force due to oil pressure acting on its piston. It means that in the instant when a driving-down boat turns up on the ramp the ramp starts deflecting until the above mentioned forces balance each other. It should be mentioned that the loading due to weight will start lowering the ramp beginning from the instant of immersing the end of the ramp buoyancy element, and the hydraulic force will be greater and greater as a result of increasing pressure in the accumulator. It makes it possible to decrease the overload which acts on people and the device during launching the boat in heavy sea conditions. The winch motor is fitted with a stopping brake and a hydraulic release. The opening process of the ramp is realized gravitationally at a steady speed controlled by means of a two-way flow controller and, if necessary, a centrifugal brake. The drive and control system of the ramp is complex. It contains additional elements which serve to pull closer and block the ramp in the voyage position.

The ramp together with the line hoisting winch fixed on the ship's hull just before the ramp constitutes a system for hoisting the boats out of water after evacuation trials. The boats are pulled one by one onto the ramp and further onto the slipway where they are placed on the chain lift catches and after that the lift is put into motion. In the instant when a boat is displaced upward to a level assigned on the boat arrangement scale, that is controlled by sensors, the chain lift is automatically stopped until a successive boat is taken out of water and placed on the catches, and after that the mechanism is put into operation, the process is repeated again and again up to the last boat.

To drive the mutually coupled chain lifts four winches fitted with a double-chain wheel and high-torque hydraulic motor equipped with a blocking brake, hydraulic release and, if necessary, additional centrifugal brake, are used. Speed of boat lowering is stabilized and controlled by a two-way flow controller. A schematic diagram of the hydraulic drive and control system is presented in the next section. Fast and efficient evacuation of people from all decks of the ship is ensured by an appropriate form of staircases and a visual and acoustic system for directing the people to the life boats. The concept is based on that the doors leading from the staircases are located just opposite the entrances to the boats. Moreover, an emergency passage connecting successive levels, placed just behind the casing, is provided to facilitate displacing the people in emergency. Moreover, in this area anti-slipping materials are used to prevent people from slipping and falling down.

HYDRAULIC DRIVE AND CONTROL SYSTEM FOR THE PORT-RAMP

The hydraulic drive and control system for the port-ramp is presented in Fig. 7. The main aim of the system is to ensure safe opening the ramp and launching all the boats with people inside, placed on the chain lift, at an appropriate, possibly uniform speed in the conditions of lack of energy supply from ship's power network. Moreover it was assumed that it should be possible to stop and restart the boat launching process from a post on board the ship, and that the system should make it possible to hoist all the boats fitted with standard equipment but only with operators inside, and to close and block the ramp in voyage position.

Run of action during realization of basic operations of the device is presented below.

Before initiation of opening process of the ramp the gate valves 23 and hooks 24 which secure it in voyage position, should be unblocked. The unblocking is realized by switching over the distributors 8c and 7c to the right, that results in oil flowing under pressure from the hydraulic - gas accumulator 17a to the cylinders of the gate valve blockade 23 and hook blockade 24. In should be mentioned that the set of blockades is so designed as to obtain the pressure value necessary to unblock the gate valves lower than that to unblock the hooks, that ensures the desirable sequence of triggering the mechanisms. In normal conditions the accumulator 17a is supplied by the constant capacity pump 2a driven by the electric motor 4a. Starting and stopping process of the motor is controlled by the
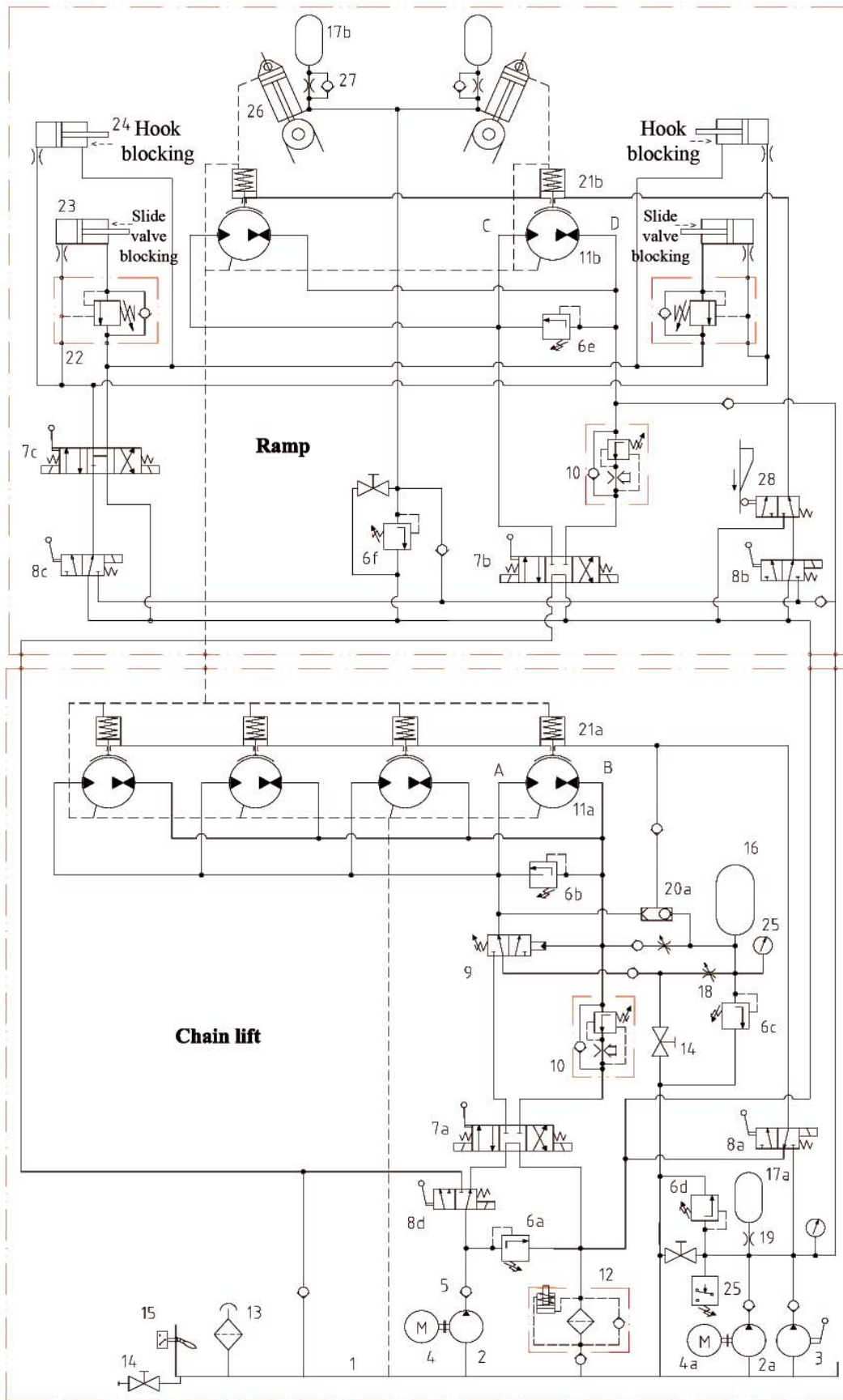
Fig. 7. Schematic diagram of the drive and control system for the stern port-ramp device and life boat chain lift. Notation: **1)** tank, **2)** constant capacity pump, **2a)** hand pump, **3)** hand pump, **4)** electric motor, **4a)** electric motor controlled by pressure transducer, **19)**, **5)** check valves, **6a)** – **6e)** overflow valves, **7a)** – **7c)** four-way three-position distributors; **8a** – **8d)** three-way two-position distributors, **9)** pressure - controlled three-way two-position distributor; **10a)** and **10b)** two-way flow controllers; **11a)** and **11b)** hydraulic motors of constant absorbing capacity; **12)** returning oil filter; **13)** inlet filter, **14)** cut-off valves, **15)** oil level relay, **16)** and **17a)** – **17b)** hydraulic-gas accumulators; **18)** throttle valves; **19)** throttling reducers, **20)** pressure -controlled valves; **21)** hydraulic brake release; **22)** brake valves, manometers; **23)** hydraulic cylinders of gate valves blocking the ramp, **24)** hook blocking hydraulic cylinders, **25)** pressure transducer, **26)** hydraulic cylinder, **27)** throttling check valve, **28)** three-way two-position distributor (limit switch), **A)**, **B)** and **C)**, **D)** stand for main circuit pipe branches of the chain lift and stern ramp, respectively

pressure transducer 25 in such a way as to keep the pressure in the accumulator within a determined range of values. To increase reliability of the device in long-lasting failure conditions the additional hand pump 3 was applied.

The gravitational opening process of the ramp is initiated by switching over the distributors 8b and 7b to the right. The distributor 8b makes oil flowing from the accumulator 17 to the brake releases 21b of the line hoisting winches. Then the distributor 7b connects both the main pipe branches C and D of the motors 11b with the oil tank, that makes suitable circulation of oil during pumping work of the motors while opening the ramp, possible. The two-way flow controller 10b located in the pipe branch D, throttling oil flow, will maintain ramp opening speed on the preset level, causing this way an increase of oil pressure in the upper part of the pipe branch. Owing to this a part of oil will flow from the branch to the accumulator 17a, recovering its charging state lowered by the operations of unblocking and freeing the brakes. Because of a relatively small capacity of the accumulator 17a and the throttling reducer 19 installed in it the charging process does not influence significantly a transient rise of opening speed of the ramp. After reaching by the ramp its nominal opening position the limit switch 28 connects brake releases with the outflow pipe branch and causes the ramp stopping in this position.

After the checking of the ramp opening state and appropriate placing people within the boats, readiness of the boats to launching is controlled and then the devices which secure the lift in its voyage position are released. The lowering of the boats as well as the opening of the ramp is performed by means of gravity forces at switched - off electric motor 4. The putting into motion the chain lifts with the boats is realized by remote switching over the distributors 8a and 7a to the right from the upper boat, or locally from the wheelhouse. It makes oil flowing from the accumulator 17a to the hydraulic brake releases 21a and a sudden rise, caused by external load, of oil pressure in the right pipe branch B of the circuit of the motors 11a. As a result, the distributor 9 is switched over to the left, making oil flow from the tank 1 through the distributors 7a and 9 up to the motors 11a, and their pumping operation due to action of the weight of the boats with people inside, possible. Speed of the motion is stabilized by means of the two-way flow controller 10a. In the first phase of the process the motion will be faster because of a high, loading - dependent oil pressure value as well as due to the fact that a part of the oil pressed from the branch B is gradually drained through the check & throttling valve 18 to the accumulator 16. The accumulator is applied to ensure continuity of lowering motion as well as for the reason that in the phase of placing the last boat on the slipway rollers and its freeing-out from the chain lifts, i.e. when external load of the motors 11a may appear too low to overcome friction forces in the system and to ensure their pumping work. When oil pressure in the branch B drops to its threshold value set by the spring of the distributor 9, it will be switched over to the position of connecting the accumulator (16) with the charging branch (A) of the motors (11) that will ensure continuity of work of the chain lift.

The hoisting operations of the boats out of the water and placing them into the voyage position, e.g. after a trial evacuation, are performed by using ship's power network. The boats are towed-out one by one onto the ramp and farther to the slipway by means of the line hoisting winch placed in the fore part of the slipway.

On the slipway the boats are placed onto the chain lift catches and then the lift is put into motion by switching-on the motor 2 of the pump 4 and switching over the distributor 7a to the left. This way oil pressure in the branch B will be increased,

the distributor 9 switched over to the left as well as the pressure controller switched over into the position connecting the branch in question with the brake releases 21a, that results in starting the hoisting process of the boats. After hoisting the boats to the level which makes it possible to fasten a successive, just taken out of water, life boat, the distributor 7a is switched over into its central position in order to stop motion of the chain lift for a period necessary to fasten the successive boat on the lift, then the chain lift is put into motion and stopped again and again up to the instant of fastening the last boat.

To start the closing process of the port-ramp it is necessary to switched over the distributors 8d and 8b to the right and then the distributor 7b to the left. As a result, the oil from the pump 2 will now flow to the branch D of the motors 11b, and the oil from the accumulator 17a will reach the brake releases 21b and, after freeing the brakes, the line hoisting winch will start in the direction of hauling away the line, closing this way the port - ramp. After its closing, the ramp is to be blocked for ship voyage period that is realized by switching over the distributors 8c and 7c to the right.

FINAL COMMENTS

On the basis of a broader comparative analysis between the elaborated concept of evacuation system and the systems have been applied so far, the following advantages of the novel concept can be presented:

1. A greater safety and comfort of evacuation from the point of view of passengers:
   - easy and safe access to life boats stiffly kept on different levels inside ship's hull without mutual displacements and a sight of rough sea,
   - a lower loading applied to boats and people as a result of lack of panting the boats against ship side and more gentle, bow-forward launching the boats.
2. Facilitation and simplification, hence a shorter duration time, of evacuation:
   - on average, a shorter distance and easier to be covered (now horizontally only) by evacuating persons,
   - simultaneous access to all the boats on particular decks, which makes process of managing and embarking people to boats simpler, faster and facilitated,
   - easiness of process of preparation and initiation of launching all the boats simultaneously and at an uniform speed, that radically speeds up evacuation process,
3. More advantageous technical features:
   - easiness of simultaneous control of readiness of all the boats – as hatchways or doors with glass eyeholes are provided in the casing walls, that makes it possible to find and reach a boat,
   - an integrated drive and control system which makes it possible to start and control evacuation process by a few operators only,
   - collision-free lowering and launching the boats and prompt sailing away from the ship in opposite direction along fairway free of obstacles (e.g. floating ice), that greatly shortens duration of evacuation and increases its safety - boat's engine is started already when the boat goes down along the slipway,
   - application of the ramp capable of increasing its deflection angle, that ensures a relatively gentle contact of a boat going down along it, with water, even in the conditions of an unfavourable ship trim forward and elevation of its end above water,
   - process of opening the port-ramp and lowering the boats runs automatically under action of gravity forces,

- the design of the chain lifts is relatively simple as it contains a smaller number of mechanisms than the systems with side life boats, that increases its reliability and lowers its cost,
- the life boats applied in the solution in question are similar to those used in free-fall boat systems but they are not to satisfy so high strength requirements, hence they can be cheaper,
- the device fastening the boat to the chain lift can be released by means of the hydrostatic release, that makes it possible to free the boat and maintain it on sea surface in the case of ship's sinking,

4. Another merits:
   - all the evacuation system occupies a relatively small area as the boats are located one by one, and in the relatively least favourable and useful zone of ship,
   - lower resistance to ship motion,
   - elevated aesthetic image of ship.

Bibliography

1. Dymarski Cz., Dymarski P.: *Life saving and rescue appliances for ships – research and design projects* (in Polish). 10th International Scientific Technical Conference on „Safety at Sea and Sea Environment Protection", 5th Marine Forum, Koszalin - Kołobrzeg 2006, Ed. S. Piocha. - Koszalin, NOT, 2006.
2. Dymarski Cz., Łubiński P.: *Safe evacuation of people from ships - projects realized in the frame of the European Research Project SAFECRAFTS* (in Polish). In: "Development Prospects of Transport Systems": 8th Conference on Shipbuilding and Ocean Engineering, Międzyzdroje, June 2006. Publ. Szczecin University of Technology, 2006.
3. Dymarski Cz., Kraskowski M., Sperski M.: *Investigation of motion of the lifeboat lowered from ship's deck.* Polish Maritime Research. - Vol. 13, No.3, 2006.
4. Dymarski Cz., Dymarski P.: *An evacuation system of people from multi-deck ship – passenger carrier in particular* (in Polish).Patent application No. P 379355 of 03.04.2006.
5. Dymarski Cz., Łubiński P., Dymarski P.: *Ramp and chain-lift-launched lifeboats - radical concepts for evacuating cruise ships.* Naval Architect, October 2006.
6. Dymarski Cz.: *A concept of drive and control system of a novel device for people evacuating from large passenger ships*. Polish Maritime Research Vol. 17, No. 4 (67) 2010
7. http://www.amarnetraffic.com/ais/pl/showallphotos.aspw?mmsi=235762000
8. http://www.alltechn.com/2009/07/01/royal-caribbean-international/

CONTACT WITH THE AUTHOR

Prof. Czesław Dymarski
Faculty of Ocean Engineering
and Ship Technology,
Gdańsk University of Technology
Narutowicza 11/12
80-233 Gdańsk, POLAND
e-mail: cpdymars@pg.gda.pl

Evolutionary approach to ship's trajectory planning within Traffic Separation Schemes

Rafał Szłapczyński, Ph. D.
Gdańsk University of Technology

ABSTRACT

The paper presents the continuation of the author's research on evolutionary approach to ship trajectory planning. While the general problem of the evolutionary trajectory planning has already been solved, no one has yet touched one of its specific aspects: evolutionary trajectory planning within Traffic Separation Schemes. Traffic Separation Scheme (TSS) is a traffic-management route-system complying with rules of the International Maritime Organization. In brief, the ships navigating within a TSS all sail in the direction assigned to a particular traffic lane or they cross at a course angle as close to 90 degrees as possible. This and other TSS rules largely affect the evolutionary method. The paper presents a proposal of the extended evolutionary method, with a focus on changes that have to be made to obey TSS rules, especially the changes in the phases of evaluation and specialised operators of the evolutionary cycle.

Keywords: marine navigation; Traffic Separation Schemes; collision avoidance manoeuvres; evolutionary computing

INTRODUCTION

As for now, nearly all aspects of marine navigation have been subjects to scientific research, with most of the navigational processes having been modelled and the decision problems described formally. Especially, there are many numerical methods for planning ship routes or collision-avoidance manoeuvres. Even though some of them have not been applied yet, these problems are generally considered to be solved from the basic research point of view. Traffic Separation Scheme (TSS) rules however are an exception and have not been thoroughly investigated yet. In particular, there are no algorithms based on them while the rules themselves are too ambiguous to implement them directly.

The Traffic Separation Scheme (TSS) is a route management system complying with rules of the International Maritime Organization (IMO). TSS's are used to regulate the traffic at busy, confined waterways (usually port waters) or around capes. Typically a TSS consists of at least one traffic lane in each main-direction, turning-points, deep water lanes, separation zones between the main traffic lanes and inshore zones. The body of water between two opposite lanes is an area where navigating is only allowed under special circumstances (collision avoidance manoeuvres or crossing the lanes). As a result of lane separation, a risk for head-on collisions is greatly reduced. Where needed, there are special zones where a lane splits into

two channels: one on-going and the other to the nearby ports. In most TTS schemes there are also Inshore Traffic Zones between the traffic-lanes and the coast. The inshore traffic zone is unregulated and should not be used for on-going traffic: it is meant for local traffic, fishing and small craft only.

There are a number of methods of solving multi-ship encounter situations: they can be divided into deterministic and heuristic ones. Deterministic approach is based on differential games and has been proposed by Lisowski [10]. Of the heuristic ones the most successful and flexible is searching for a ship's trajectory by genetic or evolutionary algorithms. The method has been first proposed by Smierzchalski and Michalewicz [12] and since then similar approaches has been tried by other researchers: evolutionary computation (EC) may be applied for finding an optimal path [16, 21] and genetic algorithms (GA) are used for optimization of collision avoidance manoeuvres [8, 18]. Other related approaches include trajectory optimization by using genetic annealing algorithm [1] and ship collision avoidance route planning by ant colony algorithm [17]. Summaries of applying GA and EC to maritime collision avoidance and trajectory planning have been presented in [13, 20] among others. In short, EC and GA approach to the problem use algorithms which for a given set of pre-determined input trajectories find a solution that is optimum according to a given fitness function. In this paper is introduced an extension to the evolutionary approach previously proposed by the author [15],

which allows the evolutionary method to support special rules that have to be obeyed within Traffic Separation Schemes.

Handling the TSS rules affects two phases of the evolutionary method: evaluation (where breaking the rules is detected and penalized by fitness function) and specialised operators which aim at eliminating the violations of the rules by adjusting the trajectories of ships. Therefore it is these two phases that the paper focuses on. The rest of the paper is organized as follows. In the next section a more formal description of the problem is given, including the particular TSS rules which have to be obeyed. Then the ways of detecting constraints violations, including violations of TSS rules, are discussed. This is followed by the summarised foundations of the evolutionary method, with a brief explanation of each of the phases of the cycle. Then detailed descriptions of phases of interest (evaluation and specialised operators) are provided. Finally example results of the method and the conclusions are presented.

OPTIMISATION PROBLEM

It is assumed that the following data are given:
- stationary constraints (such as landmasses and other obstacles),
- positions, courses and speeds of all ships involved,
- ship domains,
- times necessary for accepting and executing the proposed manoeuvres.

Ship positions and ship motion parameters are provided by ARPA (Automatic Radar Plotting Aid) and AIS (Automatic Identification System) systems. A ship domain can be determined on the basis of the ship's length, its motion parameters and type of water region. Since the shape of a domain is dependent on type of water region, the author has decided to use a ship domain model by Davis [5], which updated Goodwin model [7], for open waters and to use a ship domain model by Coldwell [3], which updated Fuji model [6], for restricted waters. The last parameter – the necessary time, is computed on the basis of navigational decision time and the ship's manoeuvring abilities. By default a 6-minute value is used here.

There are also some additional COLREGS-related assumptions, namely:
- the method is applied for good visibility conditions,
- all considered ships are equally privileged,
- all considered ships have motor engines and are not restricted in their ability to manoeuvre: no sailing ships or damaged ships are taken into account – such ships should be always given way to (COLREGS, Rule18 - responsibilities between vessels),

Knowing all the above mentioned parameters, the goal is to find a set of trajectories which minimizes the average way loss spent on manoeuvring, while fulfilling the following conditions:
- none of the stationary constraints are violated,
- none of the ship domains are violated,
- the minimal acceptable course alteration should not be too small (the minimal alteration of 15 degrees has been assumed here),
- the maximal acceptable course alteration should not be too large (the maximal alteration of 60 degrees has been assumed here),
- speed alteration are not to be applied unless necessary (collision cannot be avoided by course alteration up to 60 degrees),

- a ship only manoeuvres when she is obliged to,
- in case of head-on and crossing encounters, manoeuvres to starboard are favoured over manoeuvres to port board.

As for the first two conditions, all obstacles have to be avoided and the ship domain is an area that should not be violated by definition. All the other conditions are either imposed by COLREGS [2, 4] and good marine practice or by economics. In particular, very small course alterations might be misleading for the ARPA systems (and therefore may lead to collisions) and very large course alterations are not recommended due to efficiency reasons. Also, ships should only manoeuvre when necessary, since each manoeuvre of a ship makes it harder to track its motion parameters for the other ships' ARPA systems. Apart from the main constraints, additional constraints – selected COLREGS rules have to be directly handled. In brief, the basic COLREGS rules of interest here are:
- Rule 13 – overtaking: an overtaking vessel must keep well clear of the vessel being overtaken.
- Rule 14 - head-on situations: when two power-driven vessels are meeting head-on both must alter course to starboard so that they pass on the port side of the other.
- Rule 15 - crossing situations: when two power-driven vessels are crossing, the vessel, which has the other on the starboard side must give way.
- Rule 16 - the give-way vessel: the give-way vessel must take early a substantial action to keep well clear.
- Rule 17 - the stand-on vessel: the stand-on vessel may take action to avoid collision if it becomes clear that the give-way vessel is not taking appropriate action.

The behaviour of ships within TSS is specified by Rule 10 whose key points are as follows:
a) A vessel using a traffic separation scheme shall:
   - proceed in the appropriate traffic lane in the general direction of traffic flow for that lane,
   - so far as practicable keep clear of a traffic separation line or separation zone,
   - join or leave a traffic lane at the termination of the lane, but when joining or leaving from either side shall do so at as small an angle to the general direction of traffic flow as practicable.
b) A vessel shall so far as practicable avoid crossing traffic lanes, but if obliged to do so shall cross on a heading as nearly as practicable at right angle to the general direction of traffic flow.
c) A vessel shall not use an inshore traffic zone when she can safely use the appropriate traffic lane within the adjacent traffic separation scheme unless:
   - it is a vessel of less than 20 metres in length, sailing vessel or that engaged in fishing,
   - it is on route to or from a port, offshore installation or structure, pilot station or any other place situated within the inshore traffic zone, or to avoid immediate danger.
d) A vessel other than a crossing vessel or a vessel joining or leaving a lane shall not normally enter a separation zone or cross a separation line except:
   - in cases of emergency to avoid immediate danger,
   - to engage in fishing within a separation zone.

In the following sections it is analysed how the violations of all these constraints can be detected, and how severely should they be penalized during the evaluation phase by the fitness function of the evolutionary method.

DETECTING VIOLATIONS OF CONSTRAINTS

Detecting violations of static constraints (collisions with landmasses and safety isobaths)

The method uses a vector map of a given area. However it is not processed directly for detection of constraints violations, but for generating bitmap of an area, which is done offline and only once for each area. Then, when the method is running in real time, each bitmap cell, which the trajectory of a ship traverses, is read and checked for belonging to landmass or safety isobaths. For a bitmap whose detail level reflects this of a given vector map, the computational time would be proportional to the number of traversed cells and thus acceptable. This approach is also quite flexible in terms of future implementation of bathymetry: if every cell contained information on the water depth, it would be easy to check whether a cell is passable or not for a particular ship.

Detecting ship domain violations

The algorithm for detecting ship-to-ship collisions is as follows. Each ship's trajectory is checked against all other ships. For each pair of ships, the start time and end time of each trajectory's segments are computed. If two segments of the two trajectories overlap in time, they are checked for geometrical crossing. In case of a crossing, the approach factor value is computed. Then, if the approach factor value indicates collision, the type of an encounter (head-on, crossing or overtaking) is determined on the basis of the ships' courses and it is decided, which ship is to give way (both ships in case of head-on). The collision is only registered for the give-way ship and the information on the collision are stored in the trajectory's data structure.

Detecting general COLREGS violations

The three most common types of COLREGS violations are as follows:
- a ship does not give way, when it should,
- a ship gives way, when it should not (making unexpected and misleading manoeuvres),
- a ship manoeuvres to port-board when it should manoeuvre to starboard.

Each of these three situations may happen on either open or restricted waters, which gives a total of six cases to handle. Unfortunately, when analysing a set of ship trajectories for a multi-target encounter, it is sometimes impossible to recognize the reason for a particular manoeuvre: which ship was given way intentionally, and which one benefited from it only as a side effect. As a result, not all violations can be detected. The final COLREGS violations detection rules applied in the method are:

1) In open waters:
   a) if a ship is not obliged to give way to any other ship, any manoeuvre it performs is registered as COLREGS violation,
   b) if a ship is obliged to give way and does not perform a manoeuvre, it is registered as COLREGS violation,
   c) all manoeuvres to port board are registered as COLREGS violations.

2) In restricted waters: here, as explained before, every trajectory node which is a part of a manoeuvre, contains information on the reason why this particular node has been inserted or shifted: land or other stationary obstacle avoidance, target avoidance or accidental manoeuvre generated by evolutionary mechanisms. Based on this, COLREGS violations are registered as follows:
   a) if a ship does not initially have to give way to any target and its first manoeuvre has reason other than static constraint violation avoidance, it is registered as COLREGS violation,
   b) any manoeuvre to port board of reason other than static constraint violation avoidance is registered as COLREGS violation.

Detecting TSS rules violations

The possible lawful types of routes which are the results of applying the COLREGS rule 10 are shown in Fig. 1. For a TSS sector shown in Fig. 1 the preferred tracks that the ships should follow are:
- Track A – through traffic,
- Track B – traffic using a lane and crossing another lane to reach inshore zone; notice the small angle at which it leaves the lane to reach separation zone and altering course within the separation zone,
- Track C – traffic crossing TSS at right angle,
- Track D – traffic joining lane from the side,
- Track E – traffic leaving the inshore zone, crossing one lane and joining the other lane,
- Track F – traffic leaving the lane at small angle.
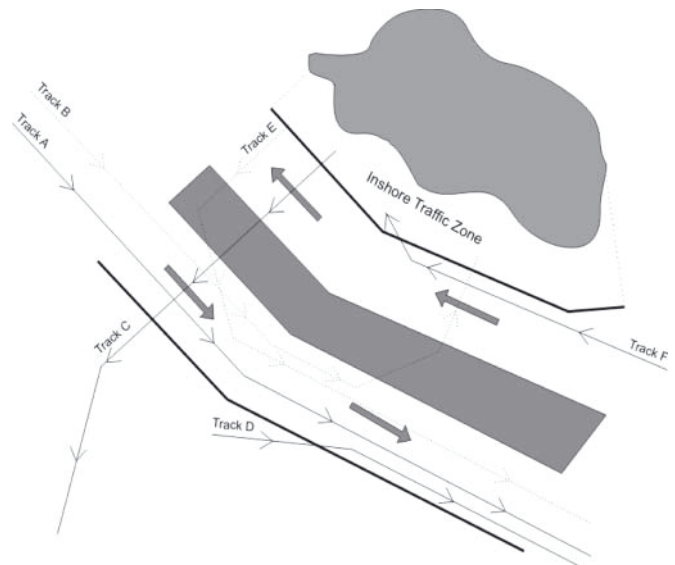
Fig. 1. TSS and different routes through a sector

The algorithm for TSS rules' violation detection is given as follows. The first step for checking for a TSS rule violation is always the checking if a trajectory's segment has crossed with a certain TSS system. If so, then each of the TSS's parts will be checked. Since each part of a TSS is a polygon it is enough to detect a crossing of a trajectory's segment with one of the polygon's edges. Once such crossing has been detected the further conditions for violations will be checked, depending on the particular TSS part. The following types of TSS violations have been identified and used in this research (the violations have been grouped into three major categories, which are shown in Fig. 2-4):
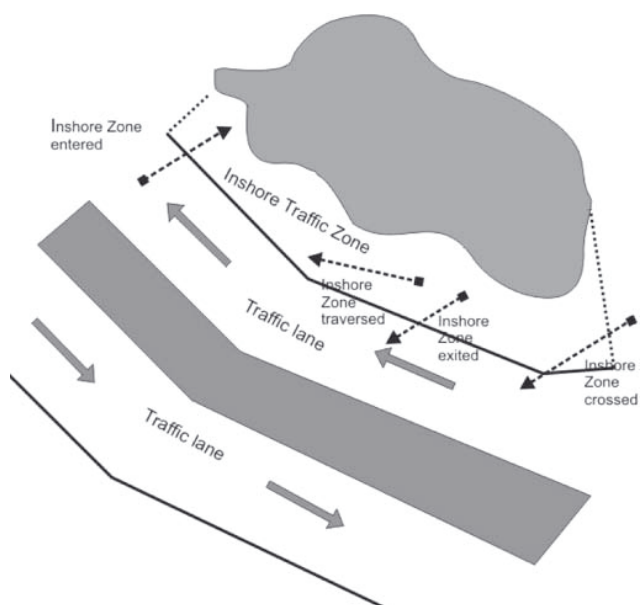
Fig. 2. Violations of Inshore Zone
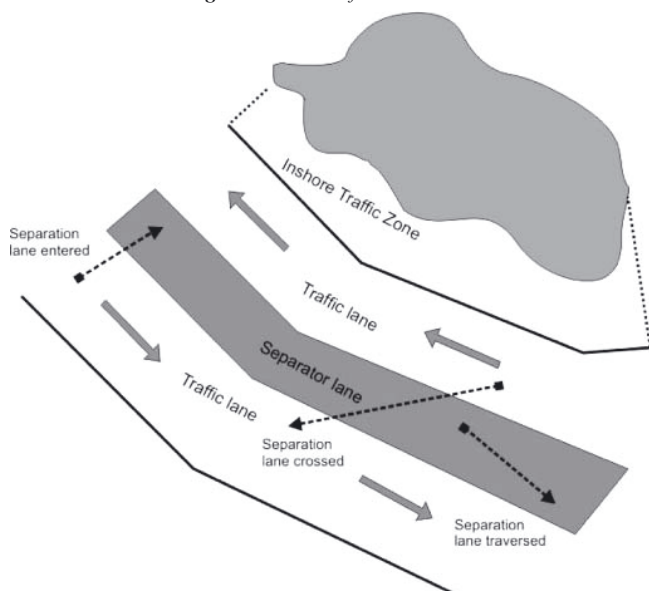
Fig. 3. Violations of Separation lane
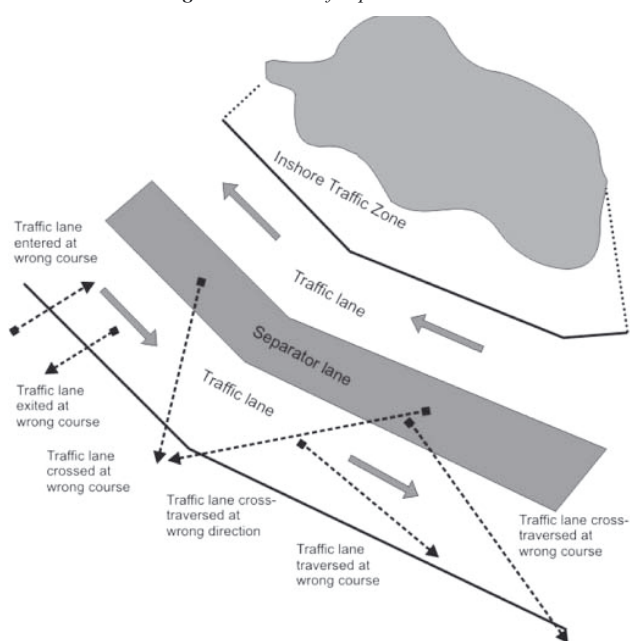
Fig. 4. Violations of traffic lane

1. Inshore Zone entered: the first endpoint of a trajectory's segment is outside the Inshore Zone and the second one is inside.
2. Inshore Zone traversed: both endpoints of a trajectory's segment are inside the Inshore Zone.
3. Inshore Zone crossed: both endpoints of a trajectory's segment are outside the Inshore Zone and the segment crosses Inshore Zone boundaries.
4. Inshore Zone exited: the first endpoint of a trajectory's segment is inside the Inshore Zone and the second one is outside.
5. Traffic lane entered at a wrong course: the first endpoint of a trajectory's segment is outside the traffic lane and the second one is inside. The course of entrance differs from the lane's direction by more than 20 degrees.
6. Traffic lane traversed at a wrong course: both endpoints of a trajectory's segment are inside the lane. The course of a segment differs from the lane's direction by more than 5 degrees.
7. Traffic lane cross-traversed at a wrong course: both endpoints of a trajectory's segment are outside the lane. The course of a segment differs from the lane's direction by more than 5 degrees but less than 45 degrees.
8. Traffic lane cross-traversed at a wrong direction: both endpoints of a trajectory's segment are outside the lane. The course of a segment differs from the lane's direction by more than 135 degrees.
9. Traffic lane crossed at a wrong course: both endpoints of a trajectory's segment are outside the lane. The course of a segment differs from the perpendicular to the lane's direction by more than 5 degrees and less than 45 degrees.
10. Traffic lane exited at a wrong course: the first endpoint of a trajectory's segment is inside the traffic lane and the second one is inside? The course of a segment differs from the lane's direction by more than 20 degrees.
11. Separation lane entered: the first endpoint of a trajectory's segment is outside the separation lane and the second one is inside.
12. Separation lane traversed: both endpoints of a trajectory's segment are inside the separation lane.
13. Separation lane crossed: both endpoints of a trajectory's segment are outside the separation lane.
14. Separation lane exited: the first endpoint of a trajectory's segment is inside the separation lane and the second one is outside.

The identified violation types of TSS rules are shown in Fig. 2 (Inshore Zone violations), Fig. 3 (Separation lane violations) and Fig. 4 (Traffic lane violations).

EVOLUTIONARY COMPUTING - GENERAL IDEA

Before proceeding further with the details of the method which solves the above formulated optimization problem, some basic information on evolutionary programming are provided in this section. The general idea of evolutionary computing [11] is shown in Fig. 5.

First, the initial population of individuals (each being a potential solution to the problem) is generated either randomly or by other methods. Usually none of the individuals is optimal or even close to that. Sometimes none of the individuals is acceptable. This initial population is a subject of subsequent iterations of evolutionary algorithm. Each of the iterations consists of the following steps:
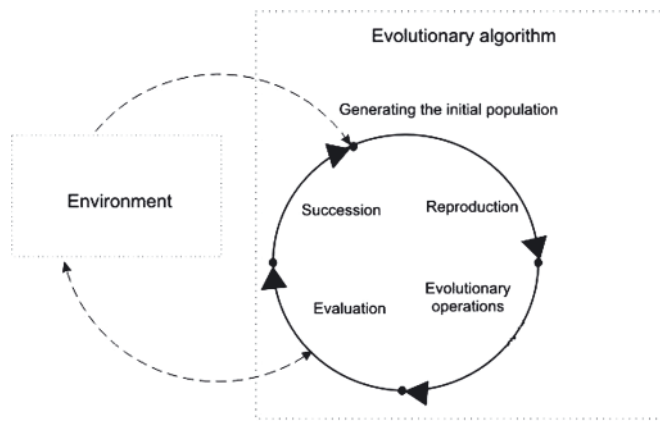
Fig. 5. Evolutionary algorithms - general idea

1. Reproduction: sets of parents (usually pairs) are selected from all of the individuals and they are crossed to produce offspring. The offspring inherits some features from each parent.
2. Evolutionary operations: the offspring is modified by means of random mutation operators as well as specialized operators dedicated to the problem.
3. Evaluation: each of the individuals (including parents and the offspring) is assigned a value of a fitness function which reflects the quality of the solution represented by this individual.
4. Succession: the next generation of individuals is selected. The selection is based on the results of the evaluation. Usually the individuals are chosen randomly with the probability strictly depending on the fitness function value.

The evolutionary algorithm ends when one of the following happens:
- maximum acceptable time or number of iterations is reached,
- the satisfactorily high value of fitness function has been reached by one of the individuals,
- further evolution brings no improvement.

The main difference between the evolutionary computing and pure genetic algorithms is that in the former the individuals directly represent the potential solutions to the problem, without being translated to chromosomes first. This allows for specialised operators dedicated to the problem, which, for some classes of optimisation tasks, greatly speed up the evolutionary process, resulting in a much lesser number of generations needed and much lower computational time. The method discussed in the paper, focuses on specialised operators thus fully utilizing the possibilities of evolutionary computing.

EVALUATION

In the evolutionary method all individuals (sets of trajectories) are evaluated by the specially designed fitness function which should reflect optimisation criteria and constraints [11]. In this section it is shown how this fitness function is formulated.

Basic criterion – minimizing way loss

The basic criterion is the economic one – minimizing way loss of a ship. A trajectory_economy_factor is computed according to the formula (1).

$$\text{trajectory\_economy\_factor} = \tag{1}$$

$$= \left(\frac{\text{trajectory\_length} - \text{way\_loss}}{\text{trajectory\_length}} \right)$$

where:
trajectory_length – the total length of the ship's trajectory [nautical miles],
way_loss – the total way loss of the ship's trajectory [nautical miles] computed as a difference between the trajectory length and length of a segment joining trajectory's start point and endpoint.

As can be seen, the trajectory_economy_factor is always a number from a (0,1] range.

Penalizing static constraint violation

After the trajectory economy factor has been computed the static constraints are handled by introducing penalties for violating them. For each trajectory its static constraint factor scf is computed. The static constraints are always valid and their violations must be avoided at all costs, therefore penalties applied here are the most severe – hence the square in the formula (2).

$$\text{scf} = \left(\frac{\text{trajectory\_length} - \text{trajectory\_cross\_length}}{\text{trajectory\_length}} \right)^2 \tag{2}$$

where:
trajectory_cross_length – the total length of the parts of the ship's trajectory which violate stationary constraints [nautical miles].

The static constraint factor is a number from a [0,1] range, where "1" value means no static constraint violation (no landmasses or other obstacles are crossed) and "0" value is for trajectories crossing landmasses on their whole length.

Penalizing collisions with other ships

Analogically to the static constraint factor, collision avoidance factor caf is computed to reflect the ship's collisions with all other privileged ships as shown by (3).

$$\text{caf} = \prod_{j=1}^{n} [\min(\text{fmin}_j, 1)]^2 \tag{3}$$

where:
n – the number of ships [/],
j – the index of a target ship [/],
f_{min_j} – the approach factor [14] value for an encounter with ship j, if the own ship is the privileged one, the potential collision is ignored and the approach factor value is equal to 1 by definition. [/].

The collision avoidance factor is a number from a [0,1] range, where "1" value means no ship domain violation and "0" means a crash with at least one of the targets.

Penalizing TSS rules violations

TSS compliance factor tcf is computed according to the following formula (4).

$$\text{tcf} = 1 - \sum_{k=1}^{m} [\text{TSS\_violation\_penalty}_k] \tag{4}$$

where:
m – he number of TSS rules violation registered for the current ship [/],
k – the index of a registered violation [/],
TSS_violation_penalty_k – the penalty for the k-th of the registered TSS rules violation [/].

The TSS rules violations are penalized as follows:

1. through 4. (Inshore Zone violations):

$$\text{TSS\_violation\_penalty} = \\ = 2 \cdot \text{segment\_violation\_percentage} \quad (5)$$

5. and 10. (Traffic Lane is entered or exited at a wrong course):

$$\text{TSS\_violation\_penalty} = \\ = 2 \cdot \text{segment\_violation\_percentage} \cdot \quad (6) \\ \cdot \sin(\text{e\_dev\_angle})$$

where:
$$\text{e\_dev\_angle} = |\text{traffic\_lane\_course} - \text{ship\_course}| - 20 \quad (7)$$

6. and 7. (Traffic Lane is traversed at a wrong course or Traffic lane is cross-traversed at a wrong course):

$$\text{TSS\_violation\_penalty} = \\ = 2 \cdot \text{segment\_violation\_percentage} \cdot \quad (8) \\ \cdot \sin(\text{t\_dev\_angle})$$

where:
$$\text{t\_dev\_angle} = |\text{traffic\_lane\_course} - \text{ship\_course}| - 5 \quad (9)$$

8. (Traffic lane is cross-traversed at a wrong direction):

$$\text{TSS\_violation\_penalty} = \quad (10)$$
$$= 2 \cdot \text{segment\_violation\_percentage} \cdot \sin(\frac{\text{ct\_dev\_angle}}{2})$$

where:
$$\text{ct\_dev\_angle} = |\text{traffic\_lane\_course} - \text{ship\_course}| - 5 \quad (11)$$

9. (Traffic lane is crossed at a wrong course):

$$\text{TSS\_violation\_penalty} = \\ = 2 \cdot \text{segment\_violation\_percentage} \cdot \quad (12) \\ \cdot \sin(\text{c\_dev\_angle})$$

where:
$$\text{c\_dev\_angle} = |\text{perpendicular\_to\_traffic\_lane\_course} - \\ + \text{ship\_course}| - 5 \quad (13)$$

11. through 14. (Separation Lane violations):

$$\text{TSS\_violation\_penalty} = \\ = \frac{\text{segment\_violation\_percentage}}{2} \quad (14)$$

For all penalty formulas:

$$\text{segment\_violation\_percentage} = \\ = \frac{\text{violating\_part\_length}}{\text{segment\_length}} \quad (15)$$

Penalizing other COLREGS violations

Within TSS, the other COLREGS violations are secondary to static constraint violations, collisions with other ships and TSS rules violation and therefore the author has decided to penalize it moderately to make sure that constraints from the previous two points are met first. COLREGS compliance factor ccf is computed according to the following formula:

$$ccf = 1 - \sum_{k=1}^{m} [\text{COLREGS\_violation\_penalty}_k] \quad (16)$$

where:

m	–	the number of COLREGS violation registered for the current ship [/],
k	–	the index of a registered violation [/],
COLREGS_violation_penalty$_k$	–	the penalty for the k-th of the registered COLREGS violation [/].

The penalty values for all registered COLREGS violations are configurable in the method and are set to 0.05 by default.

Fitness function value

Once all aforementioned factors have been computed the normalized fitness function value is calculated. The fitness function is normalized for convenience of further evolutionary operations, mostly for selection purposes. As a result no additional operations on fitness function values are necessary and they can directly be used for random proportional and modified random proportional selection in the reproduction and succession phases of the evolutionary algorithm. It is also easier to measure and see progress that is made with each generation. However, normalized fitness function is harder to obtain, because one has to make sure that the high resolution of evaluating the individuals is kept, namely that various levels of penalties are used: stationary constraints, being more important than collision avoidance and collision avoidance being more important than COLREGS compliance. Here, the normalized fitness function keeps relatively high resolution of evaluation: minor stationary constraints violations are penalized similarly as major collisions with other ships and minor collisions with other ships are penalized similarly as multiple COLREGS violations. The final fitness function is as follows:

$$\text{trajectory\_fitness} = \quad (17)$$
$$= \text{trajectory\_economy\_factor} \cdot \text{scf} \cdot \text{caf} \cdot \text{tcf} \cdot \text{ccf}$$

SPECIALISED OPERATORS WHICH FIX TSS RULES' VIOLATIONS

The random mutation operators and specialised operators dedicated for static constraints' violations problem and ship collisions' problem have been introduced in [15]. Therefore in this section only new, previously not presented operators which fix TSS rules' violations are described here. In the method's data structure all TSS violations are stored and their data contains:
- VTS violation type
- numbers which identify a TSS and its part which has been violated

- a segment responsible for the violation (identified by its first node)
- recommended course for this TSS part
- violation angle (the difference between recommended course and the segment's course)
- percentage of a segment's length which violates the rule
- coordinates of entrance point (if a segment enters a TSS part)
- coordinates of exit point (if a segment exits a TSS part)

The designed operators are semi-deterministic [9], that is based on these data, and it is decided what action can be taken to fix the part of a trajectory which violates the TSS rules. The actions can be roughly classified as:
- avoiding entering a certain TSS part,
- adjusting the current course to the recommended course.

Below the operators used for fixing violations of inshore zone, separator lanes and traffic lanes are briefly described.

Fixing violations of inshore zone

For violations of inshore zone the action is always avoiding entering this part of a TSS. The operators which are used for this are:
- inserting a new segment,
- inserting a node,
- shifting the first node of a segment,
- shifting the second node of a segment,
- shifting a segment.

These operators work very similarly as collision voidance operators described in [15]. A particular operator is chosen, based on the time distance between two nodes, which constitute the violating segment and on the time remaining to violation when the ship is in the first node. It is assumed that a navigator should always have a predefined amount of time for decision making and manoeuvre execution (by default – 6 minutes) and therefore the time between two subsequent manoeuvres cannot be shorter than this predefined time. Inserting a new segment (two course alteration manoeuvres) or a new node (a single course alteration manoeuvre) should not affect the minimal time space between manoeuvres. Therefore, the choice of an operator is done as follows:
- whenever there is enough time, a new segment is inserted
- if a new segment cannot be inserted, a new node is inserted, if possible
- if a new node cannot be inserted, the violating segment or one of its nodes is moved away from the violation point (usually the entrance point). Usually the node closer to the violation point is moved or a segment is moved if the violation point is close to the middle of this segment.

The operators are illustrated in Fig. 6 through 10.

Fixing violations of separator lanes

It has been decided that violations of separator lanes, which are penalized moderately, will not be fixed because they are often side effects of collision avoidance manoeuvres. The only exception is crossing a separator lane at a wrong course. In such cases, if possible, a new node is inserted so as to cross at a course perpendicular to the lane direction. The operator is illustrated in Fig. 11.
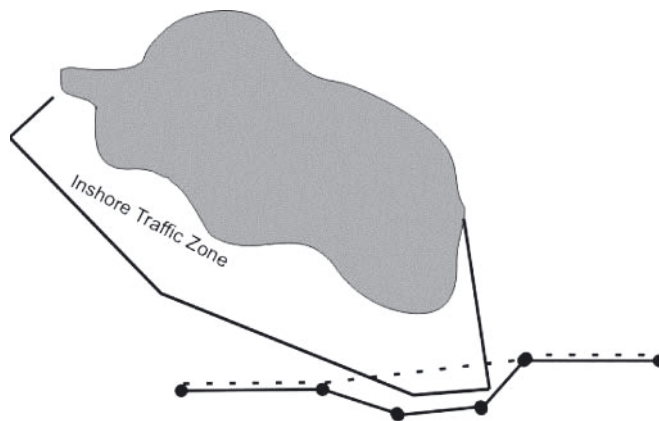

Fig. 6. Fixing violations of inshore zone - inserting a new segment
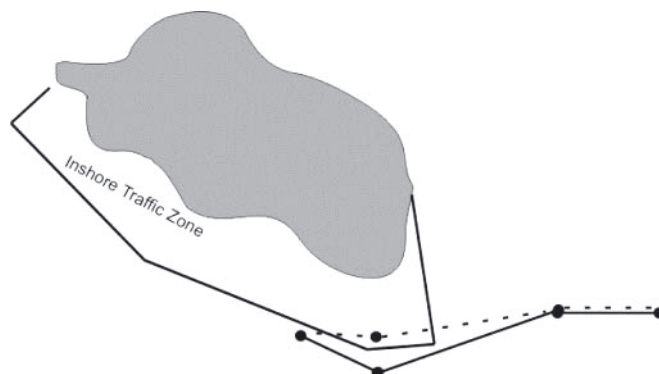

Fig. 7. Fixing violations of inshore zone - inserting a new node
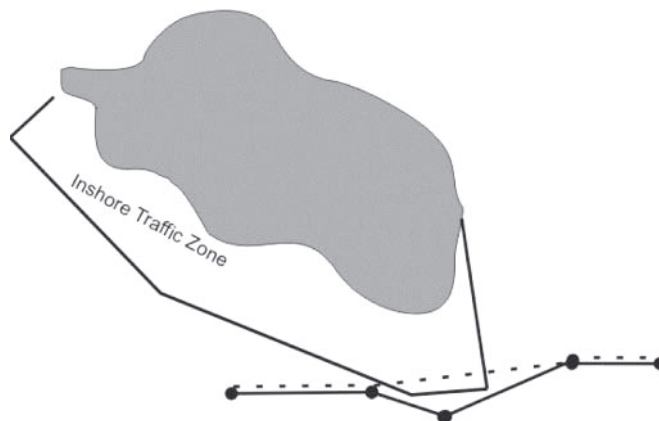
Fig. 8. Fixing violations of inshore zone -shifting the first node of a segment
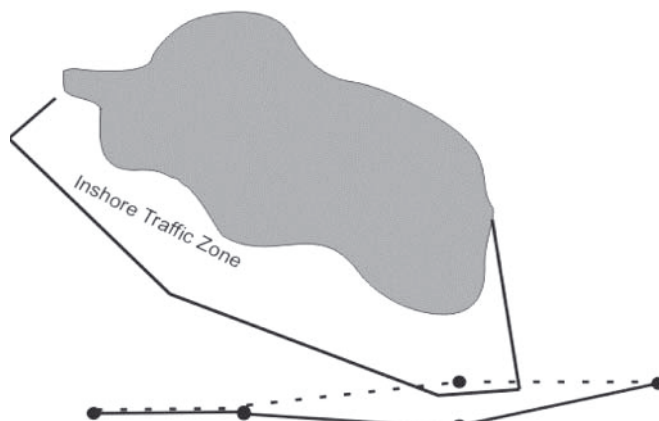
Fig. 9. Fixing violations of inshore zone - shifting the second node of a segment
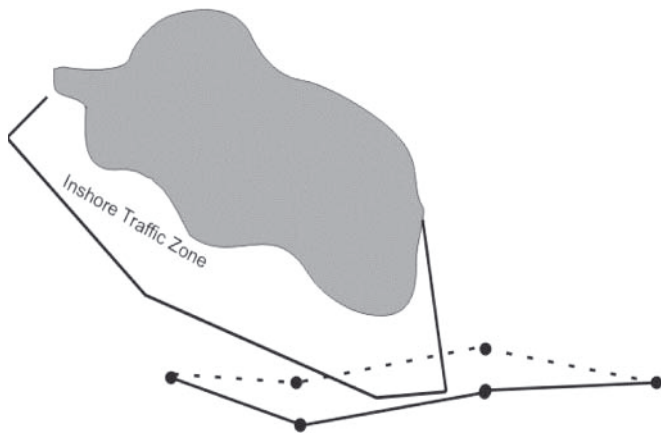
Fig. 10. *Fixing violations of inshore zone - shifting a segment*
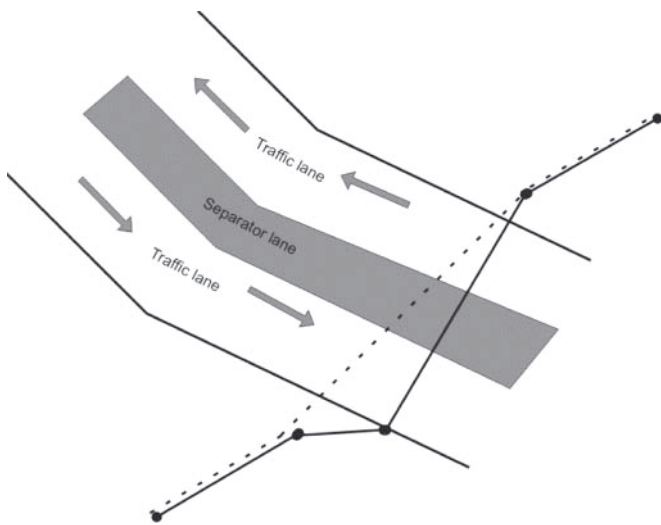
Fig. 11. *Fixing violations of separator lane - crossing the separator lane*

Fixing violations of traffic lanes

The fixing operators here work as follows:
- in case of entering or exiting at a wrong course, the second node of the segment is moved so as to change the current course to the one differing by 20 degrees from the lane direction
- in case of traffic lane traversed at a wrong course (differing from the recommended one by more than 5 degrees), the second node is moved so as to adjust the course to the recommended one. If this is not possible due to the course difference being too large, the second node of the segment is deleted.
- in case of a traffic lane crossed at wrong course, a new node is inserted so as to cross at a course perpendicular to the lane's direction, similarly as in case of crossing a separator lane
- in case of a traffic lane cross-traversed at a wrong direction, the violation is fixed similarly as in case of inshore zone violation, that is, an avoidance action is chosen
- in case of a traffic lane cross-traversed at wrong course, a new segment is inserted between the nodes of the violating segment so as to adjust movement within the lane to the traffic lane direction. If such action generates entering or exiting at wrong course, the second node of the violating segment will be additionally moved so as to change the current course to the one differing by 20 degrees from the lane direction.

The operators are illustrated in Fig. 12 through 15.
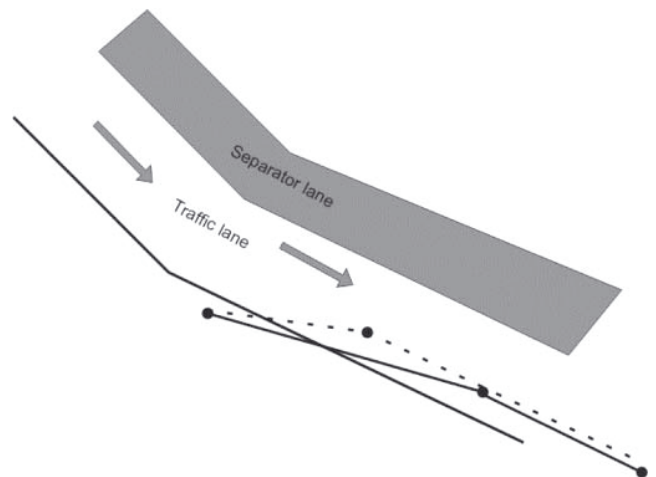
Fig. 12. *Fixing violations of traffic lane - entering or exiting the lane*
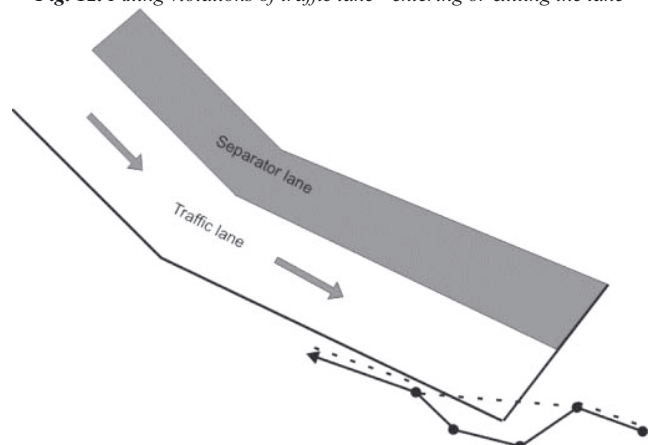
Fig. 13. *Fixing violations of traffic lane - traversing the lane*
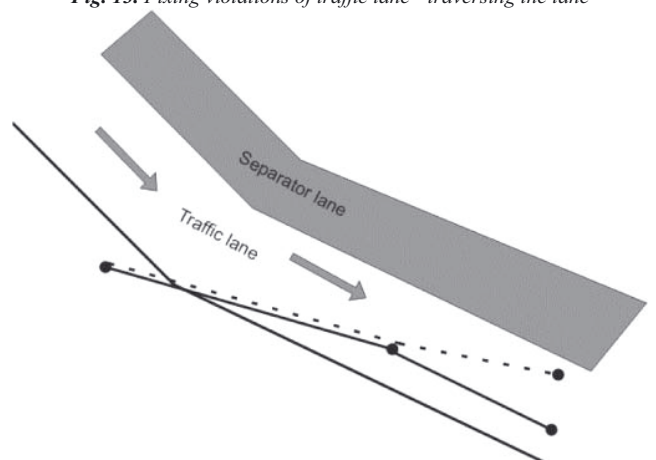
Fig. 14. *Fixing violations of traffic lane - avoiding the movement in wrong direction*
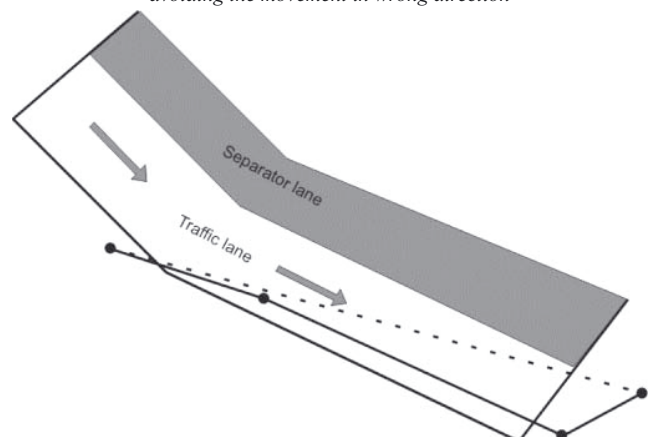
Fig. 15. *Fixing violations of traffic lane - cross-traversing the lane*

EXAMPLES OF RESULTS OF SIMULATIONS

In this section examples of ship routes planned by the method are shown (Fig. 16 and 17). Both scenarios are set in the Traffic Separation Scheme "Gulf of Gdansk" which consists of the following elements:

a) "TSS-WEST" (incoming lane and outgoing lane separated by a line – these traffic lanes are shown in a left part of each figure)
b) "TSS-EAST" (incoming lane and outgoing lane separated by a separator lane – these traffic lanes are shown in a right part of each figure)
c) "ITZ" - Inshore Traffic Zones (shown in a left part of each figure and marked with a red dotted line)
d) Recommended tracks (additional routes).

In Fig. 16 a ship traverses the incoming traffic lane of "TSS-WEST" and avoids violations of Inshore Traffic Zone, separator line and outgoing traffic lane. The ship's course is parallel to the recommended direction throughout the lane's length.

In Fig. 17 it is shown how a ship changes its course to avoid violating "TSS-WEST" and then crosses two traffic lanes and a separator lane of "TSS-EAST". The crossing is done perpendicularly to the lanes' direction.
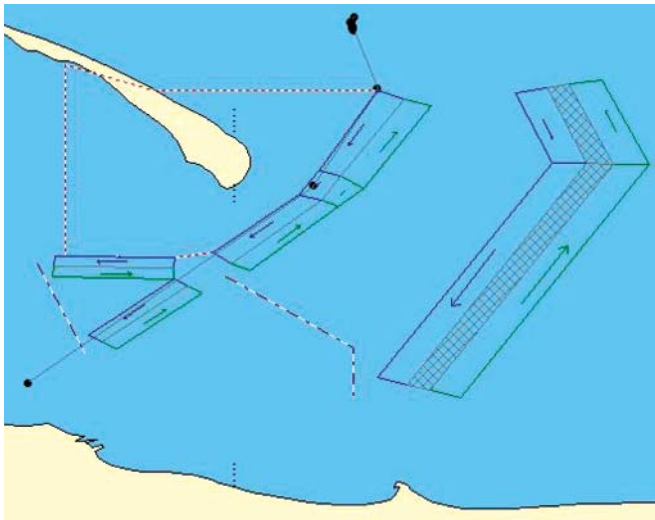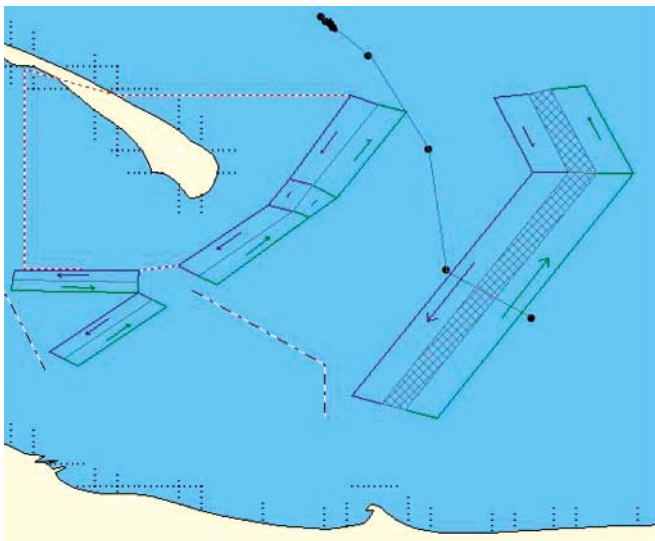

Fig. 16. A ship traversing an incoming traffic lane

Fig. 17. A ship crossing traffic lanes and a separator laneIn both cases the ships' behaviour is compliant with TSS recommendations specified by COLREGS Rule 10

SUMMARY AND CONCLUSIONS

In this paper an evolutionary trajectory planning method has been presented. The description has been focused on supporting rules abiding within Traffic Separation Schemes, which have not been handled before by similar evolutionary methods developed by other researchers. In the course of this work the following tasks have been solved. First, TSS violations have been grouped into categories. Then based on these categories, fitness function including penalties for TSS violations has been proposed. Finally a set of specialized TSS-dedicated operators has been designed to increase the effectiveness of fixing TSS violations. The preliminary tests of the method have been carried out and they have confirmed the validity of the presented approach. Examples of the method's results has been provided to illustrate how it finds a satisfying solution for basic situations. Further research of the author will be concentrated on a generalization of the presented method. The envisaged future version of the method would return a set of trajectories of all ships within jurisdiction of a VTS system supervising a given TSS region.

BIBLIOGRAPHY

1. Cheng X., Liu Z.: Trajectory Optimization for Ship Navigation Safety Using Genetic Annealing Algorithm. ICNC 2007. Third International Conference on Natural Computation, 2007, vol. 4, pp. 385-392.
2. Cockroft A.N., Lameijer, J.N.F.: A Guide to Collision Avoidance Rules. Butterworth-Heinemann Ltd.,1993.
3. Coldwell T.G.: Marine Traffic Behaviour in Restricted Waters. The Journal of Navigation, 1983, 36, 431-444.
4. COLREGS: Convention on the International Regulations for Preventing Collisions at Sea. 1972.
5. Davis P.V., Dove M.J., Stockel C.T.: A Computer Simulation of multi-Ship Encounters. The Journal of Navigation, 1982, 35, 347-352.
6. Fuji J., Tanaka K.: Traffic Capacity. The Journal of Navigation,1971, 24, 543-552.
7. Goodwin E.M.: A Statistical Study of Ship Domains. The Journal of Navigation, 1975, 28, 329-341.
8. Ito M., Feifei Z., Yoshida N.: Collision avoidance control of ship with genetic algorithm. Proceedings of the 1999 IEEE International Conference on Control Applications, 1999, vol. 2, 1791 - 1796.
9. Jozwiak L., Postula, A.: Genetic engineering versus natural evolution: genetic algorithms with deterministic operators. Journal of Systems Architecture, 2002, 48, 99-112.
10. Lisowski J.: The Dynamic Game Models of Safe Navigation. International Journal on Marine Navigation and Safety of Sea Transportation, 2007, Vol. 1, No. 1.
11. Michalewicz Z., Fogel D.B.: How To Solve It: Modern Heuristics, Springer - Verlag, 2004.
12. Smierzchalski R., Michalewicz Z.: Modeling of a Ship Trajectory in Collision Situations at Sea by Evolutionary Algorithm. IEEE Transactions on Evolutionary Computation, 2000, No. 3, Vol. 4, 227-241.
13. Statheros T., Howells G., McDonald-Maier K.: Autonomous Ship Collision Avoidance Navigation Concepts, Technologies and Techniques.The Journal of Navigation, 2008, 61, 129–142.
14. Szlapczynski R.: A unified measure of collision risk derived from the concept of a ship domain. The Journal of Navigation, 2006, 59, 477-490.
15. Szlapczynski R.: Evolutionary Sets Of Safe Ship Trajectories: A New Approach To Collision Avoidance. The Journal of Navigation, 2011, 64, 169-181.
16. Tam C.K., Bucknall R.: Path-planning algorithm for ships in close-range encounters. Journal of Marine Science Technology, 2010, vol. 15, 395–407.

17. Tsou M. C., Hsueh C. K.: The study of ship collision avoidance route planning by ant colony algorithm. Journal of Marine Science and Technology, 2010, 18(5), 746–756.

18. Tsou M.-C., Kao S.-L., Su C.-M.: Decision Support from Genetic Algorithms for Ship Collision Avoidance Route Planning and Alerts. The Journal of Navigation, 2010, 63, 167-182.

19. Xue Y., Lee B.S., Han D.: Automatic collision avoidance of ships. Proceedings of the Institution of Mechanical Engineers, Part M: Journal of Engineering for the Maritime Environment, 2009, 33-46.

20. Yang L.L., Cao S.- H.. Li B.Z.: A Summary of Studies on the Automation of Ship Collision Avoidance Intelligence. Journal of Jimei University (Natural Science), 2006, vol. 2.

21. Zeng X.: Evolution of the safe path for ship navigation. Applied Artificial Intelligence, 2003, 17, 87–104.

CONTACT WITH AUTHOR

Rafał Szłapczyński, Ph. D.
Faculty of Ocean Engineering
and Ship Technology,
Gdańsk University of Technology
Narutowicza 11/12
80-233 Gdańsk, POLAND
e-mail: rafal@pg.gda.pl

Reliability and uncertainty in determining search area during Search-and Rescue action

Zbigniew Burciu, Assoc. Prof.
Gdynia Maritime University

ABSTRACT

Sea accident occurring far away from the base of rescue ships generates – for SAR action coordinator - problem of determining search areas on the basis of information which sometimes may be incomplete and uncertain, e.g. an unknown number of launched life rafts and persons in water (PIW), as well as that of sending, to the area, a non-rescue ship nearest to place of occurrence of the accident. Variety of operational states of life rafts (number of persons on raft, drift anchor etc) produces different wind leeways as a result of which search areas for the objects would be in a different distance from the last known position (LKP), e.g.:
- search areas for life rafts without drift anchor, with an unknown number of castaways on board,
-search areas for life rafts with drift anchor, with an unknown number of castaways on board, and
- search area for the PIW.
To sweep determined search areas the coordinator makes use of a ship nearest to place of danger.
In this paper has been made an attempt to determine measures which would make SAR action coordinator capable of deciding which area should be searched first by using a ship nearest to place of the action.

Keywords: life raft; uncertainty; reliability; belief; probability;
PIW (Person In Water); search; rescue; search area; SAR

AREAS DEPENDENT ON RELIABILITY OF OBJECTS AND UNCERTAINTY

Decision made in uncertainty conditions is that whose occurrence probability of consequences of a given decision is unknown. According to [8], risk is a random event of known distribution of its occurrence probability, whereas uncertainty constitutes such kind of randomness whose probability distribution is unknown.

An uncertainty condition may be a decision of unknown future consequences and probability of their occurrence or hazard - this is occurrence probability of losses resulting from a single undesirable event occurring in a given aeronautical system [6].

Along with increasing uncertainty level decisions are made often by people than machines [9]. Hence the more uncertain information the greater probability that the SAR action coordinator (team of experts) will take part in solving a decision problem.

Risk constitutes uncertainty associated with future events or results of decisions made by the coordinator. Results of decisions lead to occurrence of an unexpected loss or reaching success of performed SAR action.

Risk assessment is a process undertaken to calculate or determine risk for an organism, population, subpopulation or ecosystem, which results from its exposure to a given factor. Risk assessment takes into account identification of accompanying uncertainties, qualities of a factor as well as features of an exposed organism, population or ecosystem [7]

Knowledge of reliability characteristics of life-saving appliances, gained by SAR action coordinator [3, 4, 5], would make it possible to increase SAR action effectiveness by making decision as to sweeping the determined area first.

COORDINATOR'S DECISION BASED ON RELIABILITY OF AN ENDANGERED OBJECT

Sea accidents which still happen, make the SAR action coordinator facing the task of determination of search areas and sweeping them as fast as possible. Lack of knowledge in which operational state a given life raft is (different leeways), results in that many such areas may appear, e.g.:
- search area of a life raft without drift anchor and an unknown number of castaways,
- search area of a life raft with drift anchor and an unknown number of castaways,

Safety function – the life raft reliability R_{tr} can be expressed as follows[4, 5]:

$$R(x) = P(Z_{tr} > x) = 1 - \int_0^x f_Z(z)dz =$$

$$= 1 - \frac{\lambda_1^{\alpha_1}\lambda_2^{\alpha_2}}{3^{\alpha_1}2^{\alpha_2}B(\alpha_1,\alpha_2)}\int_0^x \frac{z^{\alpha_2-1}}{(\frac{\lambda_1}{3}+\frac{\lambda_2}{2}z)^{\alpha_1+\alpha_2}}dz \quad z>0$$

$$\text{(1)}$$

where:

$R(x)$ – life raft reliability, safety function
Z_{tr} – maximum value of life raft speed (wind leeway)
x – wind speed
y – numerically expressed life raft speed
a, b – mean values of the independent non-negative random variables A, B
A – random variable of the gamma distribution $G(\alpha_1, \lambda_1)$
B – random variable of the gamma distribution $G(\alpha_2, \lambda_2)$.

20-person life raft
Example:

Realization of a SAR action – the searching of 20-person life rafts with accounting for reliability: the life raft performance reliability determined for 48-knot wind speed (9°B), 5 h period of action and 10°C temperature of water.

Tab. 1. Safety function, reliability values for selected 20-person life rafts [4]

Type of object		Reliability R(48)
20-person life raft with drift anchor, 20 persons on board	–	0.7368
20-person life raft with drift anchor, 2 persons on board	–	0.5234
20-person life raft without drift anchor, 20 persons on board	–	0.7275
20-person life raft without drift anchor, 2 persons on board	–	0.5234
PIW (castaway in water)	–	0.4800

As results from the above presented reliability data, the 20-person life rafts with 2 persons on board are less safe (their reliability is lower) than those with 20 persons on board, excluding the PIW.

6-person life raft
Example:

Realization of a SAR action – the searching of 6-person life rafts with accounting for reliability: the life raft performance reliability determined for 52-knot wind speed (10°B), 5 h period of action and 10°C temperature of water.

Tab. 2. Safety function, reliability values for selected 6-person life rafts [4]

Type of object		Reliability R(48)
6-person life raft without drift anchor, 1 person on board	–	0.7785
6-person life raft without drift anchor, 6 persons on board	–	0.9962
6-person life raft with drift anchor, 1 person on board	–	0.7122
6-person life raft with drift anchor, 6 persons on board	–	0.9943
PIW (castaway in water)	–	0.480

As results from the above presented reliability data, the 6-person life rafts with 2 persons on board are less safe (their reliability is lower) than those with 20 persons on board, excluding the PIW.

UNCERTAIN INFERENCE IN SAR ACTION

As real situation – threat to life at sea, sea accident situation – never can be described in detail therefore information dealing with a danger at sea are usually unprecise, incomplete or uncertain. A way of inference depends on a kind of information at our disposal. Hence the following classification of inference methods was assumed [1, 2, 10]:
- methods of uncertain information processing,
- methods of incomplete information processing.

The classification is obviously conventional and working, and methods of both the groups can be used jointly. Among the methods of the first group prevails the numerical approach in which a.o. multi-value, fuzzy, probabilistic schemes, Dempster-Shafer (DS) theory called also belief function or mathematical theory of evidence, can be distinguished.

The DS theory is applied in the following cases:
- incomplete knowledge,
- belief updating,
- evidence composing.

One of the most important problems in incertainty processing is differentiation between uncertainty and lack of knowledge. The differentiation between the two things is just the aim of the DS theory in which are determined probabilities with which given hypotheses can be proved on the basis of information being at disposal. It shows one of the ways of mathematical probability application to subjective assessment [1, 2, 10], e.g. that made by SAR action coordinator.

The DS theory[1] makes it possible to prove a given hypothesis on the basis of information at disposal:
- it allows to combine different pieces of evidence of information gained by SAR action coordinator – knowledge updating,
- new subsets of hypotheses, new probability values, are formed,
- realization – knowledge updating lasts as long as new pieces of evidence i.e. information achieved by SAR action coordinator are acquired.

$$Bel(A) \leq P(A) \leq Pl(A)$$

The association of two values: the belief $Bel(A)$ and the likelihood $Pl(A)$, forms the upper and lower limit of belief and likelihood of the hypothesis A.

As time is running the obtained new pieces of evidence, i.e. information achieved by SAR action coordinator, make the interval between the upper and lower limit, $Bel(A)$ and $Pl(A)$ narrower and narrower, causing uncertainty of information smaller.

The measure m is constrained by the conditions:

$$m(\varnothing) = 0$$

$$\sum_{A \subseteq \Theta} m(A) = 1$$

The function m is called the basic assignment of probability (differentiating frame) for the set of all hypotheses, Θ.

---

[1] Dempster-Shafer theory is widely described in literature and internet sources.

The belief function is:

$$Bel(A) = \sum_{B \subseteq A} m(B)$$

for every $A \subseteq \Theta$.

The likelihood function is:

$$Pl(A) = \sum_{B \cap A \neq \varnothing} m(B)$$

for every $A \subseteq \Theta$.

The synthesis of knowledge, i.e. the combining of knowledge achieved from various sources, can be expressed as follows:

$$m(A) = \frac{\sum_{A_i \cap B_j = A} m_1(A_i) m_2(B_j)}{1 - \sum_{A_i \cap B_j = \varnothing} m_1(A_i) m_2(B_j)}$$

Application of DS theory which makes it possible to combine (integrate) information achieved from different sources and concerning identification of hazard to life at sea, constitutes an element of SAR action planning and managing.

Search areas loaded with uncertain information

SAR action planning by its coordinator will met initially a lack of sufficient information which may be imprecise, incomplete or uncertain.

The basic question for the coordinator is: who is searched and whether a castaway (- s) are in water or placed on life saving appliances and which ones. The DS theory application makes it possible e.g. to determine priorities of sweeping sequence of the determined search areas.

The example scenarios of the DS theory application, which make it possible to account for information flowing to SAR action coordinator, i.e. pieces of evidence of information reaching him and updating his knowledge (computer aided), are as follows:
- Information on reception a SOS signal.

- Additional information on:
  · an object calling for help,
  · life saving appliances (rules, knowledge, practice, coordinator's experience).

Differentiating frame, result
1. kind of object facing danger at sea:
   a. merchant ship,
   b. fishing ship,
   c. yacht – sporting boat,
   d. ferry.

The largest probability value was obtained for merchant ship: $P_{(SH)} = 0.9760$ [4]

Differentiating frame, result
2. Sea accident (of merchant ship), castaways and life rafts in water:
   a. 6-person life raft,
   b. 10-person life raft,
   c. 20-person life raft,
   d. the PIW.

The largest probability value was obtained for 20-person life raft: $P_{(tr\ 20)} = 0.4240$, and, $P_{(PIW)} = 0.4240$.

Differentiating frame, result
3. Castaways and 20-person life rafts in water:
   a. 20-person life raft with drift anchor – 20 persons on board,
   b. 20-person life raft with drift anchor – 2 persons on board,
   c. 20-person life raft without drift anchor – 20 persons on board,
   d. 20-person life raft without drift anchor – 2 persons on board,
   e. a castaway in water, PIW.
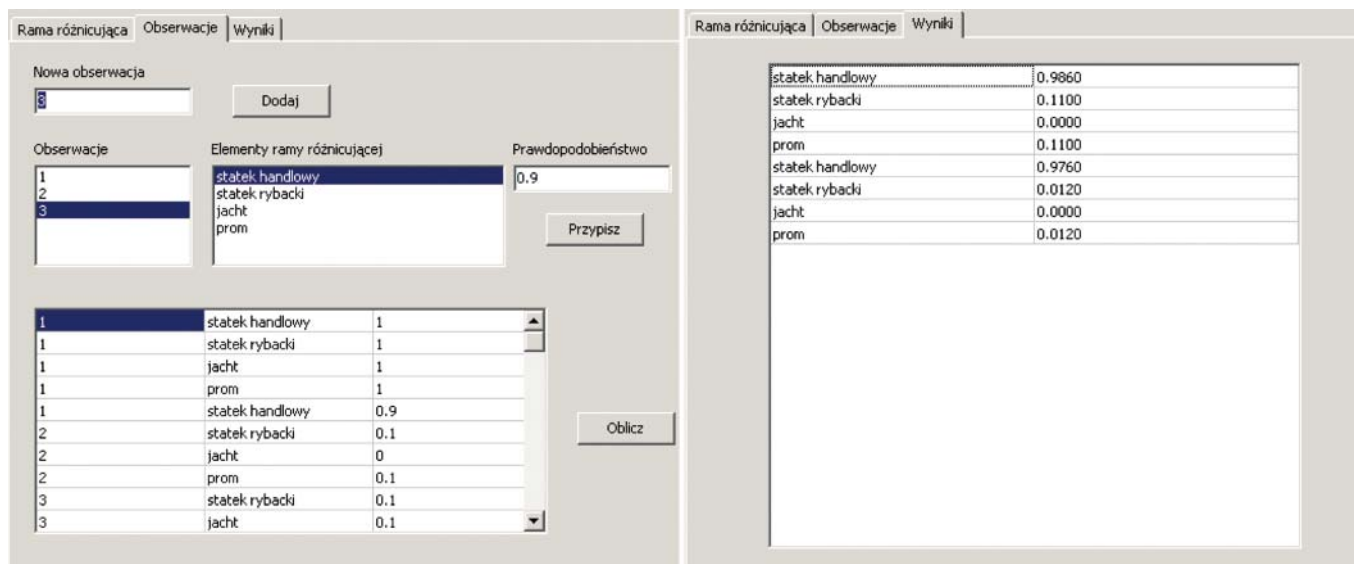
Translation:
Rama różnicująca - Differentiating frame, **Obserwacje** - Observations, **Wyniki** - Results;
Nowa obserwacja - New observation, **Dodaj** - Introduce;
Obserwacje - Observations, **Elementy ramy różnicującej** - Elements of differentiating frame, **Prawdopodobieństwo** - Probability;
Przypisz - Attribute;
statek handlowy - merchant ship, **statek rybacki** - fishing ship, **jacht** - yacht, **prom** - ferry;
Oblicz - Calculate

Fig. 1. Differentiating frame for a kind of object facing danger at sea

Translation:
Rama różnicująca - Differentiating frame, **Obserwacje** - Observations, **Wyniki** - Results;
Nowa obserwacja - New observation, **Dodaj** - Introduce;
Obserwacje - Observations, **Elementy ramy różnicującej** - Elements of differentiating frame, **Prawdopodobieństwo** - Probability;
Przypisz - Attribute;
tratwa ratunkowa 6 os. - 6-person life raft, **tratwa ratunkowa 10 os.** - 10-person life raft, **tratwa ratunkowa 20 os.** - 20-personlife raft, **PIW** - the PIW (person in water);
Oblicz - Calculate

Fig. 2. Differentiating frame for a sea accident – castaways and life rafts in water [4]

Translation:
Rama różnicująca - Differentiating frame, **Obserwacje** - Observations, **Wyniki** - Results;
Nowa obserwacja - New observation, **Dodaj** - Introduce;
Obserwacje - Observations, **Elementy ramy różnicującej** - Elements of differentiating frame, **Prawdopodobieństwo** - Probability;
Przypisz - Attribute;
tr. 20 os. z/d 20 os. - 20-person life raft with drift anchor - 20 persons on board, **tr. 20 os. z/d 2 os.** - 20-person life raft with drift anchor - 2 persons on board, **tr. 20 os. b/d 20 os.** - 20-person life raft without drift anchor - 20 persons on board, **tr. 20 os. b/d 2 os.** - 20-person life raft without drift anchor - 2 persons on board, **PIW** - the PIW (person in water);
Oblicz - Calculate

Fig. 3. Differentiating frame for 20-person life raft and castaways in water [4]

Tab. 3. The calculated values of the probability m for the example situation: 20-person life raft and a castaway in water

Kind of object		Probability [m]
20-person life raft with drift anchor – 20 persons on board	–	0.2730
20-person life raft with drift anchor – 2 persons on board	–	0.2420
20-person life raft without drift anchor – 20 persons on board	–	0.1820
20-person life raft without drift anchor – 2 persons on board	–	0.0303
PIW – a castaway in water	–	0.2730

Translation:

Rama różnicująca - Differentiating frame, **Obserwacje** - Observations, **Wyniki** - Results;
Nowa obserwacja - New observation, **Dodaj** - Introduce;
Obserwacje - Observations, **Elementy ramy różnicującej** - Elements of differentiating frame, **Prawdopodobieństwo** - Probability;
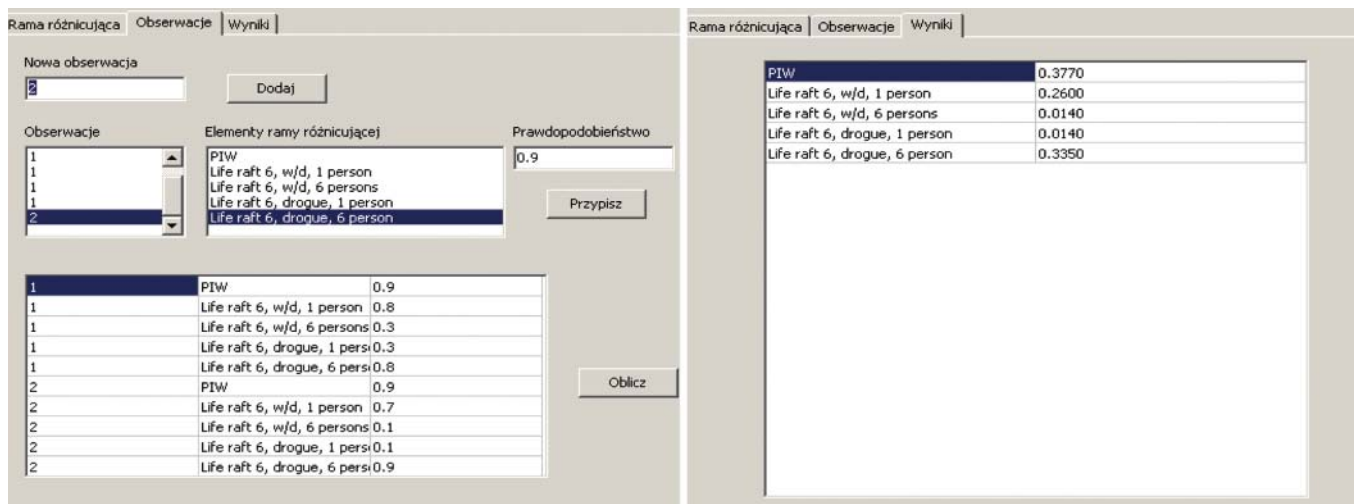**Przypisz** - Attribute;
Oblicz - Calculate

***Fig. 4.** Differentiating frame for 6-person life raft [4]*

***Tab. 4.** The calculated values of the probability m for the example of 6-person life raft and a castaway in water (PIW)*

Kind of object		Probability [m]
6-person life raft without drift anchor – 1 person	–	0.260
6-person life raft without drift anchor – 6 persons	–	0.014
6-person life raft with drift anchor – 1 person	–	0.014
6-person life raft with drift anchor – 6 persons	–	0.335
PIW – a castaway in water	–	0.377

The obtained results show importance and sweeping sequence of the search areas. The areas were determined by using the author's method for the following data: a castaway in water (PIW) and 20-person life raft.

For the SAR action coordinator it may serve as an indication as to sequence in which a given search area should be swept. The sweeping should start from the PIW's area (P = 0.273), next should be swept the areas of the life rafts with drift anchor, both fully (100%) manned (P = 0.273) and with 2 persons on board (P = 0.242), and then the areas of the life rafts without drift anchor, both with 2 persons on board (P = 0.182) and fully manned (P = 0.0303).

Example:

6-person life raft; the PIW;
52 kn wind speed; 5 h search period.

The presented method is one of many which make SAR action coordinator capable of deciding which search area should be swept in the first place.

As during SAR action an uncertainty of information and unreliability of life saving appliances take place a measure has been proposed to account for the parameters. The measure of uncertainty and unreliability of a searched object, M_{nz}, is as follows [4]:

$$M_{nz} = m \cdot (1 - R_o)$$

where:
M_{nz} – measure of uncertainty and unreliability,
m_{tr} – life raft uncertainty measure,
R_o – object reliability (of life raft or PIW)
$1 - R_o$ – object unreliability.

In Tab. 5 is presented the decision matrix for 20-person life raft and PIW, which makes it possible to make decision as to choice of area sweeping sequence, depending on R, m, $R \cdot m$, $M_{nz} = m \cdot (1 - R_o)$, and in Tab. 6 – the same for 6-person life raft and PIW.

***Tab. 5.** The decision matrix for 20-person life raft and PIW [3, 4]*

For: - 48 kn wind speed (10°B), - 5 h period of action, - 10°C temperature of water			Reliability R	1 - R	Uncertainty [m]	R · m	(1-R) · m	Decision - making sequence on sweeping search area depending on parameters			
								R	m	R · m	$M_{nz} = (1-R_o) \cdot m$
Person in water (PIW)			0.4800	0.520	0.2730	0.131	**0.142**	1	1	1	**1**
20-person life raft	with drift anchor	10%	0.5234	0.4766	0.2420	0.127	**0.115**	2	3	3	**2**
		100%	0.7275	0.2725	0.2730	0.199	**0.074**	4	2	2	**4**
	without drift anchor	10%	0.5234	0.4766	0.1820	0.095	**0.087**	2	4	4	**3**
		100%	0.7368	0.2632	0.0303	0.022	**0.008**	3	5	5	**5**

Tab. 6. *The decision matrix for 6-person life raft and PIW [3, 4]*

For: - 52 kn wind speed (10°B), - 5 h period of action, - 10°C temperature of water			Reliability R	1 - R	Uncertainty [m]	R · m	(1-R) · m	Decision - making sequence on sweeping search area depending on parameters			
								R	m	R · m	$M_{nz} = (1-R_o) \cdot m$
Person in water (PIW)			0.4800	0.520	0.377	0.181	**0.196**	1	1	1	**1**
6-person life raft	with drift anchor	10%	0.7122	0.288	0.014	0.01	**0.011**	2	4	5	**3**
		100%	0.9943	0.006	0.335	0.333	**0.002**	3	2	1	**4**
	without drift anchor	10%	0.7785	0.221	0.260	0.202	**0.057**	2	3	2	**2**
		100%	0.9962	0.004	0.014	0.014	**0.00006**	4	4	4	**5**

Fig. 5. *The determined search areas for 20-person life raft both with drift anchor and without it as well as for a castaway in water[2], with assigned numbers of sweeping sequence and values of the occurrence probability m [4]*

Fig. 6. The determined search areas for 6-person life raft both with drift anchor and without it as well as for a castaway in water[3], with assigned numbers of sweeping sequence and values of the occurrence probability m [4]

Tab. 7. The decision matrix for 6-person life raft and PIW [3, 4]

For: - 52 kn wind speed (10°B), - 5 h period of action, - 10°C temperature of water			Decision - making sequence on sweeping search area depending on parameters			
			R	m	R · m	$M_{nz} = (1-R_o) \cdot m$
Person in water (PIW)			**1**	1	1	**1**
6-person life raft	with drift anchor	10%	**2**	4	5	**3**
		100%	**3**	2	1	**4**
	without drift anchor	10%	**2**	3	2	**2**
		100%	**4**	4	4	**5**

Tab. 8. *The decision matrix for 20-person life raft and PIW, where wind speed was accounted for. Sweeping sequence of the determined search areas*

For: - 48 kn wind speed (10°B), - 5 h period of action, - 10°C temperature of water			Decision - making sequence on sweeping search area depending on parameters			
			R	m	R · m	$M_{nz} = (1-R_o) \cdot m$
Person in water (PIW)			1	1	1	1
6-person life raft	with drift anchor	10%	2	3	3	2
		100%	4	2	2	4
	without drift anchor	10%	2	4	4	3
		100%	3	5	5	5

Fig. 7. *The search areas determined for 6-person life raft both with drift anchor and without it as well as for a castaway in water[4]. Sweeping sequence of the determined areas depending on R, M_{nz}*

[4]   The Search and Rescue Computer Aided Sysytem SARCAS 2000 for supporting life saving action at sea, Research project No. 2288/C.T12-9/98 sponsored by KBN (State Committee for Scientific Research). Project manager: Z. Burciu.

Model input parameters

No. of wind's parameters changes: 5

No. of wind's parameters changes - on scene: 5

Object 1
Life raft type: 20-Person without drogue — Loading: 10 %

Object 2
Life raft type: 20-Person without drogue — Loading: 100 %

Object 3
Life raft type: 20-Person with drogue — Loading: 10 %

Object 4
Life raft type: 20-Person with drogue — Loading: 100 %

☑ Deterministic model
☑ Random model
☑ Monte Carlo — Distribution: normal
☐ Show counting results

Input data - time to approach

	T1	T2	T3	T4	T5
T [h]	0,5	0,5	0,5	0,5	0,5
Kw [°]	045	045	090	090	125
WDE [°]	0	0	0	0	0
Vw [kn]	48	48	48	48	
WSE[kn]	0	0	0	0	0

Input data - on - scene

	T1	T2	T3	T4	T5
T [h]	0,5	0,5	0,5	0,5	0,5
Kw [°]	125	145	145	160	160
WDE [°]	0	0	0	0	0
Vw [kn]	48	48	48	48	
WSE [kn]	0	0	0	0	0

Disaster position:
Lat. = 55.00,0 [°]
Long. = 016.00,0 [°]

Set

Start

PIW
**1 R
1 Mnz**

20-person life raft with drift anchor, 20 persons
**4 R
4 Mnz**

20-person life raft with drift anchor, 2 person
**2 R
2 Mnz**

20-person life raft without drift anchor, 20 persons
**3 R
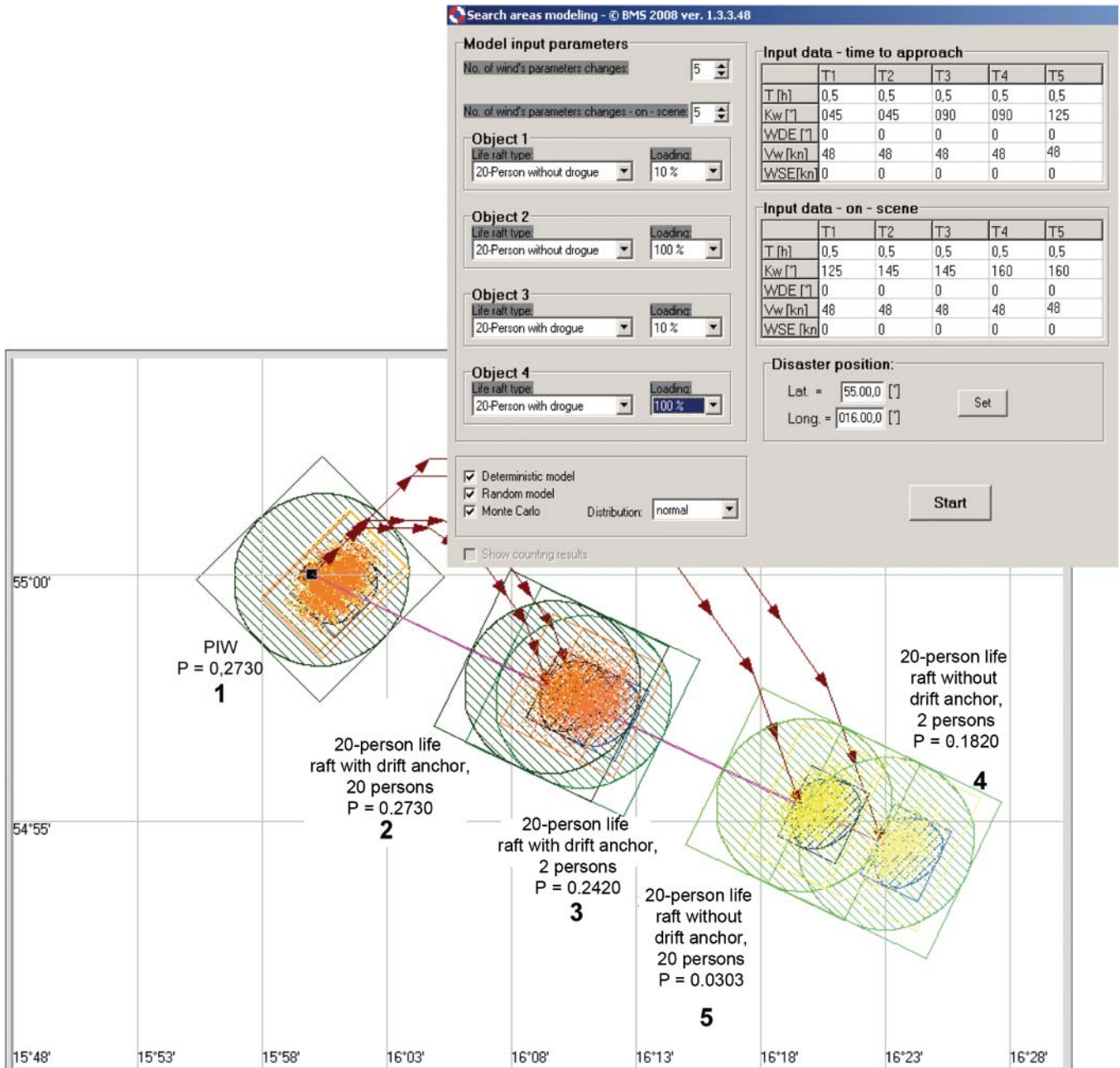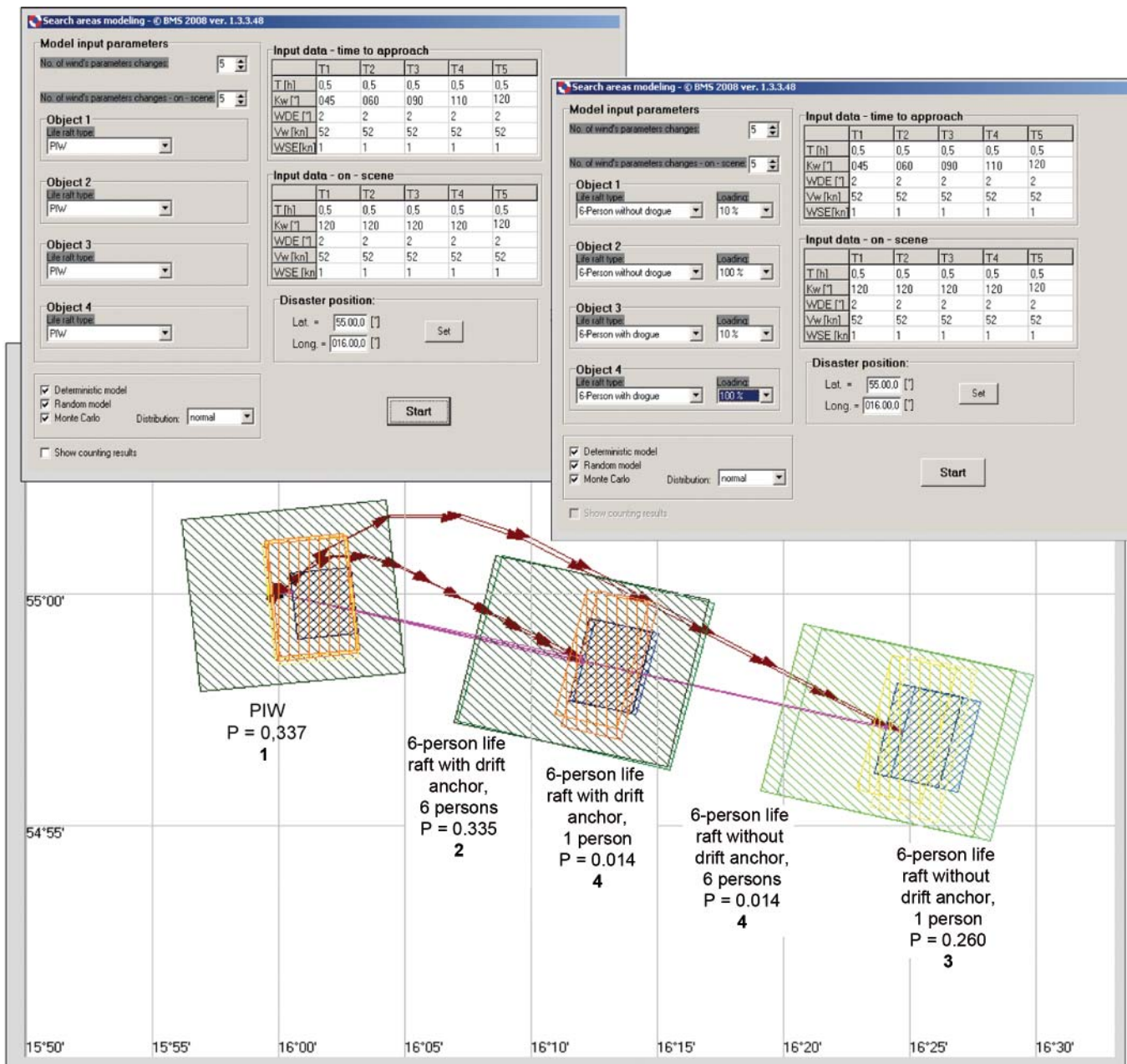5 Mnz**

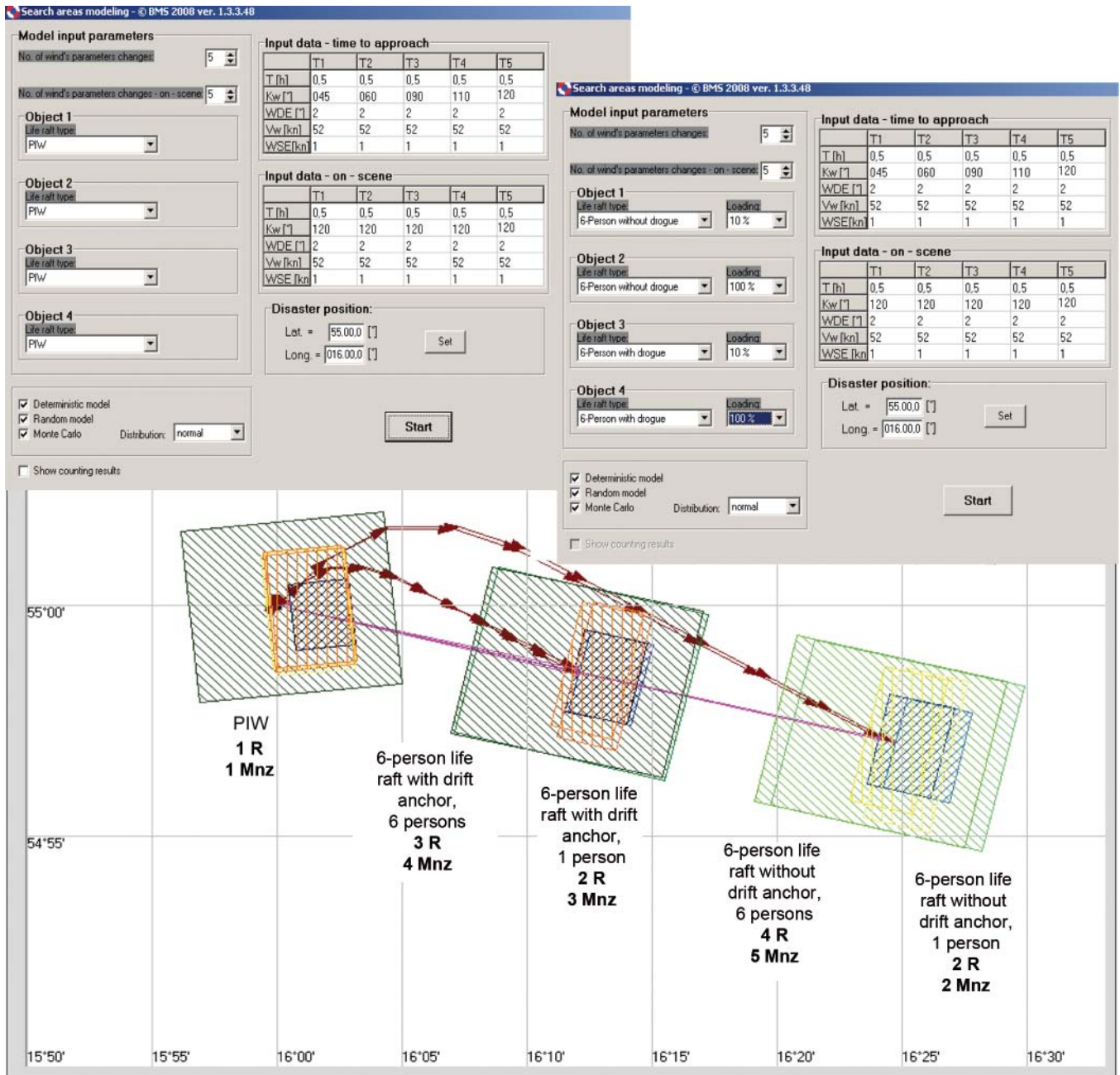20-person life raft without drift anchor, 2 person
**2 R
3 Mnz**

Fig. 8. The search areas determined for 20-person life raft both with drift anchor and without it as well as for a castaway in water[5]. Sweeping sequence of the determined areas depending on R, M_{nz}

R(tr)
m(tr)

m (tr)

The area of decision based on reliability
R(tr)

The area of coordinator's decision based on uncertainty
m(tr)

The area of coordinator's decision based on reliability and uncertainty
$[1-R(tr)] \cdot m(tr)$

R(tr)

44 - 48 kts.
(9°B - 10°B)

Wind speed [knots]

Time
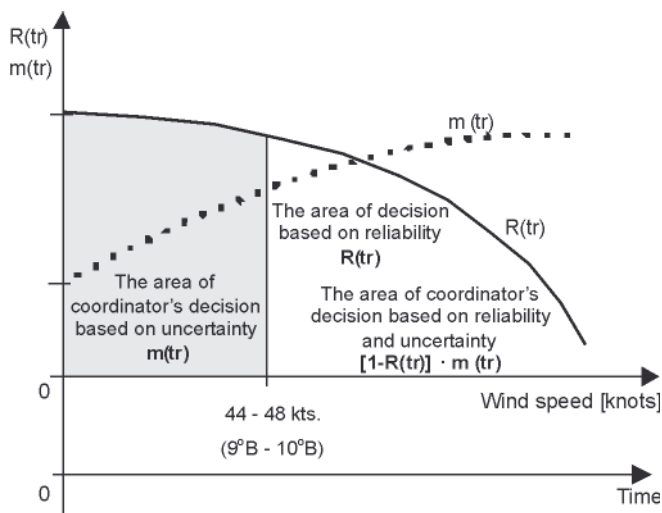
Fig. 9. Areas of decision – making based on uncertain information and reliability of life raft [4]

m (tr)

R(tr)

Reliability
R

Uncertainty
m

44 - 48 kts.
(9°B - 10°B)

Wind speed [knots]
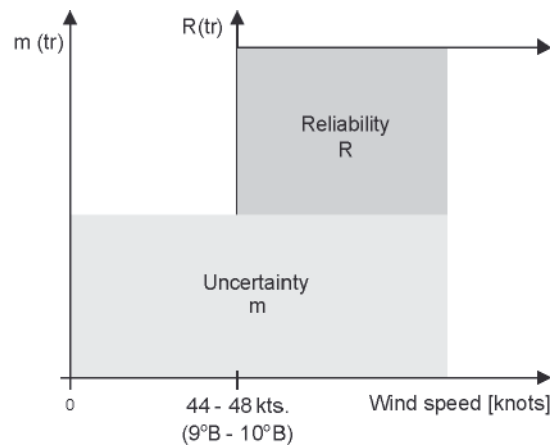
Fig. 10. Areas of uncertainty and reliability measures for the presented example [4]

---

[5] The Search and Rescue Computer Aided Sysytem SARCAS 2000 for supporting life saving action at sea, Research project No. 2288/C.T12-9/98 sponsored by KBN (State Committee for Scientific Research). Project manager: Z. Burciu.
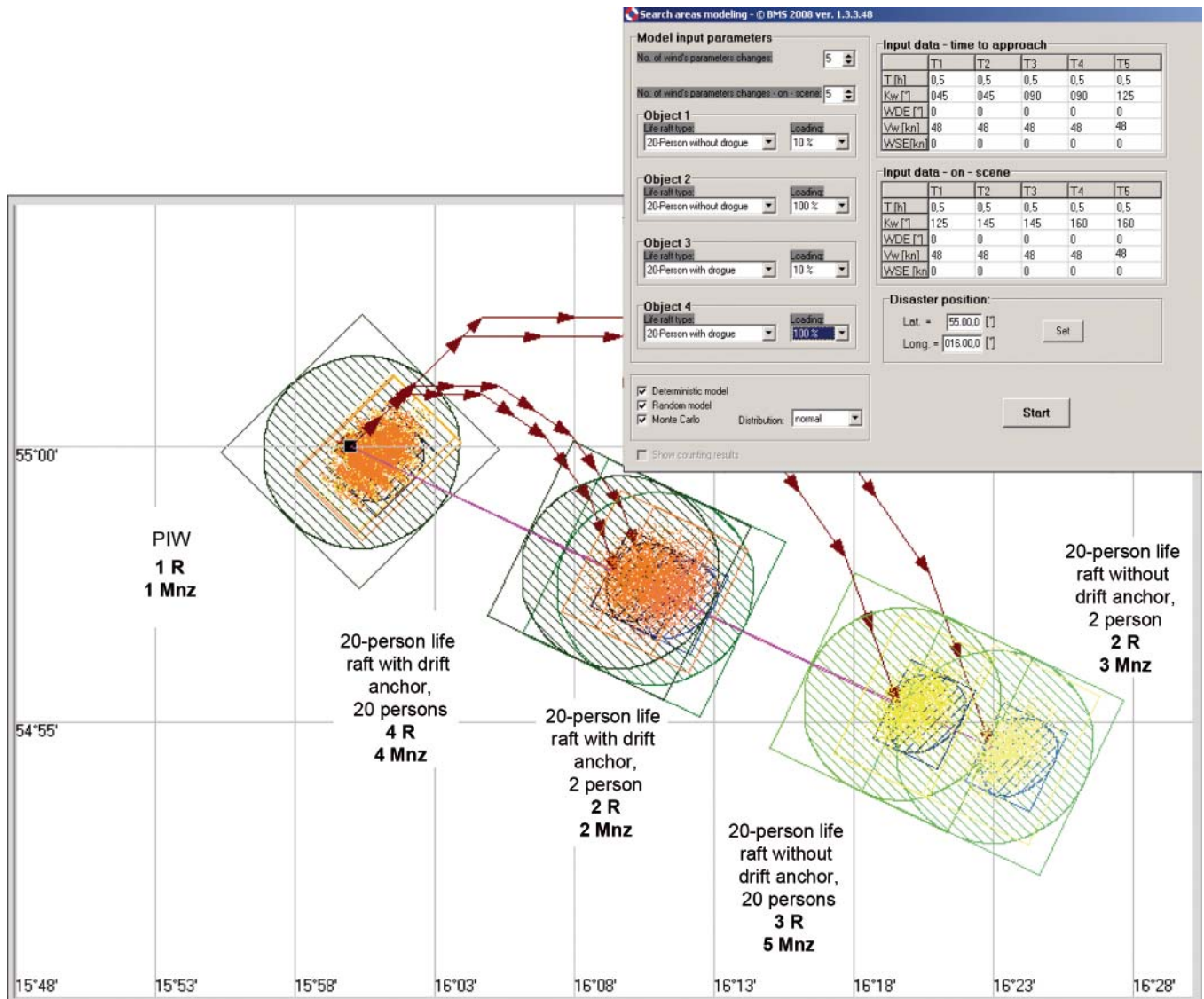
The areas of decision - making by SAR action coordinator:
- in the case of wind speed lower than 48 knots the information uncertainty m_{tr} should serve as the decison measure.
- in the case of SAR action planning at the wind speed greater than 48 knots the coordinator should take into account both the reliability of life saving appliances and the measure of uncertainty and unreliability, $M_{nz} = m \cdot (1 - R_o)$.

The reliability of person in water, $S_p(t)$, depends on time and water temperature [3, 4].

CONCLUSIONS

Both the above presented solution in which the reliability model – functions of searched object, was used, and that of Dempster and Shafer, make the coordinator capable of taking decision on sweeping first a search area in which an object of a low reliability is located (safety function) and when it is simultaneously quite sure that it is placed just in the area.

BIBLIOGRAPHY

1. Biernacki M., Tarnowski A., Truszczyński O.: *Risk in aeronautical operations and a method of its optimization* (in Polish). [in:] *Psychology of hazardous behaviour. Concepts, research, practice* (in Polish) by Goszczyńska M., Studenski R. (Ed.), Wydawnictwo Akademickie „Żak" („Żak" academic publishing house),Warsaw, 2006.
2. Bolc L., Brodziewicz W., Wójcik M.: *Fundamentals of processing uncertain and incomplete information* (in Polish), PWN (State scientific publishing house), Warsaw, 1991.
3. Burciu Z.: *Bayesian methods in reliability of search and rescue action*. Polish Maritime Research, No. 4(67), Vol 17, Gdańsk, 2010
4. Burciu Z., *Safety in shipping by sea - Search and Rescue (SAR)*. A monograph (to be published)
5. Burciu Z., Grabski F.: *The experimental and theoretical study on the reliability of life rafts.* Submitted for publication in Reliability Engineering & System Safety, Elsevier
6. Makarowski R.: *Risk limits. Psychological paradigm* (in Polish). Oficyna Wydawnicza „Impuls" („Impuls" Publishing House). Cracow, 2006
7. Seńczuk W.: *Contemporary toxicology* (in Polish). PZWL (Medical publishing house), Warsaw, 2005
8. Sikora W.: *Operational research* (in Polish). Polskie Wydawnictwo Ekonomiczne. (Polish economic publishing house) Warsaw, 2008
9. Syska E.: *Cash-Flow sources from using informatic systems* (in Polish). Gazeta IT, e-czasopisma (e-publications) 22.05.2003
10. Tołwiński M.: *Inferencing in uncertainty conditions. Dempster-Shafer theory.* (in Polish). Electronic script: aragorn. pb.bialystok.pl/~radev/ai/sosn/tolwinski.doc 25.03.2010.

CONTACT WITH THE AUTHOR

Zbigniew Burciu, Assoc. Prof.
Faculty of Navigation,
Gdynia Maritime University
Aleja Jana Pawła II 3
81-345 Gdynia, POLAND
e-mail: zbj@am.gdynia.pl

Numerical model to study the valve overlap period in the Wärtsilä 6L 46 four-stroke marine engine

Lamas, M. I., Assoc. Prof.
Rodríguez, C. G., M. Sc.
Rebollido, J. M., Assoc. Prof.
Escola Universitaria Politécnica. Universidade da Coruña, Spain.

ABSTRACT

In this paper, a CFD (Computational Fluid Dynamics) analysis was carried out to study the Wärtsilä 6L 46 medium-speed, four-stroke marine engine. For the purpose, the commercial software ANSYS Fluent 6.3 was employed. The aim is to analyze the scavenging of gases, especially during the valve overlap period. Particularly, the pressure, velocity and mass fraction fields were numerically obtained. In order to validate the CFD results, the in-cylinder pressure was successfully compared to experimental measurements for the exhaust, intake and compression strokes of the cylinder operation.

This model can be used in future works to improve the performance of these engines because the information provided is very useful to identify regions in which the pressure, velocity or distribution of gases are inadequate. Besides, to compute the quantity of burnt gases which remain inside the cylinder, fresh charge which is expelled through the exhaust valves and study the influence of parameters such as the exhaust and intake pressures, engine speed, cam profile design, etc.

Keywords: Four-stroke engine; computational fluid dynamics (CFD); marine engine

INTRODUCTION

The compression ignited internal combustion engine (also known as diesel engine) has two main designs, the four-stroke cycle, and the two-stroke cycle. Both are very common in marine applications because of their high efficiency compared with other types of heat engines and the possibility of employing heavy fuel oil, which is a low cost fuel [1]. Merchant ships such as tankers, chemical tankers, bulkcarriers, OBO, container ships, etc, in the power range between 5000 and 15000 kW have recently experienced a change in their tendency. Traditionally, these ships were propelled by two-stroke engines, but nowadays medium-speed (400-600 rpm), four-stroke engines are highly employed in this power range. Fuel consumption have become similar in two and four-stroke engines, and the lower weight, size and cost of four-stroke engines make them very competitive in the market, although the disadvantage of requiring a gear reducer.

In the field of four-stroke marine engines, the Wärtsilä 6L 46 has become very popular on new cruise vessels, bulk carriers, cargo vessels, ferries, fishing boats, tankers, etc since it was launched onto the market in 1988. As the Wärtsilä 6L 46 is a non-reversing engine, in marine applications it is used as auxiliary engine (electric generator) or as main engine connected to a controllable pitch propeller. Some examples of recent applications are the large Spain tuna fish vessels "Albatun 2" and "Panamá Tuna". Other example is the chemical tanker "Stend Idun" and the cruise vessel "Oasis of the Seas", equipped with six Wärtsilä 46 engines. Due to its high popularity, the Wärtsilä 6L 46 marine engine was chosen to carry out the present work.

For years, the study of the fluid flow inside engines has been mainly supported by experimental tests such as PIV (Particle Image Velocity), LDA (Laser Doppler Anemometry), ICCD cameras, etc. However, in the field of medium and large marine engines, experimental tests are very laborious, expensive, and restricted to a small portion of the whole cylinder, and down-scale models are sometimes not accurate enough. As an alternative solution to experimental techniques, CFD (Computational Fluid Dynamics) has recently become a useful tool to study the fluid flow inside engines. CFD is a branch of fluid mechanics that uses numerical methods and algorithms to analyze problems that involve fluid flows, even complex simulations such as compressible or turbulent flows. Computers are used to perform the calculations by dividing the domain of interest in a large number of sub-domains called mesh or grid. In recent years, CFD has been significantly improved, especially thanks to the performance of computing, allowing more accurate and fast simulations. In the field of engines, CFD is especially useful to design complex components such as combustion chambers, manifolds, injectors or other parameters. Although CFD was integrated in 1960s on the aerospace industry, the first simulations of engines appeared in 1980s. In the last few years, examples of numerical works about

four-stroke engines are those of [2-8], however, they were not applied to medium or large marine engines. Examples of large engines are those of Lamas and Rodríguez [9] and Nakagaya [10], both of them two-stroke type. So far, the field of medium and large four-stroke marine engines has not been investigated extensively enough employing CFD codes. Accordingly, the present paper presents a CFD study of the Wärtsilä 6L 46 four-stroke marine engine. It is the aim of this paper to present results of the flow characteristics inside the cylinder, especially during the valve overlap period, which has a crucial influence on the performance of the engine.

DESCRIPTION OF THE ENGINE

Geometry and specifications

A cross section of the Wärtsilä 6L 46 is shown in Fig. 1 and the main technical characteristics are summarized in Table 1. This engine has six cylinders in line, and every cylinder has two inlet and two exhaust valves. The valve follower is of the roller tappet type, where the roller profile is slightly convex for good load distribution. The valve mechanism includes rocker arms working on yokes guided by pins. The Wärtsilä 46 is provided with Spex (Single pipe exhaust) system and with high efficiency turbocharger.
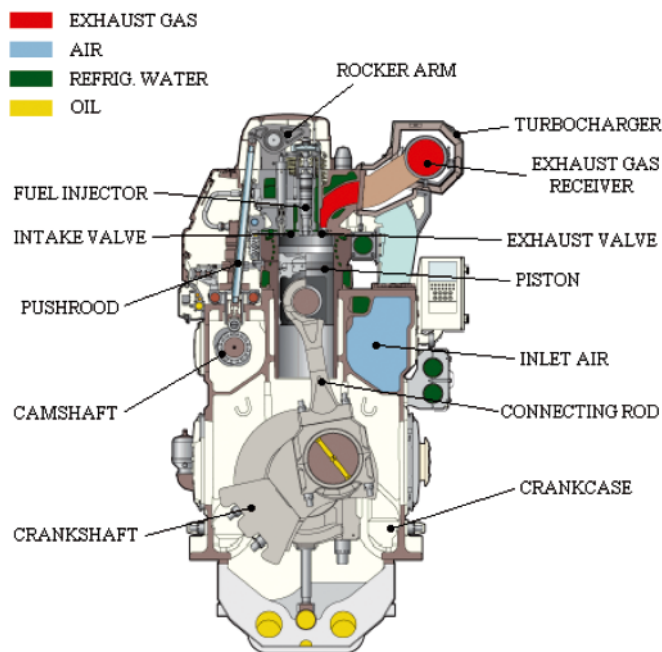

Fig. 1. Cross section. Adapted from Wärtsilä [11]

Tab. 1. Engine specifications at maximum continuous rating

Parameter	Value
Output [kW]	5430
Mean effective pressure [bar]	22.5
Speed [rpm]	500
Cylinder displacement volume [cm³/cyl]	96400
Bore [mm]	460
Stroke [mm]	580
Connecting rod length [mm]	1381
Number of cylinders	6
Number of valves per cylinder	2 inlet valves 2 exhaust valves

Engine operation

Before proceeding with the calculations, the cycle of operation and the valve overlap period will be explained. The principle of operation of a four-stroke engine is as follows. Air is induced into the cylinder by an intake stroke of the piston from TDC (top dead center) to BDC (bottom dead center), thereby increasing the cylinder volume, Fig. 2a. Thus, as the piston moves from TDC to BDC (note that the arrows indicate the direction of the piston), the cylinder is filled with air. After reaching BDC, the piston rises and the intake valves are closed, Fig. 2b. In this compression stroke, the pressure and temperature increases noticeably. A few instants before the piston reaches TDC, the fuel is injected and combustion takes place. After that, the piston descends on the power stroke, Fig. 2c, pushed by the very high pressures caused by the combustion. This pushing force on the piston gives a torque on the crank. After reaching BDC, the products of combustion are expelled through the exhaust valves, Fig. 2d. Finally the piston reaches TDC and the cycle starts again.
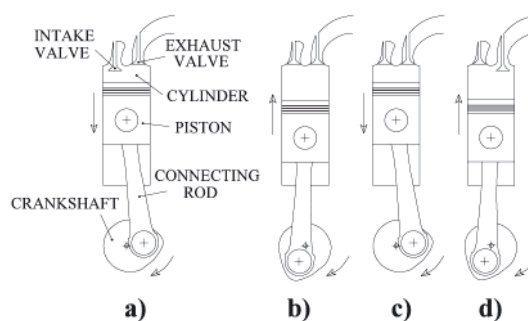

Fig. 2. Engine operation: a) Intake stroke, b) compression stroke, c) power stroke, d) exhaust stroke

Particularly, the valve timing events for the Wärtsilä 6L 46 are shown in Fig. 3. As can be seen, the exhaust valves open 53º before BDC and close 44º after TDC. On the other hand, the intake valves open 50º before TDC and close 26º after BDC.
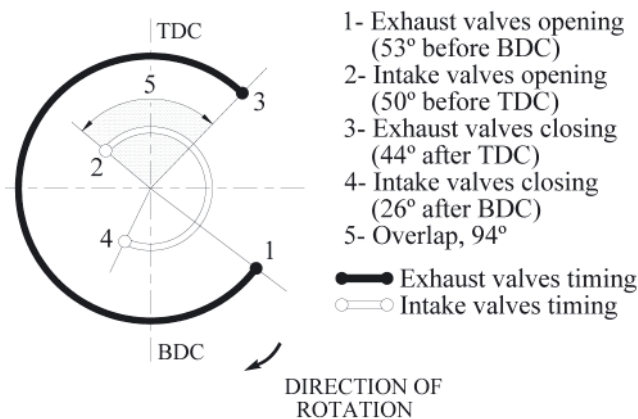
Fig. 3. Valve timing events

As can be seen in Fig. 3, there is a period of 94º between the exhaust and intake strokes when the intake valves are opening and the exhaust valves are closing, i.e., all valves are opened simultaneously. This is called the valve overlap period, and is very important in large four-stroke diesel engines with high turbocharging because the expelling of the burnt gases by the fresh air is more efficient. The overlap period is also useful to refrigerate (the entering air at low temperature refrigerates the walls of the combustion chamber, piston head and exhaust

valves. Besides, this air mixes with the burnt gases, which are directed to the turbocharger turbine. If these gases were too hot, the turbine blades would be damaged).

For these reasons, the overlap period is very necessary. Unfortunately, the potential for mechanical or gas flow mayhem during the overlap period is obvious. If the cylinder and exhaust pressures are too high, large quantities of exhaust gas can be shuttled into the intake tract. This gas is hot, maybe 1000ºC, and can cause fuel residues on the back of the intake valves. Besides, if exhaust gas occupies the inlet conduct, only a fraction mass of air can be induced into the cylinder. If the air is not enough, the combustion is incomplete and the consequence is that an excess of unburned hydrocarbon emissions are expelled to the atmosphere. Hence, the design process of the engine during the valve overlap period is a very critical issue. In this regard, CFD is a very useful tool.

Experimental results

Experimental measurements were carried out by means of several pressure and temperature sensors situated at different parts of a Wärtsilä 6L 46. These measurements were carried out at 96% load and 499.6 rpm. For these conditions, the indicated power was 7153 kW and the consumption was 172 g/kWh (note that this low value of consumption is comparable to a two-stroke engine). The engine performance analyzer MALIN 6000 (Malin Instruments, Ltd.) was employed to obtain the Fig. 4, which represents the in-cylinder gauge pressure versus the position of the piston.
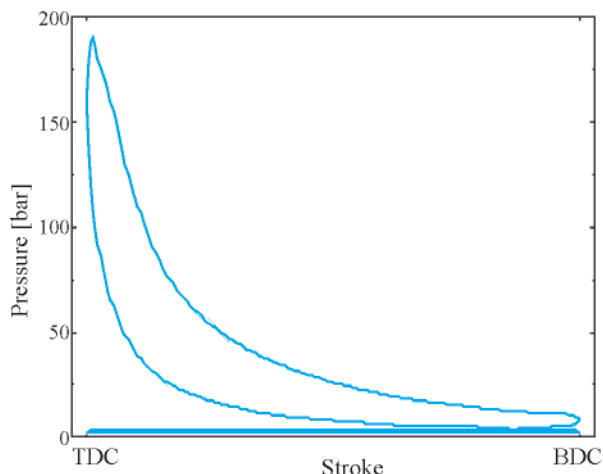

Fig. 4. In-cylinder pressure experimentally measured
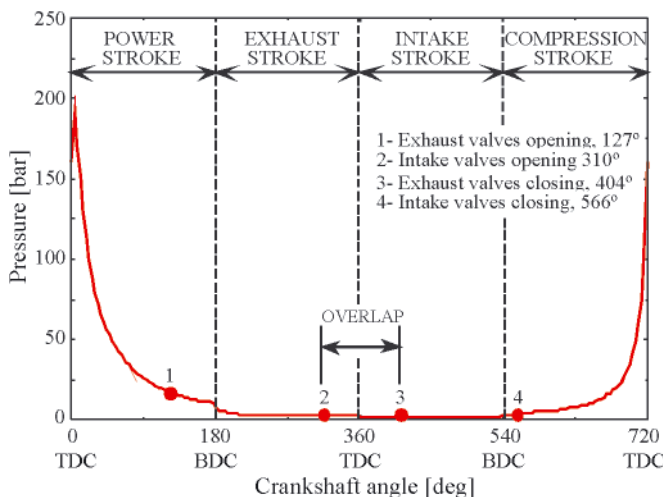

Fig. 5. In-cylinder pressure experimentally measured, opened diagram

In the present paper, the crank angles will be given with reference to the top dead center at the beginning of the power stroke. From this point, the different instants will be referred as this reference position. Accordingly, the opened pressure-crankshaft diagram is shown in Fig. 5. In this reference system, the exhaust valves open at 127º and close at 404º and the intake valves open at 310º and close at 566º. The valve overlap period takes place between 310º and 404º.

Other representative values obtained from the experimental measurements are shown in Table 2.

Tab. 2. Engine test summary.

Parameter	Value
Load [%]	96
Speed [rpm]	499.6
Indicated power [kW]	7154
Maximum pressure [bar]	192
Indicated mean effective pressure [bar]	29.7
Boost pressure [bar]	2.8
Ambient temperature [ºC]	25
Intake temperature [ºC]	55
Exhaust temperature, before turbocharger [ºC]	451
Exhaust temperature, after turbocharger [ºC]	350
Exhaust temperature, cylinder [ºC]	371

MUMERICAL PROCEDURE

Simplifications

As the measurements of all cylinders were practically identical, only one of them was studied. The exhaust, intake and compression strokes were simulated. The combustion stroke is out of range of the present work due to its mathematical complexity. In order to simplify the model, only two components were simulated, air and burnt gases. All actual components could be computed but, since no combustion was simulated, there would not be much difference on the results.

Governing equations

The governing equations of the turbulent flow inside the cylinder are the RANS (Reynolds-Averaged Navier-Stokes) equations. The energy equation is also needed to compute the thermal problem. Finally, as there are two components (air and burnt gases), one more equation must be added to characterize the mass fraction field. These equations are briefly described in what follows.

In Cartesian tensor form, the continuity equation is given by:

$$\frac{\partial \rho}{\partial t} + \frac{\partial}{\partial x_i}(\rho u_i) = 0 \qquad (1)$$

where:
u – Reynolds average velocity
ρ – the density.

The flow was considered an ideal gas, so the density is given by the equation of state of ideal gasses:

$$\rho = \frac{p}{RT} \qquad (2)$$

The momentum conservation equation can be expressed as:

$$\frac{\partial}{\partial t}(\rho\, u_i) + \frac{\partial}{\partial x_j}(\rho\, u_i u_j) =$$

$$= -\frac{\partial p}{\partial x_i} + \frac{\partial \tau_{ij}}{\partial x_j} + \frac{\partial}{\partial x_j}(-\rho\,\overline{u_i' u_j'}) \qquad (3)$$

Equations (1) and (3) are called Reynolds-Averaged Navier-Stokes (RANS) equations. They have the same general form as the instantaneous Navier-Stokes equations, with the velocities and other solution variables representing time-averaged values. In Eq. (3), u denotes the mean velocities, u' are the turbulence fluctuations about the ensemble average velocity, τ_{ij} is the stress tensor and the term $-\rho\,\overline{u_i' u_j'}$ represents the Reynolds stresses (the over bar denotes the averaging process). In this case, the Reynolds stresses were computed using the Boussinesq hypothesis and the k- ε model. More details of this procedure can be found in [12] and [13]. The k- ε model was chosen because it is robust, computationally economic and reasonable accurate for a wide range of turbulent flows, including the present study.

Concerning the heat transfer problem, the energy equation is given by the following expression:

$$\frac{\partial}{\partial t}(\rho\, E) + \frac{\partial}{\partial x_i}[u_i(\rho\, E + p)] =$$

$$= \frac{\partial}{\partial x_j}\left[\left(k_t + \frac{C_p \mu_t}{Pr}\right)\frac{\partial T}{\partial x_j} + u_i \tau_{ij}\right] \qquad (4)$$

where:
E   –   total energy
k_t –   the turbulent kinetic energy [12, 13].

Finally, the equation used to characterize the local mass fraction of air is given by:

$$\frac{\partial(\rho Y_{air})}{\partial t} + \nabla \cdot (Y_{air} \rho \vec{V}) = 0 \qquad (5)$$

where:
Y_{air} –   the mass fraction of the air.

The mass fraction of the burnt gases, Y_{gas}, is given by the fact that the total mass fraction must sum to unity:

$$Y_{gas} = 1 - Y_{air} \qquad (6)$$

Boundary and initial conditions

The experimentally measured data summarized in Table 2 were used to establish the boundary conditions. An inlet flow of 2.8 bar and 55ºC was imposed at the intake ducts. On the other hand, an outlet condition was employed at the exhaust ducts, at 2.4 bar and 371ºC.

As the combustion process was not simulated, the start of computation was chosen at 90º crankshaft angle, which takes place after the completion of the combustion. On the other hand, the end of computation was chosen at 630º crankshaft angle, before the beginning of the combustion of the next cycle. It can be seen in Fig. 5 that the in-cylinder gauge pressure at 90º crankshaft angle is 25.9 bar. Unfortunately, the in-cylinder temperatures can not be measured experimentally because a temperature sensor is not fast enough to accurate capture the in-cylinder temperature along the whole cycle, only being possible to measure the inlet and exhaust temperatures, which are practically constant along the cycle. For this reason, the in-cylinder initial temperature was estimated from an adaptation of

the ideal thermodynamic cycle. Details of the procedure can be found in most undergraduate textbooks on internal combustion engines or thermodynamics, so it is not repeated here. The result at 90º crankshaft angle is 1337ºC. Concerning the initial velocity, a value of zero was assumed in the exhaust and intake ducts. Nevertheless, in the cylinder, the initial velocity was assumed as the lineal velocity of the piston at 90º crankshaft angle, i.e., 15.5 m/s.

Computational mesh

The principle of operation of CFD codes is subdividing the domain into a number of smaller, non-overlapping sub-domains. The result is a grid (or mesh) of cells (or elements). In this work, a grid generation program, Gambit 2.4.6, was used to generate the mesh, which is shown in Fig. 6.
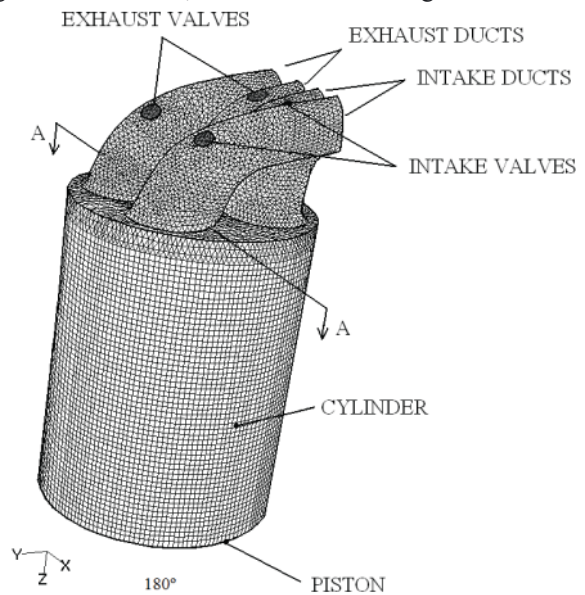
Fig. 6. Computational mesh at 180º crankshaft angle

Due to the movement of the piston and valves, the domain changes into a new position of the calculation and the grid must be automatically reconstruct at each time step. Figure 7 shows the A-A cross section of the mesh at 180º (with the piston at bottom dead center, the intake valves closed and the exhaust

Fig. 7. A-A section of the mesh: a) 180º crankshaft angle, top dead center, b) 360º crankshaft angle, bottom dead center

valves opened) and 360º (with the piston at top dead center, with all valves opened). The number of elements varies from 40000 at top dead center, Fig. 7a to 500000 at bottom dead center, Fig. 7b. In order to minimize the number of cells and obtain good convergence, hexahedral elements were used to mesh the cylinder. Unfortunately, hexahedral elements do not adapt properly to the complex geometry of the valves and ducts, for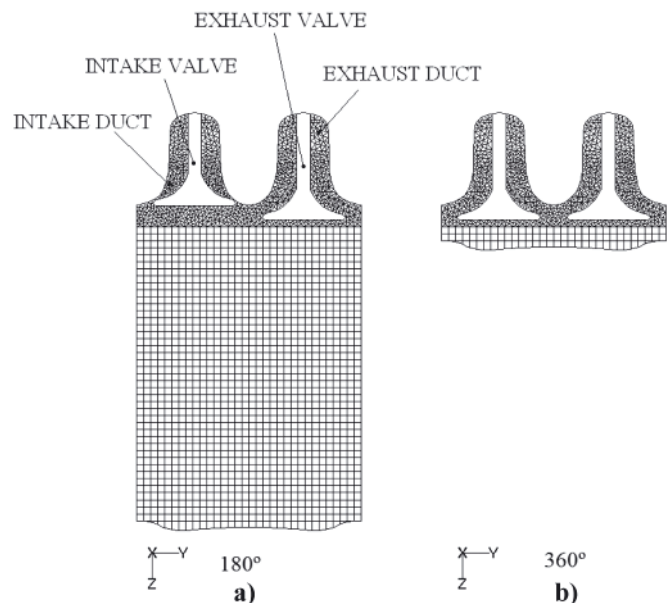 this reason, tetrahedral elements were employed to the cylinder head and ducts. The cylinder head, especially around valves, was refined in order to capture the complex characteristics of the flow.

Resolution of the equations

The governing equations were solved using the commercial software Ansys Fluent 6.3, based on the finite volume method. A simple backward Euler scheme was used for the temporal treatment, with a constant time step equivalent to 0.1º crank angle. A second order scheme was chosen for discretization of the continuity, momentum, energy and mass fraction equations, and the PISO algorithm was employed for the pressure-velocity coupling. The computation time was about 4 days in an AMD Phenon II processor with 4 Gb RAM.

RESULTS AND DISCUSSION

Validation of the code

In order to ensure that the CFD model is accurate enough, numerical results were compared to experimental measurements in terms of the in-cylinder pressure. For the interval of time studied, from 90º to 630º crankshaft angles, the numerical and experimental results are shown in Fig. 8. Note that an acceptable concordance is obtained between CFD and experimental results, being the average error around 10%.
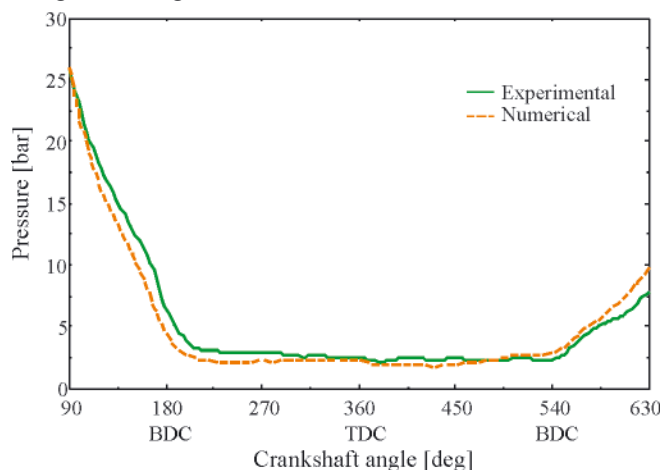

Fig. 8. *In-cylinder pressure numerically and experimentally obtained*

Figure 9 shows the pressure field on the A-A cutting plane (see Fig. 7) at several crankshaft angles. This plane was chosen in order to appreciate the opening/closing of the exhaust and intake valves. As can be seen, the initial in-cylinder pressure, Fig. 9a is 25.9 bar. At the beginning of the simulation, the pressure descends drastically due to the expansion of the piston. When the exhaust valves are opened, Fig. 9b, the in-cylinder pressure is slightly superior to the exhaust pressure, therefore burnt gasses are expelled through the exhaust ducts. When the intake valves are also opened, Fig. 9c, the in-cylinder pressure has an appropriate value, between the exhaust and intake pressures. Consequently, air enters through the intake ducts and burnt gases continue being expelled through the exhaust ducts.

Finally, when all valves are closed, the piston is ascending and the gasses are compressed, Fig. 9d.
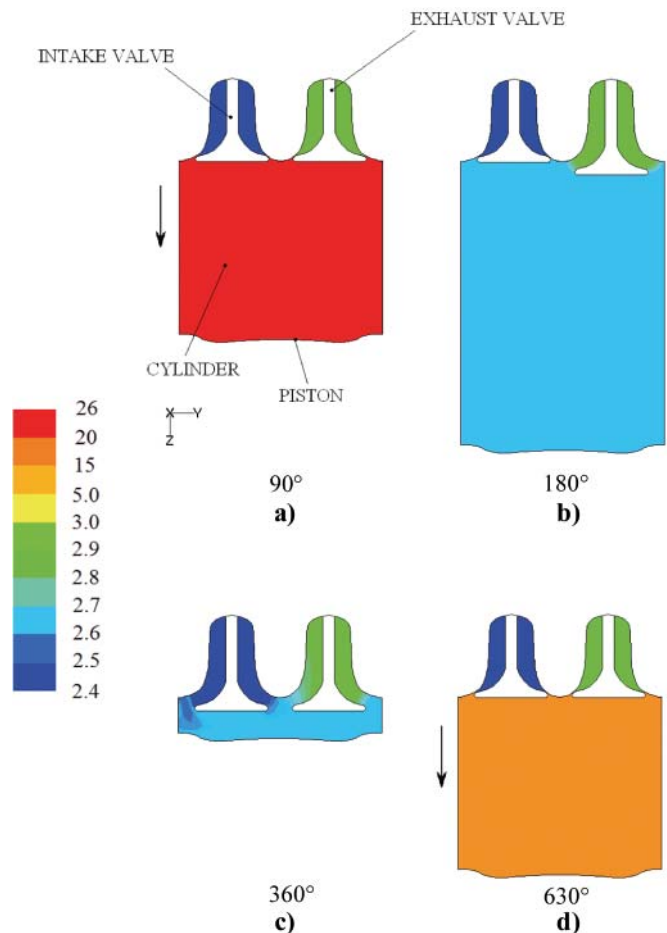

Fig. 9. *Pressure field (bar) at several crankshaft angles*

Mass fraction and velocity fields

Figure 10 shows the velocity field overlaid with the pressure field on the A-A cutting plane. As initial conditions, Fig. 10a, the velocity inside the cylinder was imposed as the lineal velocity of the piston and it was assumed that the cylinder and exhaust ducts are full of burnt gases (red color), while the intake duct is full of air (blue color). When the exhaust valves are opened, Fig. 10b, high velocity burnt gases are expelled trough the exhaust ducts. A short time later, the inlet valves are opened and air enters through the intake ducts and burnt gases are expelled through the exhaust ducts, Fig 10c-e. This process of entering fresh air and expelling burnt gases was verified during all the overlap period, i.e., between 310º and 404º. No retrocession of burnt gases to the intake ducts was produced. This means that these operating conditions are adequate. Finally, at the end of the simulation, all valves are closed and residual velocities remain into the cylinder.

CONCLUSIONS AND FURTHER DEVELOPMENTS

In this work, numerical and experimental tests were performed over a commercial four-stroke marine engine, the Wärtsilä 6L 46. A CFD model has been used to simulate the exhaust, intake and compression strokes. Special attention was focused on the overlap valve period, which has a crucial influence on the performance of the engine. It was verified that the fluid flow during the overlap period is correct (no reverse flow was obtained). This work was validated, verifying
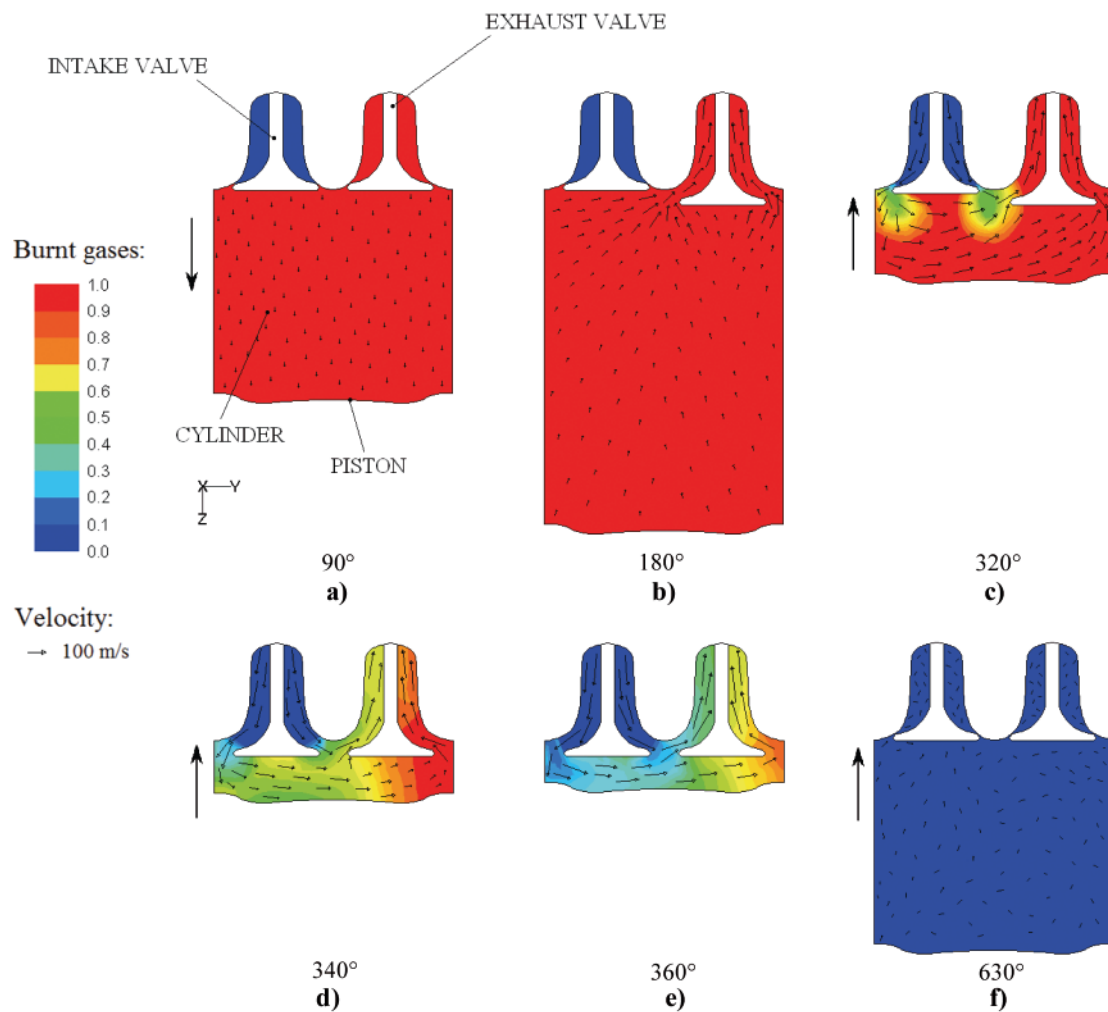
Fig. 10. *Velocity field (m/s) overlaid with mass fraction of burnt gases field (-) at several crankshaft angles*

that CFD results were in good agreement with experimental measurements of the in-cylinder pressure. This model is an unprecedented opportunity for engineers to understand the highly complex flow interactions that occur in an engine, providing extra information which can not be analyzed with experimental techniques. Besides, this is a very useful tool do improve the performance of the new designs of engines because it is very easy and reasonably cheap to study the influence of parameters such as the exhaust and intake pressures, engine speed, cam profile design, etc.

Although the numerous advantages, it is very important to mention the disadvantages of this CFD procedure. The most important is that it requires high computational resources. For example, the computation time for this problem was four days in an AMD Phenon II processor with 4 Gb RAM memory. Other disadvantage of CFD codes is that the process of generation of the mesh is very delicate. It is very easy to have convergence errors or loose accurate due to an inadequate mesh. In order to obtain good results, it is necessary to make several meshes and ensure that the results are independent of the mesh. Other disadvantage is that some CFD problems are very complicated. In this case, the geometry of the engine, coupled with the complex nature of the motion, in which the valves and piston move, make this a dificult problem to solve.

Acknowledgements

NOMENCLATURE

BDC	–	Bottom Dead Center
E	–	energy
g	–	gravity
k_t	–	turbulent kinetic energy
p	–	pressure
Pr	–	Prandtl number
R	–	gas constant
t	–	time
T	–	temperature
TDC	–	Top Dead Center
u	–	velocity
Y	–	mass fraction

Special characters

μ	–	dynamic viscosity
μ_t	–	turbulent viscosity
ρ	–	density
τ_{ij}	–	stress tensor

Subscripts

i	–	Cartesian coordinate (i = 1, 2, 3)
j	–	Cartesian coordinate (j = 1, 2, 3)

REFERENCES

1. Woodyard, D.: *Pounder´s marine diesel engines and gas turbines*. 8th Edition. Amsterdan. Elsevier 2004.

2. Milton, B.E.; Behnia, M.; Ellerman, D.M.: *Fuel deposition and re-atomization from fuel/air flows through engine inlet valves.* International Journal of Heat and Fluid Flow, vol. 22, pp. 350-357, 2001.

3. Payri F.; Benajes J.; Margot X.; Gil, A.: *CFD modeling of the in-cylinder flow in direct-injection diesel engines.* Computers & Fluids, vol.33 p.995-1021, 2004.

4. Moureau, V.; Angelberger, C.: *Towards large eddy simulation in internal combustion engines: simulation of a compressed tumble flow.* SAE Paper 011995, 2004.

5. Huang, R.F.; Huang, C.W.; Chang, S.B.; Yang, H.S.; Lin, T.W.; Hsu, W.Y.: *Topological flow evolutions in cylinder of a motored engine during intake and compression strokes.* Journal of Fluids and Structures, vol. 20, pp. 105-127, 2005.

6. Yang, S.L.; Siow, Y.K.; Teo, C.Y.: *A Kiva code with Reynolds-stress model for engine flow simulation.* Journal of Energy Conversion, vol. 30, pp. 427-445, 2005.

7. Semin; Idris, A.; Bakar, R.A.: *Effect of port injection CNG engine using injector nozzle multi holes on air-fuel mixing in combustion chamber.* European Journal of Scientific Research, vol. 34, pp. 16-24, 2009.

8. Ramajo, D. E.; Nigro, N. M.: *In-cylinder flow CFD analysis of a tour-valve spark ignition engine: comparison between steady and dynamic tests.* Journal of Engineering for Gas Turbines and Power, vol. 132, 2010.

9. Lamas, M.I.; Rodríguez, C.G.: *CFD analysis of the scavenging process in the MAN B&W 7S50MC two-stroke diesel marine engine.* Submitted to Journal of Ship Research.

10. Nakagawa, H.; Kato, S.; Tateishi, M., Adachi, T., Nakashima, M.: *Airflow in the cylinder of a 2-stroke cycle uniflow scavenging diesel engine during compression stroke,* JSME International Journal, series II, vol. 33, No. 3, pp. 591-598, 1990.

11. Wärtsilä 46. *Project guide for marine applications.* 2001.

12. *Fluent 6.3 Documentation,* 2006. Fluent Inc.

13. Versteeg H K, Malalasekera W.: *An introduction to computational fluid dynamics: the finite volume method.* 2nd Edition. Harlow: Pearson Education, 2007.

CONTACT WITH THE AUTHORS

Lamas M. I., Assoc. Prof.
Rodríguez C. G., M. Sc.
Rebollido, J. M., Assoc. Prof.
Escola Universitaria Politécnica. Universidade da Coruña.
Avda. 19 de Febreiro s/n - 15405 Ferrol - A Coruña. SPAIN.
e-mail: isabellamas@udc.es

Dynamic properties of 7000 - series aluminum alloys at large strain rates

Wojciech Jurczak, Ph. D.
Polish Naval Academy in Gdynia
Lesław Kyzioł, Assoc. Prof.
Gdynia Maritime University

ABSTRACT

This paper presents test results of mechanical properties of EN AW-AlZn5Mg1Zr and EN AW-AlZn5Mg1,5CuZr aluminum alloys for various tensile strain rates. Static tests were conducted with the use of MTS 810.12 tension test machine, and dynamic tests - with RSO rotary impact test machine. The work was aimed at determination of effects of strain rate and notch geometry of specimens on their material mechanical properties and damage mechanisms.

Keywords: High resistance aluminum alloys; Dynamic characteristics; Analysis, RSO rotary impact

INTRODUCTION

The 7000 - series aluminum alloys have been commonly used in shipbuilding industry worldwide [1, 17]. Such properties as low specific weight, amagnetism, good corrosion resistance and high strength make ship designers and production engineers willing to apply the alloys as wide as possible [2, 15, 17]. Ships built of the alloys are subjected to dynamic (impact) loads during operation and therefore to know both static and dynamic properties of the alloys is necessary. Moreover, naval ships, due to their functions, are exposed to action of enemy dynamic weapons. Hence to properly select structural materials the designers and production engineers should know their properties in a wide range of strain rates.

Strain rate under dynamic load changes strength properties of structural materials [3, 4, 19, 20] including aluminum alloys [5, 15, 16, 18]. Static and dynamic characteristics of the tested materials have been determined to assess their properties at strain rates changing from quasistatic one to V_{max} = 40 m/s.

Many contemporary military engineering constructions contain local material discontinuities in the form of notches exposed to effects of intensive short-lasting loads during operation.

In this paper are presented dynamic characteristics of 7000 - series aluminum alloys commonly used in shipbuilding industry. The tests were aimed at determination of effects of strain rate and notch geometry of specimens on their mechanical properties and damage mechanisms in fracture zone. Geometrical notch effect is usually revealed under fatigue loads [17, 18]. The problem of behaviour of notched specimens under dynamic pulse loads at changeable strain rates has been left still open.

Strain rate is a crucial factor which affects value of material yield point. In Fig. 1 for example the curve 1 corresponds to tensile strength test of non-alloy steel of 0.2% C content at the static strain rate $\dot{\varepsilon} = 10^{-2}\,\text{s}^{-1}$, and the curve 2 – to tensile strength test of the specimen of the same material at the dynamic strain rate $\dot{\varepsilon} = 10^{-2}\,\text{s}^{-1}$.
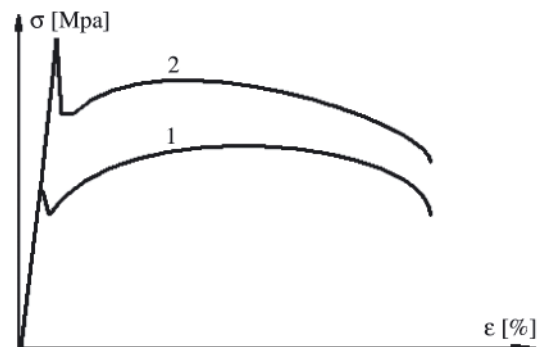

Fig. 1. Diagrams of the stress-strain relations: σ = f(ε): 1) for static strain rate, and 2) for dynamic strain rate, [6]

Under dynamic load, value of acting force depends both on mass and speed of hiting body and specimen's strain rate [6, 7].

A way of action of blast energy to ship structures depends on distance and power of blast source, and the action may be direct (contact) or intermediate one (non-contact). In both the cases a shock wave is generated (shock wave pressure pulse), which affects both the above-water (in air) and under-water parts of ship hull. a way of propagation of shock wave in the two media, i.e. air and water, is different. In the presented investigations energy of rotary impact machine claw (Fig. 2) is deemed representative for action of air pressure pulse, and its short time to failure of specimen is most similar to action of explosion- generated shock wave pressure on to ship structure [3, 8].

TESTING METHOD

The tests were performed on plate specimens made of EN AW-AlZn5Mg1Zr (7108, PA47) [21] and EN AW-AlZn5Mg1,5CuZr (7015) [21] alloys obtained from two heats of different chemical composition. The chemical compositions of the materials are given in Tab. 1 and 2. From the plates the following specimens were prepared for static and dynamic tensile tests:

- plain specimens;
- „V"- notched specimens
- „U"- notched specimens.

From the tested materials were made the specimens of the forms presented in Fig. 2, intended for static and dynamic tensile tests. The direction of cutting from plates the specimens for testing the static and dynamic properties of EN AW-AlZn5Mg1Zr and EN AW-AlZn5Mg1,5CuZr aluminum alloy of heat No.507, was in line with that of plate rolling. To assess the influence of rolling direction on dynamic properties of the tested alloy the specimens of EN AW-AlZn5Mg1,5CuZr alloy of heat No. 635 were cut in perpendicular to plate rolling direction and marked "p".
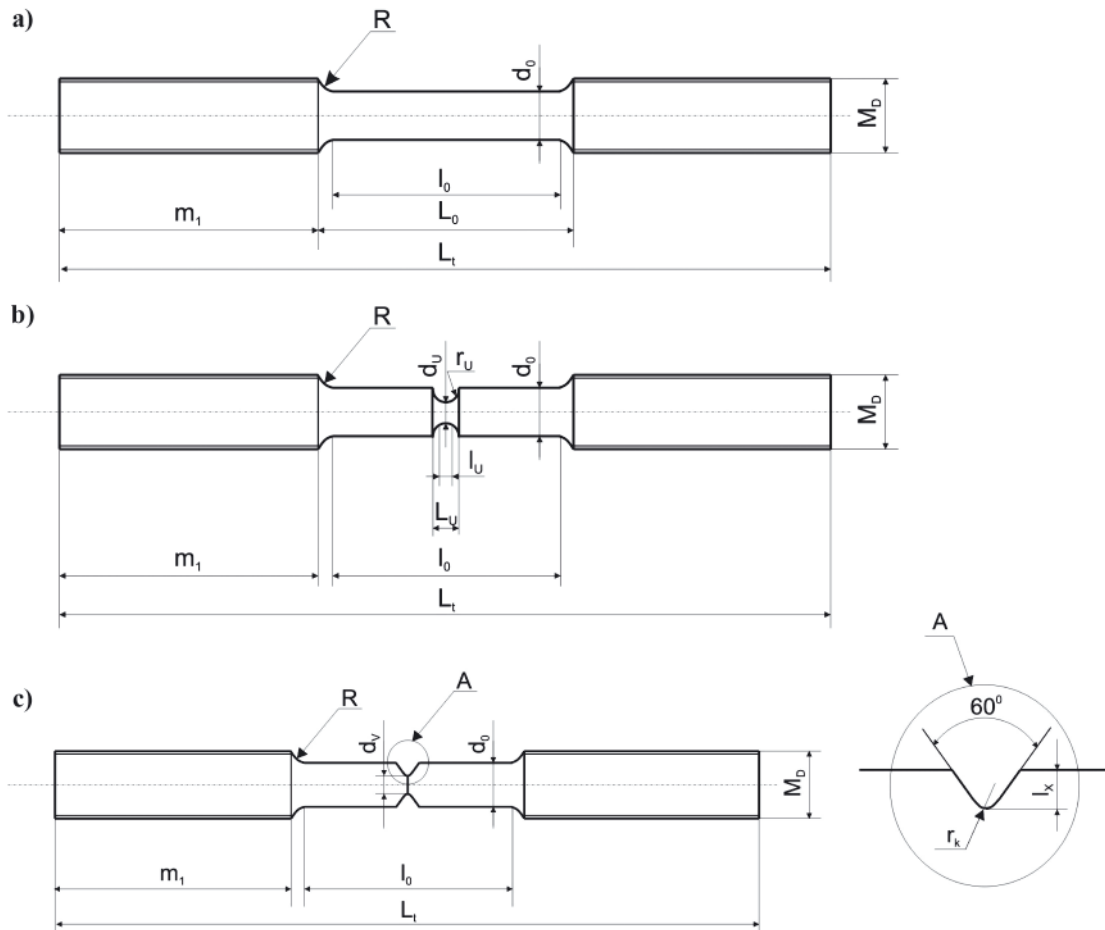

Fig. 2. *Forms and dimension symbols of specimens made of the tested Al- alloys:*
a) *plain specimen of circular cross-section,* ***b)*** *„V" notched specimens,* ***c)*** *„U"notched specimens*

Tab. 1. *Chemical composition of the tested EN AW-AlZn5Mg1Zr (7108, PA47) aluminium alloy [21, 22]*

Heat treatment state	Plate thickness [mm]	Chemical composition [mass percentage]									No. of batch and certificate
		Mg	Mn	Ti	Zn	Cr	Si	Fe	Cu	Al	
tb	12	1.25	0.18	0.034	5.3	0.14	0.16	0.32	0.05	rest /Zr = 0.04/	2945/485/4 ZN 81 MH-MN-190-06

tb: Solutioning - heating up to 480°C for 50 min, cooling down with hot water to min. 70°C, natural ageing for 0 ÷ 4 days at 20°C, two-stage artificial ageing at - two-stage artificial ageing: 95°C for 8h and at 150°C for 8h

Tab. 2. *Chemical composition of plates made of EN AW-AlZn5Mg1,5CuZr (7015) aluminium alloy [9, 21, 22]*

No. of heat	Chemical composition [mass percentage]											No. of batch and certificate
	Zn	Mg	Cr	Zr	Ti	Fe	Si	Cu	Mn	Ni	Al	
507	5.13	1.9	0.16	0.15	0.071	0.27	0.15	0.08	0.057	0.006	rest	1086
635	4.81	1.9	0.17	0.12	0.016	0.31	0.21	0.09	0.06	0.006	rest	1085

tb: Solutioning - heating up to 480°C for 50 min, cooling down with hot water to min. 70°C, natural ageing for 0 ÷ 4 days at 20°C, two-stage artificial ageing at two-stage artificial ageing: 95°C for 8h and at 150°C for 8h

The static tensile tests were conducted with the aim of the MTS 810.12 electro-hydrodynamic tension test machine fitted with computer-aided control and recording system, and the dynamic tensile tests - by means of the RSO rotary impact test machine presented in Fig. 3, which has been specially instrumented and used by the Institute of Machine Construction Fundamentals, Polish Naval University.

Owing to the fitting of the rotary impact machine with the original measuring system it was possible to perform measurements of tensile force and displacement rate with simultaneous recording the data by means of the digital oscilloscope. The force was recorded by using a resistance dynamometer and the displacement - by means of an opto-electronic sensor of displacement rate of the traverse fixed to the specimen. The force F and the displacement W was recorded by using the LS-140 digital oscilloscope. The tests were performed for four selected displacement rates: 10, 20, 30 oraz 40 ms^{-1}, which were measured with the use of the opto-electronic measuring system [5].

For the analyzing of microstructure of the tested specimens and their fracture mechanisms was used the Neophot-2 microscope, SSC-DC88P SONY digital camera, and a PC computer fitted with MultiScan v.14 CSS software of MultiScanBase.
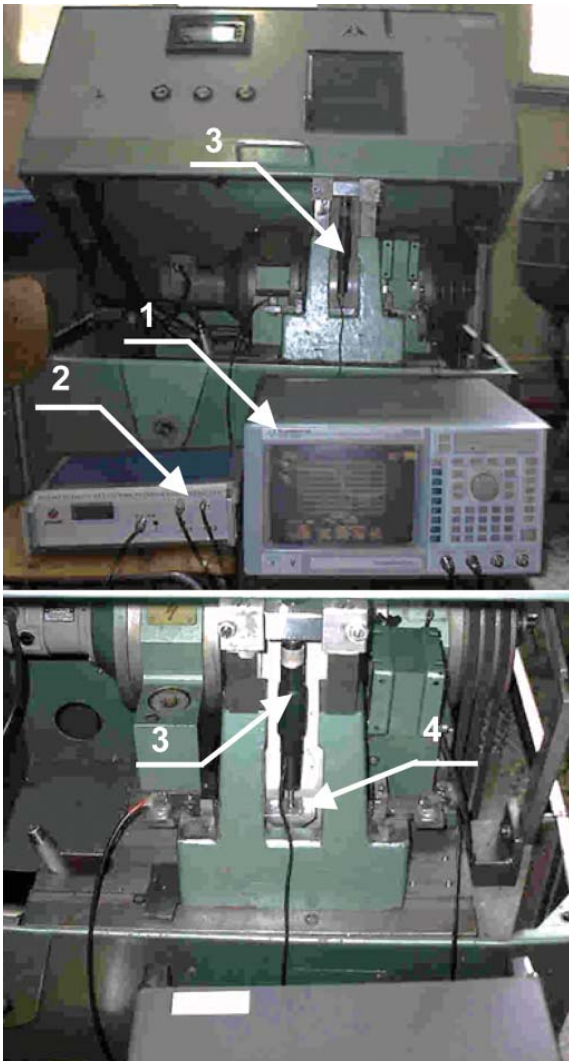

Fig. 3. *The RSO rotary impact test machine: traverse– specimen– dynamometer system. The instrumentation of the machine was consisted of: 3) the extensometric dynamometer, 2) the system's amplifier, 1) the LS-140 LeCroy digital oscilloscope. In advance of the measurements calibration was performed of the extensometric dynamometer by using the MTS, and calibration of rotational speed indications of the drum to which the ram claw (4) was fixed*

TEST RESULTS

The performed static and dynamic strength tests made it possible to determine characteristic strength properties of the tested alloys. Each of the measurement points in the diagram stands for the arithmetic mean value obtained from three specimens. In Fig. 4 and 5 are presented example time runs of force and traverse displacement recorded during dynamic tension test of the specimens made of the investigated alloys, performed by using the rotary impact test machine. Detailed test results of the tested Al - alloys are given in [10].

The results obtained from the static and dynamic tension tests of the investigated Al - alloys are presented in function of the displacement rate in Fig. 5 through 7.

Fig. 4. *Time runs of the force F(t), (marked CH1), and the traverse displacement Δl(t), (marked CH2), recorded during the dynamic tension test of a plain alloy specimen of EN AW-AlZn5Mg1Zr; performed with the use of the RSO rotary impact test machine at the tension displacement rate V = 10 ms^{-1}*
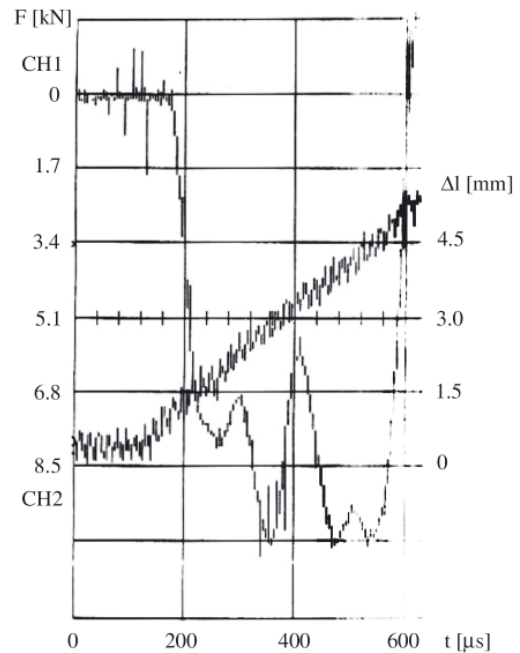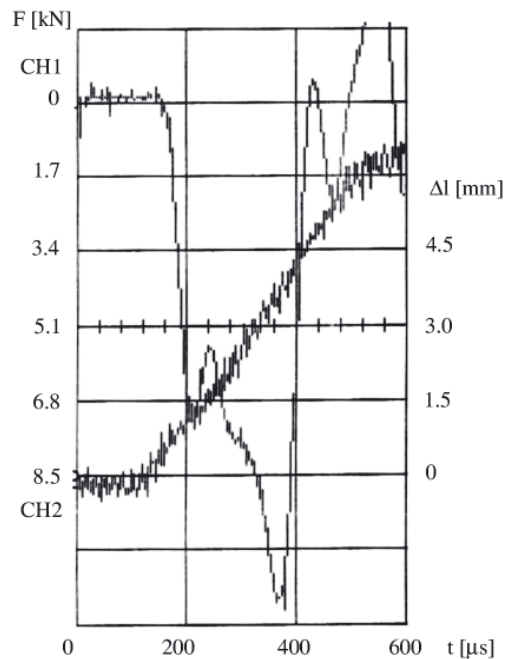

Fig. 5. *Time runs of the force F(t), (marked CH1), and the traverse displacement Δl(t), (marked CH2), recorded during the dynamic tension test of a plain specimen of EN AW-AlZn5Mg1Zr alloy, performed with the use of the RSO rotary impact test machine at the tension displacement rate V = 30 ms^{-1}*
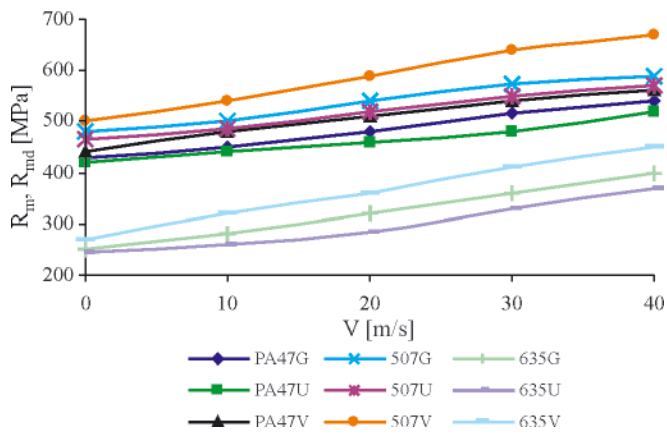
Fig. 6. *Relation of the dynamic tensile strength R_{md} of EN AW-AlZn5Mg1Zr and EN AW-AlZn5Mg1,5CuZr aluminium alloys in function of the displacement rate V for plain and notched specimens. **Notation:** **PA47** – EN AW-AlZn5Mg1Zr alloy, **507** - heat number of EN AW-AlZn5Mg1,5CuZr alloy, **635** – heat number of EN AW-AlZn5Mg1,5CuZr alloy, and: **G** – plain specimen, **U** – „U"notched specimen, **V** – „V"notched specimen*

Fig. 7. *Relation of the tensile yield point $R_{0.2d}$ of EN AW-AlZn5Mg1Zr and EN AW-AlZn5Mg1,5CuZr aluminum alloys in function of the displacement rate V for plain and notched specimens. **Notation:** **PA47** – EN AW-AlZn5Mg1Zr alloy, **507** - heat number of EN AW-AlZn5Mg1,5CuZr alloy, **635** – heat number of EN AW-AlZn5Mg1,5CuZr alloy, and: **G** – plain specimen, **U** – „U"notched specimen, **V** – „V"notched specimen*
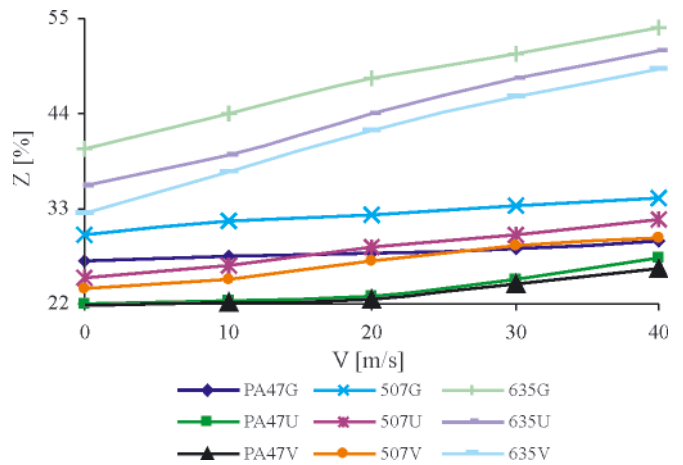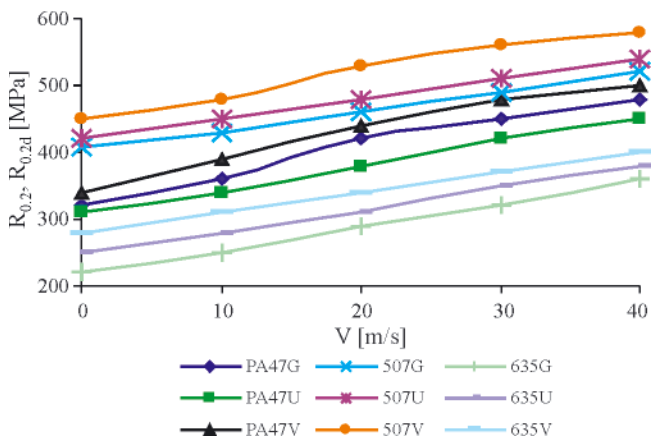

Fig. 8. *Relation of the percentage reduction of area Z of EN AW-AlZn5Mg1Zr and EN AW-AlZn5Mg1,5CuZr aluminum alloys of heat No. 507 and 635 in function of the displacement rate V for plain and notched specimens. **Notation:** **PA47** – EN AW-AlZn5Mg1Zr alloy, **507** - heat number of EN AW-AlZn5Mg1,5CuZr alloy, **635** – heat number of EN AW-AlZn5Mg1,5CuZr alloy, and: **G** – plain specimen, **U** – „U"notched specimen, **V** – „V"notched specimen*

ANALYSIS OF THE TEST RESULTS

Static properties of the tested Al- alloys

The static strength tests performed on plain specimens showed that the highest values were obtained for the EN AW-AlZn5Mg1,5CuZr alloy of heat No. 507 for the load direction in line with rolling direction. The smallest values were obtained for the specimens of EN AW-AlZn5Mg1,5CuZr alloy of heat No. 635p, loaded in perpendicular to the rolling direction. The tests confirmed the earlier strength test results of Al-alloys as regards relation of loading and rolling direction. Data from literature sources indicate that values of strength properties of the alloys of the heats No. 507 and 635, obtained from the specimens of the same heat treatment, subjected to loading in line with rolling direction, are close to each other. This results from that the heats are of the similar chemical composition [2] and somewhat higher strength properties, as regards the EN AW-AlZn5Mg1Zr alloy, due to a lower summary content of Zn + Mg [2]. The strength tests confirmed - on the example of the heat No. 635p - the effect of rolling direction on strength

Tab. 2. *Relative maximum values of the dynamic yield point $R_{0.2d}$ and the dynamic tensile strength R_m (at V = 40 m/s) against respective values of the static yield point $R_{0.2}$ and tensile strength R_m for the alloys: EN AW-AlZn5Mg1Zr and EN AW-AlZn5Mg1,5CuZr– heat No.507, EN AW-AlZn5Mg1,5CuZr – heat No.635p, based on tests for plain and notched specimens*

Alloy	Type of specimen	Diameter	R_{md} / R_m	R_{ed} / $R_{0.2}$
EN AW-AlZn5Mg1Zr	plain cylindrical	5.0$^{+0.1}$	1.25	1.50
	with U – notch of 1.9 mm radius	5.0/ 4.3$^{+/-0.1}$	1.24	1.45
	with V – notch of 0.2 mm radius	5.0/ 4.3$^{+/-0.1}$	1.27	1.47
EN AW-AlZn5Mg1,5CuZr -507	plain cylindrical	5.0$^{+0.1}$	1.23	1.27
	with U – notch of 1.9 mm radius	5.0/ 4.3$^{+/-0.1}$	1.23	1.28
	with V – notch of 0.2 mm radius	5.0/ 4.3$^{+/-0.1}$	1.34	1.28
EN AW-AlZn5Mg1,5CuZr - 635p	plain cylindrical	5.0$^{+0.1}$	1.60	1.63
	with U – notch of 1.9 mm radius	5.0/ 4.3$^{+/-0.1}$	1.51	1.52
	with V – notch of 0.2 mm radius	5.0/ 4.3$^{+/-0.1}$	1.66	1.47

properties of Al-alloys. The specimens subjected to tension load perpendicular to rolling direction showed almost two times smaller strength as compared with those loaded in line with rolling direction. Hence a way of arranging the sheet made of the tested alloy on plating of ship hull or its superstructure should take into account direction of operational stresses.

Dynamic properties of AlZn5Mg2CrZr alloy in function of strain rate

In order to assess real impact strength of ship structure it is necessary to know impact mechanical properties of its material.

In Tab. 2 are given values of the dynamic yield point $R_{0.2d}$ and the dynamic tensile strength R_{md} related to respective values of the static yield point $R_{0.2}$ and the tensile strength R_m.

As results from the performed analysis of results of the tests on plain specimens of the alloys in question, the greatest increase of the dynamic tensile strength and yield point at V = 40 m/s, as compared with the static strength, was revealed by the EN AW-AlZn5Mg1,5CuZr - 635p. However, as already mentioned, the alloy showed low strength properties as a result of cutting the specimens from the sheets in perpendicular to rolling direction. The absolutely greatest increase of the $R_{0.2d}$ was revealed by the EN AW-AlZn5Mg1,5CuZr alloy – heat No. 507. The results of the tests are illustrated in Fig. 9.
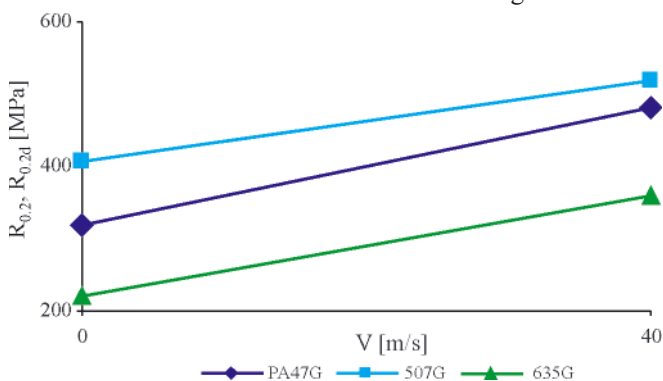

Fig. 9. *The dynamic tensile yield point $R_{0.2d}$ of EN AW-AlZn5Mg1Zr and AlZn5Mg1,5CuZr of the heats 507 and 635 in function of the displacement rate V.* ***Notation:*** ***PA47*** *– EN AW-AlZn5Mg1Zr alloy,* ***507*** *- heat number of AlZn5Mg1,5CuZr alloy,* ***635*** *– heat number of AlZn5Mg1,5CuZr alloy,* ***G*** *– plain specimen,* ***U*** *– „U"notched specimen,* ***V*** *– „V"notched specimen*

Along with increasing strain rate values the plastic properties of the tested Al-alloys reach greater values in contrast to such properties of steel which are as a rule dropping. The tests aimed at determination of effects of notch form and strain rate demonstrated that the greatest increase of the strength properties was revealed by the „V" – notched specimens of the EN AW-AlZn5Mg1,5CuZr alloy – heat No. 507. Moreover, the remaining Al-alloys, of which the notched specimens were made, showed the greatest increase of strength properties. The test results are illustrated in Fig. 10.

Character of phenomena which occur under dynamic loads is very complex because of influence of many factors such as: stress wave propagation, stress concentration, temperature, strain rate distribution etc. Increasing strain rate results in increasing resistance to plastic deformation of metals, which leads to yield point, strength and hardness increasing. Notch form influences very much fatigue strength of materials [17, 18]. Under the assumption that plastic flow of metals is based on a thermally activated process which determines motion of dislocations through crystal network containing point defects,
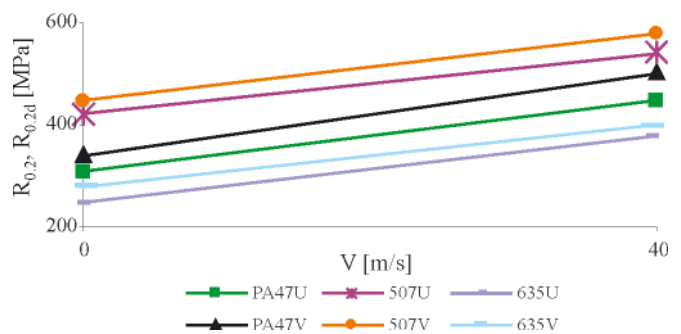

Fig. 10. *The dynamic tensile yield point $R_{0.2d}$ of EN AW-AlZn5Mg1Zr and AlZn5Mg1,5CuZr PA47 alloy – heat No. 507 and 635 in function of the displacement rate and notch form.* ***Notation****: PA47 – EN AW-AlZn5Mg1Zr alloy,* ***507*** *- heat number of AlZn5Mg1,5CuZr alloy,* ***635*** *– heat number of AlZn5Mg1,5CuZr alloy,* ***G*** *– plain specimen,* ***U*** *– „U"notched specimen,* ***V*** *– „V"notched specimen*

tensile strain rate can be usually described in the form of Arhenius equation as follows:

$$\varepsilon = \varepsilon_0 \exp[-\Delta G(\sigma)/kT]$$

where:
$\Delta G(\sigma)$ – activation energy dependent on the stress σ,
k – Boltzman constant,
T – temperature,
ε_0 – material constant.

Making use of the above given relations one can relate the obtained values of yield point and tensile strength to the activation energy $\Delta G(\sigma)$.

Microscopic examinations of non-etched microsections taken from the area reveal occurrence of voids in the microstructure, hence a loss of material continuity, Fig. 11.
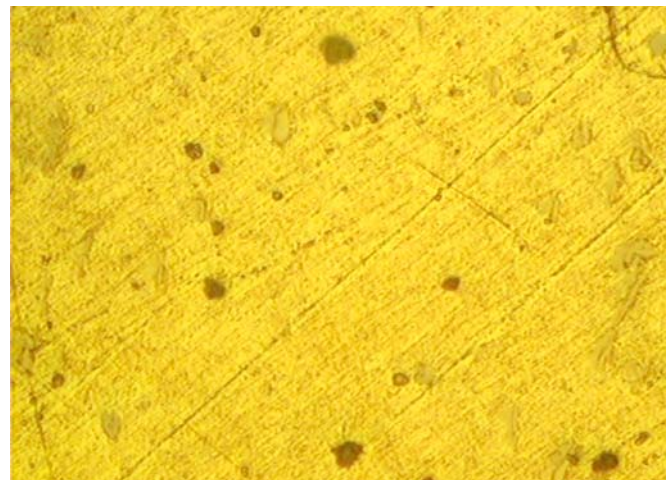
Fig. 11. *Non-etched micro section of a EN AW-AlZn5Mg1Zr alloy specimen under tension; maximum void diameter: 5 μm, mean void diameter: 4 μm*

Material plastic flow is not usually accompanied with a change in material volume. Therefore occurrence of voids may be deemed equivalent to material deterioration or damage process. Such damage may be defined by means of a function dependent on stresses, plastic strain energy, pressure, strain rate and temperature [11].

In the dynamic modelling of damages proper models of process of voids nucleation and grow are necessary. On the basis of metallographic observations of plastically damaged areas, models of spherical voids are assumed for description of plastic damage processes both in neck of tension specimens and specimen of colliding plates, [12, 13, 14].

FINAL CONCLUSIONS

From the performed static and dynamic tests on plain and notched specimens made of EN AW-AlZn5Mg1Zr and EN AW-AlZn5Mg1,5CuZr alloys, as well as the performed analysis of the test results, the following conclusions can be drawn:

1. Rolling direction is of essential influence on static and dynamic mechanical properties of the tested materials.
2. The lowest susceptibility to dynamic loading, this way also to strain rate, was found for the „V"- notched specimens. The „V" notched specimens both of EN AW-AlZn5Mg1Zr and EN AW-AlZn5Mg1,5CuZr alloy revealed higher increase of strength properties than the plain specimens and the „U"- notched ones at increasing strain rate.
3. As a result of dynamic loading an increase of strength indices of the tested Al-alloys was observed as compared with those obtained from static tension test.

The conclusions drawn from the performed static and dynamic tests may be applied to the modelling of dynamic deformation of Al-alloys considered elastic – visco-plastic materials.

Financing

BIBLIOGRAPHY

1. Levedahl W., Capable A.: *Affordable 21st - Century Destroyer*. Naval Engineers Journal. May 1993
2. Jurczak W.: *Influence of chemical composition and heat treatment on mechanical properties and corrosion resistance of Al-Zn-Mg alloys applicable to welded ship structures* (in Polish). Doctoral thesis, Gdańsk University of Technology, 1998.
3. Cudny K., Powierża Z.: *Selected problems of impact strength of ships* (in Polish). Printed course lectures, Polish Naval University, Gdynia, 1978.
4. Wiśniewski A.: *Armours – construction, design and tests* (in Polish). WNT (Scientific Technical Publishing House), Warsaw, 2001.
5. Dobrociński St., Fila J., Jurczak W., Kolenda J.: *Impact and ballistic strength of a novel Al-alloy and its composites* (in Polish). Report on „BALIDUR" research project, Polish Naval University, Gdynia, 2001.
6. Kinslov R. at al.: *High-Velocity Impact Phenomena*. Academic Press, New York and London, 1970
7. Fila J.: *Research on influence of loading state and strain rate on strength and toughness of ship materials* (in Polish). The conference on" Impact strength of structures ", Polish Naval University, Gdynia, 1993.
8. Fila J., Zatorski Z. at al.: *Reports: No. 1/1993, No.1/94 and No. 2/95/IPBMO / "Powłoka" - AMW-KBN*, 1993÷95, AMW Gdynia, str. 216.
9. Material certificate of AlZn5Mg2CrZr alloy, IMN-OML Skawina nr 4550/91, 336 OML/91.
10. Kyzioł L.: *Dynamic characteristics of materials intended for marine structures* (in Polish). Report on „KONSTRUKTOR" research project, 3rd phase, Polish Naval University, Gdynia, 2004, (unpublished).
11. Han Zheng, Ze – Ping Wang: *Spall damage in aluminium alloy*. International Journal Solids and Structures, 32 (1995) 1135÷1148.
12. Johnson J. N.: *Dynamic fracture and spallation in ductile solids*, Journal Applied Physics, 52 (1981) 2812÷2824.
13. Lewiński T., Sokołowski J.: *Energy change due to the appearance of cavities in elastic solids*, International Journal of Solids and Structures, 40 (2003) 1765÷1803.
14. Zukas J. A.: *High velocity impact dynamics*. John Willey & Sons Inc. U.K., 1990.
15. Bugłacki H.: *Influence of thermal treatment and chemical content of filler metals on mechanical properties and stress corrosion of AlZn5Mg1 alloy used for welded ship structures* (in Polish). Doctoral thesis. Gdańsk University of Technology, Gdańsk, 1981.
16. Bugłacki H., Jasiński R., Cudny K.: *Mechanical properties in function of strain rate for metal alloys used in shipbuilding* (in Polish). The conference on „ Impact strength of structures", Polish Naval Academy, Gdynia, 1993.
17. Cudny K., Puchaczewski N.: *Metal alloys for ship hulls and offshore engineering structures* (in Polish). Gdańsk University of Technology, Gdańsk, 1995.
18. Jasiński R.: *Influence of work hardening coefficient on impact properties and limited fatigue strength of aluminum alloys used in ship structures* (in Polish). Doctoral thesis. Gdańsk University of Technology, Gdańsk, 1976.
19. Perzyna P.: *Theory of visco-plasticity* (in Polish). PWN (State Scientific Publishers), Warsaw, 1969.
20. Perzyna P: *Application of visco-plasticity* (in Polish). Ossolineum,1971.
21. PN-EN 573-3: *Aluminum and its alloys– Chemical composition and kinds of plastically worked products– Part 3: Chemical composition* (in Polish).
22. PN-EN 515: *Aluminum and its alloys–Plastically worked products–Denotation of states* (in Polish).

CONTACT WITH THE AUTHORS

Wojciech Jurczak, Ph. D.
Faculty of Mechanical and Electrical Engineering
Institute Construction and Operation of Ships
Polish Naval Academy in Gdynia
Śmidowicza 69
81-103 Gdynia, POLAND
e-mail: W.Jurczak@amw.gdynia.pl

Lesław Kyzioł, Assoc. Prof.
Faculty of Marine Engineering,
Gdynia Maritime University
Morska 81/87
81-225 Gdynia, POLAND
e-mail: lkyz@skrzynka.pl , lkyz@am.gdynia.pl

The influence of the constraint effect on the mechanical properties and weldability of the mismatched weld joints

Part I

Eugeniusz Ranatowski, Prof.
University of Technology and Life Science, Bydgoszcz

ABSTRACT

The process of welding has dynamic character and is related with the local change of the internal energy E of welded system and can be defined by general dependence between intensive φ_j and extensive ψ_j parameters. The knowledge of the run of thermo-dynamical process under welding indicates on the possibility of active modelling of weldability and the control of welding process: $\varphi_j = \partial E / \partial \psi_j$. Hence, these process can be enhanced by mathematical modelling and numerical analysis of weldability models of, i.e. welding processes of material behaviour in welding and the strength of welded structures. The main attention is focused on the assessment of susceptibility of materials under defined welding conditions using fracture mechanics parameters. The analysis is based on the normalised parameters such as: ∂/∂_c, K_{Ith}/K_{IC}, as a measure of the susceptibility of materials in welding process. The deformation process and fracture parameters calibrations are influenced by constraint; hence the importance of determining the deformation behaviour and fracture parameters as a function of constraint. Furthermore, there established analytically the condition of welding process in mismatched weld joints for strength equal to base metal. Finally, same analytical examples which present new capabilities of weldability estimates and mechanical properties of mismatched weld joints are presented.

Keywords: weld joint; weldability; weldability analysis; thermal cycle;
heat source model; heat flow analysis; heat affected zone

INTRODUCTION

For some groups of welded joints, considerable local diversification of the material structure and, consequently, of the mechanical properties may occur in the weld or in the heat affected zone (HAZ). This can take place during welding of high strength steel and strain or age hardened steel, etc. Changes in the material structure are directly related to the mechanical properties.

The micro-structural models are in many cases sufficiently advanced to give accurate predictions for welds and HAZ. Till now the potential of quantitative weldability analysis and method in the design process is not so clear [1].

The problem of optimal design of welded structures is very complex and various attempts have been made to obtain effective methods which might be used in engineering, which requires appropriate dimensioning of materials and constructions. The application of the classical strength effort hypothesis is inconsiderable when defects, such as cracks, occur.

The discontinuities, such as cracks, show that the Huber – Mises equivalent of stress exceeds critical value at low load. The

elasticity solutions of problems involving stress concentrations show that the stress becomes singular as the notch root radius tends to zero; the theoretical stress at the notch is singular. Various approximate methods of calculation are often used in designing, e.g. reducing internal forces, yet the best approach is based on fracture mechanics and its parameters and criterions. The application of fracture mechanics parameters to materials and constructions dimensioning is a great step towards effort process modelling compliant with the modelling rules [2], which justifies the aim of the present research – physical characteristics of weldability and the main parameters and criterions of fracture mechanics and its applicability to welded structure designing and dimensioning.

THE GLOBAL ESTIMATE OF THE WELDABILITY

Currently the welding as a technological process is concerned with special processes, the results of which cannot be checked in a complete degree by the subsequent control, test of production. Numerical weldability analysis is a new

powerful research and development tool which is useful for metallurgists, technologist and design engineers. Weldability denotes the possibility to join parts by welding under defined conditions of design, materials and manufacture [1]. Weldability is conventionally ascertained and further developed by testing – empirical basis. This process can be enhanced and made more efficient by mathematical modelling and numerical analysis – theoretical basis. Strictly speaking, the numerical analysis of a weldability comprises thermodynamic, thermo-mechanical and micro-structural modelling of the welding process Ref. 3-4. The result of this operation is the different step of susceptibility of the material on welding process which physical measurement is the fracture resistance and decides on the utility of welded joints.

The mathematical modelling of property – determining processes presents a modern and powerful tool to improve engineering materials and their processing such as welding process. Outgoing from the fundamental mechanisms and their physical representation in the form of equation systems, the effect of influencing factors on weldability can be simulated by numerical models. The application of this method results in a considerable reduction of the total development time and costs of experimental investigation. The mathematical modelling allows an optimisation of the numerous influencing parameters with the aim to increase the process reliability and to improve the welding construction properties. It means that the modelling of welding processes requires taking into account the physical phenomena and their interactions [5]. The analysis of the welding process from above point of view, enables to execute the algorithm which is presented in Fig. 1.

The first step of our calculation (module I) effects heat flow character in welding process and determines the nature of the weld thermal cycle and hence, in transformable alloys the metallurgical process and the microstructure of weld metal and heat affected zones (HAZ) (module II) and change of the mechanical specificity (module III). Besides, in agreement with Fig. 1 the estimate of the weldability consists with two stages:
- recurring projection process of the structure feature of weld metal and HAZ in comparison with base metal-submodules 1, 2, 3, 4,
- estimating of the result of this process through analysis of the feature of mechanical properties-submodules 5, 6, 7, 8.

According to former configuration we can ascertain that Ref.6-7:
- solute distribution during weld pool solidification is an important phenomenon resulting in segregation that can significantly affect the weldability, microstructure and properties,
- solidification in weld metal region is complicated by several factors:
  · dynamic nature of the welding process,
  · unknown weld pool shape,
  · epitaxial growth,
  · variations in temperature gradient and the weld metal cooling rate may vary from 10^2 to 10^3 °C s^{-1} for the conventional welding process to 10^5 to 10^7 °C s^{-1} for high – energy beam processes,
- weld solidification controls the size and shape of grains, segregation and defects such as porosity and hot cracks,
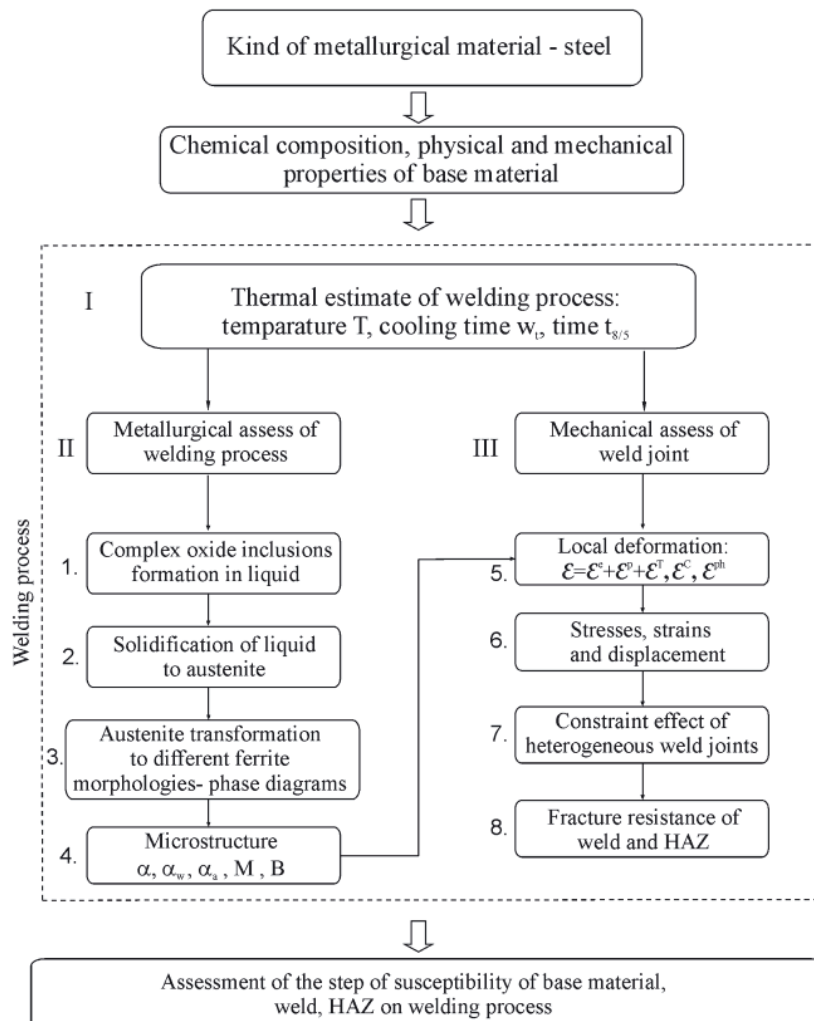

Fig. 1. Flow chart of the model to assess numerical weldability

- a lot of attention has been given to modelling the microstructure in weld metal areas and in addition to the phase transformations in solid state during weld thermal cycles,
- the austenite grain size is assumed to be inversely proportional to the nucleation rate is function of $\Delta G^{\delta \to \gamma}$ (G- Gibbs energy).
- the transformation of austenite to various ferrite morphologies in low-alloy ferritic steel weld metal is very sensitive to prior austenite grain size and there is a need for models to predict the austenite grain size as a function of weld metal compositions and welding process variables.

The mechanical analysis of the welded joints is more complex than the heat flow analysis because of the geometry changes and because of the complex stress – strain relationship. Models of the mechanical properties of base metal, HAZ and weld metal, are needed as input data for thermal analysis. The welding process has dynamic character and in general, mechanical behaviour of metals under thermal cycle can be described by module III and submodules $5 \div 8$, Fig. 1 Ref. 8-10. In this conceptual modelling, the constitutive relation: stress-strain link is the most important in the welding mechanics. One of the fundamental assumption is that the total strain can be divided into components which are produced by different physical processes – submodule 5 [11].

The coupling between thermal and mechanical fields enable to assess the thermo-mechanical diffusion equation [3]:

$$\rho c \dot{T} + \partial q_i / \partial x_j = \dot{Q}_{int} - \frac{E \alpha T}{1 - 2\nu} \cdot \dot{\varepsilon}_{ii}^e + \xi S_{ij} \dot{d}_{ij} \quad (1)$$

where:

q_i –   heat flux per unit area
Q_{int} –   internal heat generation
S_{ij} –   deviatoric stress tensor
d_{ij} –   viscoplastic strain rate tensor
ξ –   parameter characterising inelastic energy dissipation $S_{ij} \dot{d}_{ij} (\xi < 1)$.

Therefore, it is possible to divide the thermo-mechanical analysis of the welding process into two main parts – the analysis of the thermal field and the subsequent analysis of the mechanical fields for estimate residual stresses and residual deformation submodule 6.

The submodules 7 and 8 characterises the influence of constraint effect of heterogeneous welded joints on the mechanical properties. The effect of strength mis-match in steel weldments has received much attention.

The assessment of the step susceptibility of the base material on welding process is finally lean upon the fracture toughness parameter K_{mat} in terms of stress intensity factor K or his normalised value or others fracture parameters such as δ-CTOD, J.

THE VALUATION OF CONSTRAINT EFFECT IN MISMATCHED WELDED JOINTS

The theory of constrained materials in classical mechanics of deformable media is characterised by a restriction on the class of possible motions. One of the simplest mechanical constraints, namely the condition of incompressibility, has played a central role in the formulation and utilisation of constitutive equations for linear and non-linear elastic solids as well as the development of constitutive theories of other media including plasticity.

In order to solve this problem for mismatched welded joints which constitutes the aim of the present work, the simplified model is created with thin layer W (soft or hard – representing the weld metal or part of HAZ) which is taken into account and show in Fig. 2.

One of the primary features of welded structures is the macro-mechanical heterogeneity. The heterogeneous nature of the weld joints is characterised by macroscopic dissimilarity in mechanical properties. This mismatch causes constraints in macroscopic scale and local stress concentrations which are enhanced by geometric and physical parameters of the mismatched weld joints and state of loading – under tension or bending loading. The determination of local change in the stress occurring at the interface of zones (B) and (W) is then of primary importance for correct interpretation and estimation of new mechanical properties.

The components of the stress state in mismatched weld joints under static tension are determined by the equilibrium equations and the equation of the plasticity condition which fulfils the boundary condition of the interfaces of zones B and W. The stress analysis in this area has been performed in [12].

A very useful form of the stress state we can obtain by changing the parameters $\gamma \to q$:
- undermatched case:

$\gamma = k_1 / k$; $|\gamma| \leq 1$; $k = R_e^{W(un)} / \sqrt{3}$; $-k \leq k_1 \leq k$; $R_e^{W(un)} \leq R_e^B$

- overmatched case:

$\gamma = k_1 / k$; $|\gamma| \leq 1$; $k = R_e^{W(ov)} / \sqrt{3}$; $-k \leq k_1 \leq k$; $R_e^{W(ov)} \leq R_e^B$
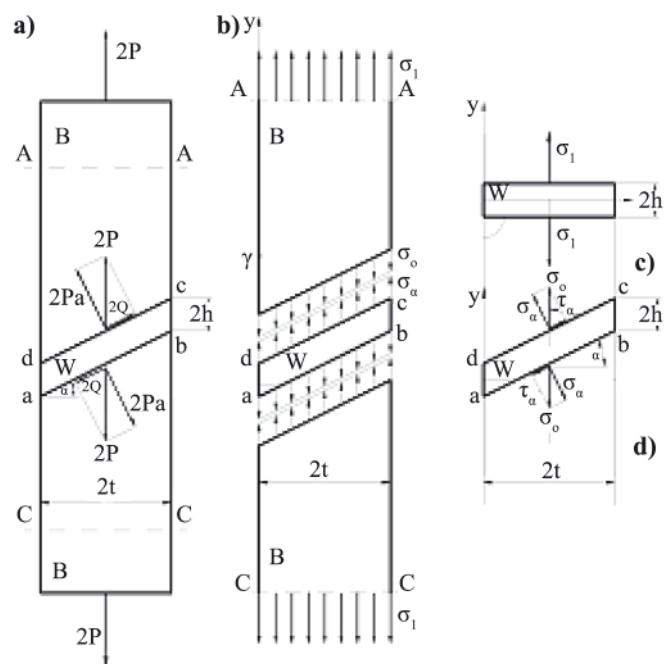

Fig. 2. Characteristic of the model of the mismatched weld joints:
a) geometrical configuration - layer W is inclined to external load;
b) distribution of external stresses σ_1 and σ_α ; c) external stress at interface for perpendicular layer; d) external stress at interface for inclined layer

The parameter γ represents the internal normalised tangential stress at interfaces and parameter q ($0 \leq q \leq 1$) represents the external normalised tangential stress caused by force 2Q. While using of the relation between γ and q as:

$$\gamma + 1 = 2q \to \gamma = 2q - 1 \quad (2)$$

and after insert the value of q:

$$q = (\sigma_1 / k) \sin 2\alpha \quad (3)$$

to equation (2) can be transformed the components of stress in the form very useful in engineering practice as follows [13]:
- undermatching case:

$$
\sigma_{xx(n)}^{un} = \frac{\sigma_{xx}^{un}}{k} = \left[\frac{1}{2 - 2 \cdot \left(\frac{\sqrt{3} \cdot \sigma_1}{2 \cdot R_e^W} \cdot \left| \sin(2 \cdot \alpha) \right| \right)} \cdot \right.
$$

$$
\cdot \left[\frac{\pi}{2} - \left[2 \cdot \left(\frac{\sqrt{3} \cdot \sigma_1}{2 \cdot R_e^W} \cdot \left| \sin(2 \cdot \alpha) \right| \right) - 1 \right] \cdot \sqrt{1 - \left[2 \cdot \left(\frac{\sqrt{3} \cdot \sigma_1}{2 \cdot R_e^W} \cdot \left| \sin(2 \cdot \alpha) \right| \right) - 1 \right]^2} +
$$

$$
- \arcsin \left[2 \cdot \left(\frac{\sqrt{3} \cdot \sigma_1}{2 \cdot R_e^W} \cdot \left| \sin(2 \cdot \alpha) \right| \right) - 1 \right] \right] + \left(1 - \frac{\sqrt{3} \cdot \sigma_1}{2 \cdot R_e^W} \cdot \left| \sin(2 \cdot \alpha) \right| \right) \cdot \frac{\xi}{\kappa} +
$$

$$
- 2 \cdot \sqrt{1 - \left[\frac{\sqrt{3} \cdot \sigma_1}{2 \cdot R_e^W} \cdot \left| \sin(2 \cdot \alpha) \right| + \left(1 - \frac{\sqrt{3} \cdot \sigma_1}{2 \cdot R_e^W} \cdot \left| \sin(2 \cdot \alpha) \right| \right) \cdot \frac{\eta}{\kappa} \right]^2} \right]
$$

(4)

$$
\sigma_{yy(n)}^{un} = \frac{\sigma_{yy}^{un}}{k} = \frac{1}{2 - 2 \cdot \left(\frac{\sqrt{3} \cdot \sigma_1}{2 \cdot R_e^W} \cdot \left| \sin(2 \cdot \alpha) \right| \right)} \cdot
$$

$$
\cdot \left[\frac{\pi}{2} - \left[2 \cdot \left(\frac{\sqrt{3} \cdot \sigma_1}{2 \cdot R_e^W} \cdot \left| \sin(2 \cdot \alpha) \right| \right) - 1 \right] \cdot \sqrt{1 - \left[2 \cdot \left(\frac{\sqrt{3} \cdot \sigma_1}{2 \cdot R_e^W} \cdot \left| \sin(2 \cdot \alpha) \right| \right) - 1 \right]^2} +
$$

$$
- \arcsin \left[2 \cdot \left(\frac{\sqrt{3} \cdot \sigma_1}{2 \cdot R_e^W} \cdot \left| \sin(2 \cdot \alpha) \right| \right) - 1 \right] \right] + \left(1 - \frac{\sqrt{3} \cdot \sigma_1}{2 \cdot R_e^W} \cdot \left| \sin(2 \cdot \alpha) \right| \right) \cdot \frac{\xi}{\kappa}
$$

(5)

$$
\sigma_{xy(n)}^{un} = \frac{\sigma_{xy}^{un}}{k} = \frac{\sqrt{3} \cdot \sigma_1}{2 \cdot R_e^W} \cdot \left| \sin(2 \cdot \alpha) \right| + \left(1 - \frac{\sqrt{3} \cdot \sigma_1}{2 \cdot R_e^W} \cdot \left| \sin(2 \cdot \alpha) \right| \right) \cdot \frac{\eta}{\kappa}
$$

(6)

where:

$$
k = R_e^W / \sqrt{3}; \quad R_e^W \leq R_e^B; \quad \kappa = 2h/2t
$$

$$
\eta = 2y/2t; \quad \xi = 2x/2t; \quad \kappa \geq \eta
$$

R_e^W – yield point of layer

R_e^B – yield point of base material.

The σ_1 can assess the following values for undermatching case:

a. B - elastic, W – elastic:

$$
\sigma_1 < R_e^W < R_e^B
$$

(7)

b. B – elastic, W – plastic:

$$
R_e^W \leq \sigma_1 < R_e^B
$$

(8)

c. B and W – plastic:

$$
\sigma_1 \geq R_e^B \geq R_e^W
$$

(9)

- overmatched weld joints:

$$\sigma_{xx(n)}^{ov} = \frac{\sigma_{xx}^{ov}}{k} = \left[\frac{1}{2 - 2 \cdot \left(\frac{\sqrt{3} \cdot \sigma_1}{2 \cdot R_e^W} \cdot \left| \sin(2 \cdot \alpha) \right| \right)} \cdot \right.$$

$$\cdot \left[-\frac{\pi}{2} + \left[2 \cdot \left(\frac{\sqrt{3} \cdot \sigma_1}{2 \cdot R_e^W} \cdot \left| \sin(2 \cdot \alpha) \right| \right) - 1 \right] \cdot \sqrt{1 - \left[2 \cdot \left(\frac{\sqrt{3} \cdot \sigma_1}{2 \cdot R_e^W} \cdot \left| \sin(2 \cdot \alpha) \right| \right) - 1 \right]^2} +$$

$$+ \arcsin \left[2 \cdot \left(\frac{\sqrt{3} \cdot \sigma_1}{2 \cdot R_e^W} \cdot \left| \sin(2 \cdot \alpha) \right| \right) - 1 \right] \right] + \left(1 - \frac{\sqrt{3} \cdot \sigma_1}{2 \cdot R_e^W} \cdot \left| \sin(2 \cdot \alpha) \right| \right) \cdot \frac{\xi}{\kappa} + \tag{10}$$

$$+ 2 \cdot \sqrt{1 - \left[\frac{\sqrt{3} \cdot \sigma_1}{2 \cdot R_e^W} \cdot \left| \sin(2 \cdot \alpha) \right| + \left(1 - \frac{\sqrt{3} \cdot \sigma_1}{2 \cdot R_e^W} \cdot \left| \sin(2 \cdot \alpha) \right| \right) \cdot \frac{\eta}{\kappa} \right]^2} \right]$$

$$\sigma_{yy(n)}^{ov} = \frac{\sigma_{yy}^{ov}}{k} = \frac{1}{2 - 2 \cdot \left(\frac{\sqrt{3} \cdot \sigma_1}{2 \cdot R_e^W} \cdot \left| \sin(2 \cdot \alpha) \right| \right)} \cdot$$

$$\cdot \left[-\frac{\pi}{2} + \left[2 \cdot \left(\frac{\sqrt{3} \cdot \sigma_1}{2 \cdot R_e^W} \cdot \left| \sin(2 \cdot \alpha) \right| \right) - 1 \right] \cdot \sqrt{1 - \left[2 \cdot \left(\frac{\sqrt{3} \cdot \sigma_1}{2 \cdot R_e^W} \cdot \left| \sin(2 \cdot \alpha) \right| \right) - 1 \right]^2} + \tag{11}$$

$$+ \arcsin \left[2 \cdot \left(\frac{\sqrt{3} \cdot \sigma_1}{2 \cdot R_e^W} \cdot \left| \sin(2 \cdot \alpha) \right| \right) - 1 \right] \right] + \left(1 - \frac{\sqrt{3} \cdot \sigma_1}{2 \cdot R_e^W} \cdot \left| \sin(2 \cdot \alpha) \right| \right) \cdot \frac{\xi}{\kappa}$$

$$\sigma_{xy(n)}^{ov} = \frac{\sigma_{xy}^{ov}}{k} = \frac{\sqrt{3} \cdot \sigma_1}{2 \cdot R_e^W} \cdot \left| \sin(2 \cdot \alpha) \right| + \left(1 - \frac{\sqrt{3} \cdot \sigma_1}{2 \cdot R_e^W} \cdot \left| \sin(2 \cdot \alpha) \right| \right) \cdot \frac{\eta}{\kappa} \tag{12}$$

where:
$$k = R_e^W / \sqrt{3} \; ; \; R_e^W > R_e^B \; ; \; \kappa = 2h/2t$$

For overmatching case the σ_1 can assess the following values:

a. B – elastic, W – elastic:

$$\sigma_1 < R_e^B < R_e^W \tag{13}$$

b. B – plastic, W –elastic:

$$R_e^B \leq \sigma_1 < R_e^W \tag{14}$$

c. B and W – plastic:

$$\sigma_1 \geq R_e^W \geq R_e^B \tag{15}$$

The conversion of stress state makes a change to mechanical properties of the different part of the mismatched welded joints. As an effective measure of constraint effect we can introduce the stress state parameter S_p as follows:

- undermatching case:

$$S_p^{un} = \sigma_m^{un} / \sigma_H^{un} \tag{16}$$

- overmatching case:

$$S_p^{ov} = \sigma_m^{ov} / \sigma_H^{ov} \qquad (17)$$

where:

$\sigma_m^{un/ov}$ – mean stress

$\sigma_H^{un/ov}$ – equivalent of stress according to Huber-Mises.

Some examples of an assessment of $S_p^{un/ov}$ are presented in Fig. 3.
These examples reveal the different tendencies of change of $S_p^{un/ov}$ with α increase and periodic character.
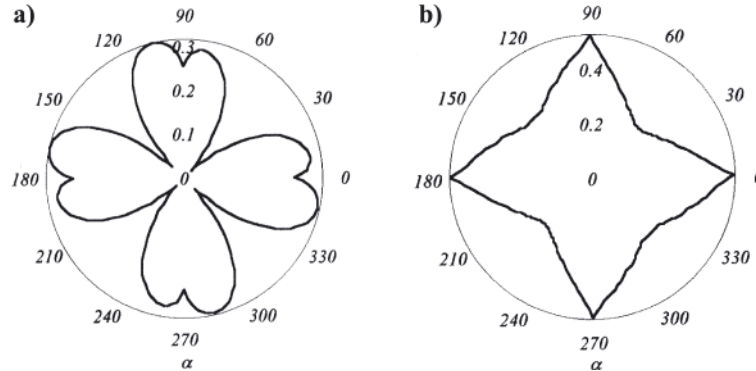

*Fig. 3. Characteristic of : **a)** S_p^{un} (σ_1 = 500 MPa, R_e^W = 434 MPa) and **b)** S_p^{ov} (σ_1 = 500 MPa, R_e^W = 605 MPa) at α = 0 ÷ 360°
in polar coordinates and geometric feature κ = 0.75 , η = 0.1 , ξ = 0.1*

Furthermore, the change analysis of stress state in mismatched models of welded joints enables estimation of constraint factors $K_W^{un/ov}$ as follows [13]:

$$
\begin{aligned}
K_W^{un} = \frac{2}{\sqrt{3}} \cdot \Bigg[& \frac{1}{4 \cdot \left(1 - \dfrac{\sqrt{3} \cdot \sigma_1}{2 \cdot R_e^W} \cdot \sin(2 \cdot \alpha)\right)} \cdot \\
& \cdot \left[\frac{\pi}{2} + 2 \cdot \left[1 - 2 \cdot \left(\frac{\sqrt{3} \cdot \sigma_1}{2 \cdot R_e^W} \cdot \sin(2 \cdot \alpha)\right)\right]\right] \cdot \\
& \cdot \sqrt{\frac{\sqrt{3} \cdot \sigma_1}{2 \cdot R_e^W} \cdot \sin(2 \cdot \alpha) \cdot \left(1 - \frac{\sqrt{3} \cdot \sigma_1}{2 \cdot R_e^W} \cdot \sin(2 \cdot \alpha)\right)} + \\
& - \arcsin\left[2 \cdot \left(\frac{\sqrt{3} \cdot \sigma_1}{2 \cdot R_e^W} \cdot \sin(2 \cdot \alpha)\right) - 1\right]\Bigg] + \left(1 - \frac{\sqrt{3} \cdot \sigma_1}{2 \cdot R_e^W} \cdot \sin(2 \cdot \alpha)\right) \cdot \frac{1}{4 \cdot \kappa} \Bigg]
\end{aligned} \qquad (18)
$$

$$
\begin{aligned}
K_W^{ov} = \frac{2}{\sqrt{3}} \cdot \Bigg[& \frac{1}{4 \cdot \left(1 - \dfrac{\sqrt{3} \cdot \sigma_1}{2 \cdot R_e^W} \cdot \sin(2 \cdot \alpha)\right)} \cdot \\
& \cdot \left[-\frac{\pi}{2} - 2 \cdot \left[1 - 2 \cdot \left(\frac{\sqrt{3} \cdot \sigma_1}{2 \cdot R_e^W} \cdot \sin(2 \cdot \alpha)\right)\right]\right] \cdot \\
& \cdot \sqrt{\frac{\sqrt{3} \cdot \sigma_1}{2 \cdot R_e^W} \cdot \sin(2 \cdot \alpha) \cdot \left(1 - \frac{\sqrt{3} \cdot \sigma_1}{2 \cdot R_e^W} \cdot \sin(2 \cdot \alpha)\right)} + \\
& - \arcsin\left[2 \cdot \left(\frac{\sqrt{3} \cdot \sigma_1}{2 \cdot R_e^W} \cdot \sin(2 \cdot \alpha)\right) - 1\right]\Bigg] + \left(1 - \frac{\sqrt{3} \cdot \sigma_1}{2 \cdot R_e^W} \cdot \sin(2 \cdot \alpha)\right) \cdot \frac{1}{4 \cdot \kappa} \Bigg]
\end{aligned} \qquad (19)
$$

The great value of $K_W^{un/ov}$ appears at small values of κ and when $\alpha = 0°$ or $\alpha = 90°$ at values of $\sigma_1 = R_e^B$ for undermatched case or $\sigma_1 = R_e^W$ for overmatching case – Fig. 4.

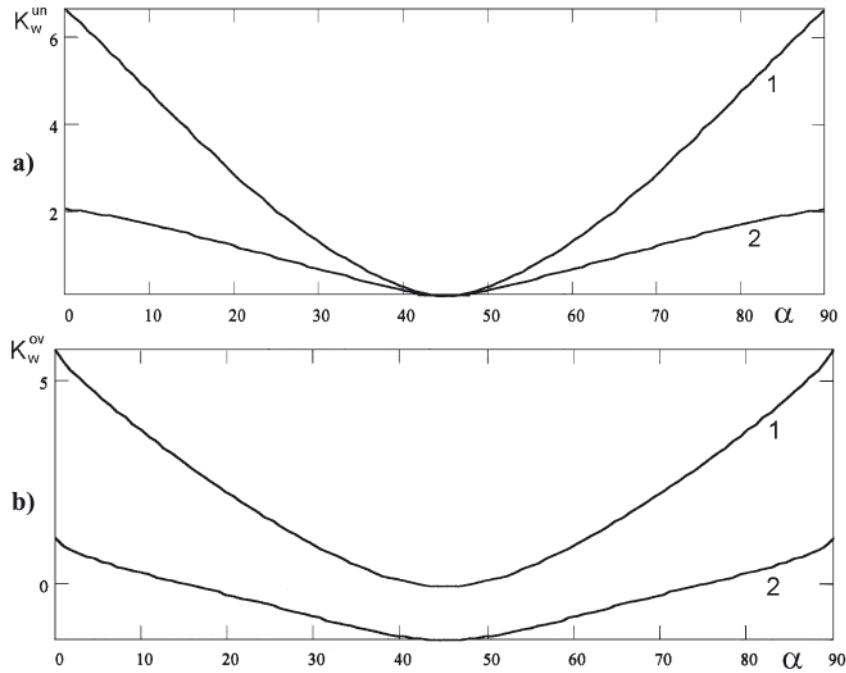**Fig. 4.** *Characteristic of K_W^{un} and K_W^{ov} for: **a)** undermatching: $R_e^W = 434$ MPA, $\sigma_1 = 500$ MPA, $\alpha = 0 – 90°$, $\kappa_1 = 0.05$; $\kappa_2 = 0.25$, curves: 1 for κ_1; 2 for κ_2; **b)** overmatching: $R_e^W = 605$ MPA, $\sigma_1 = 500$ MPA, $\alpha = 0 – 90°$, $\kappa_1 = 0.05$; $\kappa_2 = 0.25$, curves: 1 for κ_1; 2 for κ_2*

We can also transform the constraint factors $K_W^{un/ov}$ as follows [14]:

$$K_W^{un} = \frac{2}{\sqrt{3}}\left(\frac{1}{4(1-q)}\left[\frac{\pi}{2} + 2(1-2q)\sqrt{q(1-q)} - \arcsin(2q-1)\right] + (1-q)\frac{1}{4\kappa}\right) \tag{20}$$

$$K_W^{ov} = \frac{2}{\sqrt{3}}\left(\frac{1}{4(1-q)}\left[-\frac{\pi}{2} - 2(1-2q)\sqrt{q(1-q)} + \arcsin(2q-1)\right] + (1-q)\frac{1}{4\kappa}\right) \tag{21}$$

where:
$$0 \leq q < 1$$
$$\kappa = 2h/2t$$

Fig. 5. shows the dependence of the constraint factors $K_W^{un/ov}$ on the parameters κ and q.
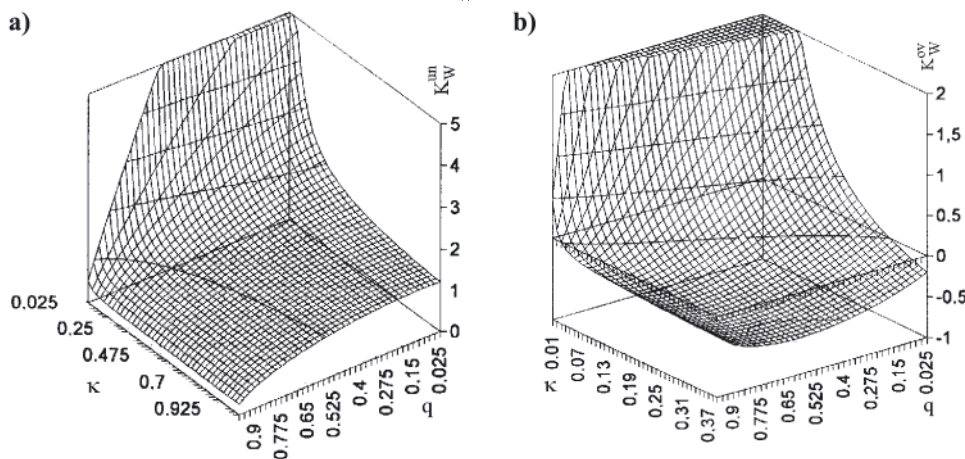

Fig. 5. *Diagrams of K_W^{un}, K_W^{ov} for: **a)** undermatched; **b)** overmatched models of weld joints*

The above data indicate that the constraint factors K_W^{un}, K_W^{ov} increases at small values of κ and q but it attains the different values for under- and overmatched cases. Under the assumption that the materials of zones B and W are perfectly ductile the new values of the yield point is given by:

- undermatching case ($R_e^W < R_e^B$):

$$R_e^{W(un)} = K_W^{un} \cdot R_e^W \tag{22}$$

- overmatching case ($R_e^W > R_e^B$):

$$R_e^{W(ov)} = K_W^{ov} \cdot R_e^W \qquad (23)$$

The values of $K_W^{un/ov}$ indicate that the constraint effect considerably influences the mechanical properties of the mismatched weld joints.

CONCLUSION

The objective in Computational Welding Mechanics is to extend the capability to analyze the evolution of temperature, stress and strain in welded structures together with the evolution of microstructure.

In narrowest sense computational weld mechanics is concerned with the analysis of temperatures, displacements, strains and stresses in welded structures.

BIBLIOGRAPHY

1. Radaj D.: *Welding residual stresses and distortion. Calculation and measurement. DVS-Verlag.* 2002.
2. Lingren Ł. E.: *Numerical modelling of welding.* Comput. Methods Appl. Mech. Eng. 195. 2006.
3. Goldak J. A. and Akhlaghi M.: *Computational welding mechanics.* Springer. 2006.
4. Dowden J. M.: *The mathematics of thermal modelling.* London. 2001.
5. Buchmayr B.*: Modelling of weldability – needs and limits. Mathematical Modelling of Weld Phenomena 2. Book* 594. Edited by H. Cerjak, H. Bhadeshia. The Istitute of Materials. London. 119-137, 1995.
6. David S. A., Babu S.S.: *Microstructure modelling in weld metal.* M*athematical* M*odelling of* W*eld* P*henomena* 3. Edited by H. Cerjak. Book 650. The Institute of Materials. London. 151-180, 1997.
7. Bhadeshia H.: *Models for the elementary mechanical properties of steel welds.* M*athematical* M*odelling of* W*eld* P*henomena* 3. Edited by H. Cerjak. Book 650. The Institute of Materials. London. 229-282, 1997.
8. Hrivnak: *Grain growth and embrittlement of steel welds. Mathematical Modelling of Weld Phenomena 2.* Edited by Cerjak H. Materials Modelling Series. Book 594. London., 1995.
9. Bhadeshia H.: *Microstructure modelling in weld metal.* M*athematical* M*odelling of* W*eld* P*henomena* 3. Edited by Cerjak H. Book 650. The Institute of Materials. UK. 249-284, 2007.
10. Murawa H., Luo Y. and Ueda Y.: *Inherent strain as an interface between computational welding mechanics and its industrial application.* M*odelling of* W*eld* P*henomena* Vol. 4. Edited by H. Cerjak. Book 695. 597-619, 2007.
11. Ranatowski E.: *Some remarks on stress state at interface of the mismatched weld joints. Mis - Matching of Interfaces and Welds.* Editors: K. H. Schwalbe, M. Koçak, GKSS Research Center Publication, Geesthacht, FRG, ISBN 3-00-001951-0, 185-196, 1997.
12 Landes J. D. et al.: *An application methodology for ductile fracture mechanics. Fracture Mechanics.* ASTM STP 1189. 2001.
13. Schwalbe K. H.: *Effect of weld metal mis-match on toughness requirements: some simple analytical considerations using the Engineering Treatment Model (ETM).* International Journal of Fracture. No 1, 2004.

CONTACT WITH THE AUTHOR

Prof. Ranatowski Eugeniusz
Faculty of Mechanical Engineerig,
University of Technology and Life Science,
Prof. S. Kaliskiego 7
85-763 Bydgoszcz, POLAND
e-mail: ranatow@utp.edu.pl

The end of Part I – to be continued in POLISH MARITIME RESEARCH, No 2/2012

Design of Inner Gate
for CRIST Shipyard Dry Dock

Marian Bogdaniuk, Ph. D., Gdańsk University of Technology
Zenon Górecki, Ph. D., Gdańsk University of Technology, IDEK Company Ltd

ABSTRACT

The paper deals with a removable steel inner gate which was designed to separate two parts of a dry dock of about 70 m in width and 380 m in length. The gate allows for independent assembly of ship structures in the two separated parts of the dock. The fore part of the dock can be flooded while the after part is dry. The gate was designed by IDEK Company Ltd in 2011 and it was soon constructed and used by CRIST Shipyard in Gdynia.

Keywords: shipyard; dry dock; dock inner gate; FEM strength analysis

INTRODUCTION

CRIST Shipyard in Gdynia, Poland specializes in the construction of medium-sized ships and offshore facilities. That is why there was a need for an inner gate to split a 380-metre-long dry dock to allow for an independent assembly of ship structures in two parts of the dock. Structures whose assembly require more time are built in the after part of the dock. At the same time other structures, not longer than 130 m, can be assembled in the fore part of the dock and then launched.

Ships, barges or pontoons transporting some structures or equipment for the objects assembled in the dock after part can enter the fore part. Then, a dock gantry crane of lifting capacity 900 tons can take these components to the dock after part.

The customer, namely CRIST Shipyard submitted the following design requirements regarding the gate:
- the gate width (measured along the dock) is to be as little as practicable not to take up too much space in the dock;
- the gate mass should not exceed 400 tons to be readily operated by the dock gantry crane;
- the maximum water depth in the flooded dock is 9.5 m.

CONCEPT AND DESIGN
OF THE INNER GATE

Some examples of inner gates for dry docks are described in [1].

The design of the gate in question has a structure slightly different from the examples given in [1]. Their transverse cross-sections in the planes parallel to the dock plane of symmetry are shown in Fig.1.
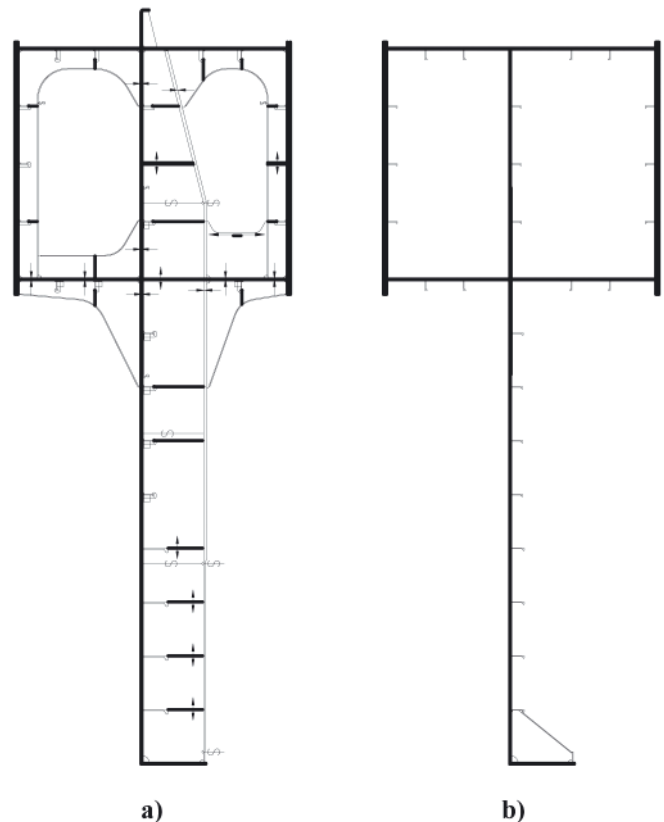

a)　　　　　　　**b)**

Fig. 1. *Transverse cross-sections of the gate:*
a) in the web frame planes, b) between the web frames

The gate is constructed of steel with the yield point 355 MPa, as a watertight vertical wall. At its upper part, a box-type structure 3.5 m wide and 3.0 high was arranged. The length of the gate is 70.3 m which is only 0.15 m less than upper part dock width.

The spacing of web frames shown in Fig. 1a is 2.5 m. The web frames support horizontal stiffeners of the watertight wall are spaced at intervals of 0.75 m.

Figures 5 and 6 showing a FEM model of the gate facilitate understanding of the gate steel structure.

The plates of the deck and bottom of the box type structure are 10.0 mm thick. The plates forming the side walls of the box type structure are 40 mm thick in the middle portion of the gate and 30 mm in way of the gate side edges.

The thickness of the watertight vertical wall of the gate is equal to 10 mm.

Horizontal stiffeners of the watertight wall are arranged as follows: BP 180x8 – in the lower portion, BP 160x8 – in middle height region and BP 140x8 – in the upper portion.

Vertical girders shown in Fig. 1a are T-type beams with web 800x10 at the lower part and 800x15 at the upper part. Their flanges are flat bars 300x20 in the lower part and 300x40 in the upper part. In the region near the side edges of the gate, T-shaped beams become slightly smaller as they are more effectively supported by the box-type structure there.

In the design process, an assumption was applied that the pressure of water acts on the side of the vertical watertight wall where its girders and the plating stiffeners are located.

The lower edge of the gate is supported by a steel threshold connected to the dock bottom concrete slab by a system of bolts (see Fig. 2). In Fig. 2, sealing system design is also shown. A rubber gasket is placed between two oak planks directly transmitting the load induced by the water filling the dock fore part to the threshold structure. The planks restrict the value of gasket deflection, too.

The gate is put in its working position by the dock gantry crane. First, the gate is put near the threshold. Then special turn-buckles connected to the threshold, to the side supporting structure and to the gate are used to exert initial compression of the gasket. Then the pressure of water filling the dock fore part acts on the gate watertight wall thus tightening the gate.

The gate is supported at its side edges by a special steel structure. In its lower part, the structure is welded to corrugated steel sheet walls of the dock. In the upper part, the supporting steel structure is connected with bolts to massive concrete girders forming side walls of the dock and resting on the corrugated side walls. These supporting structures are schematically shown in Fig. 3.

The systems for transmitting the load from the gate to the supporting structure and for tightening the gate at its side edges are similar to those shown in Fig. 2.

A considerable part of the transverse force induced by the filling water and acting on the gate, loads the upper box-type structure supporting vertical girders shown in Fig.1a. The remaining part of the force loads the threshold positioned at the lower edge of the gate.
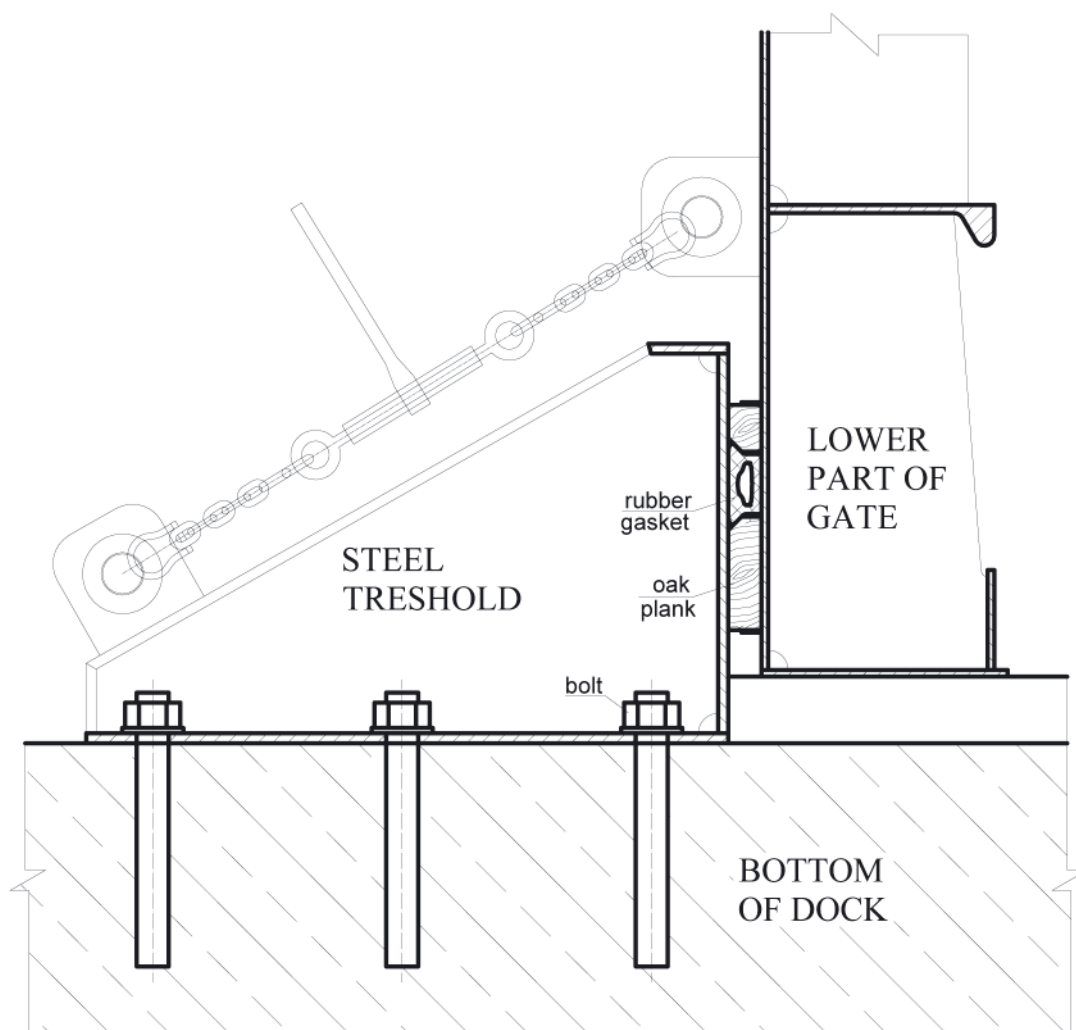

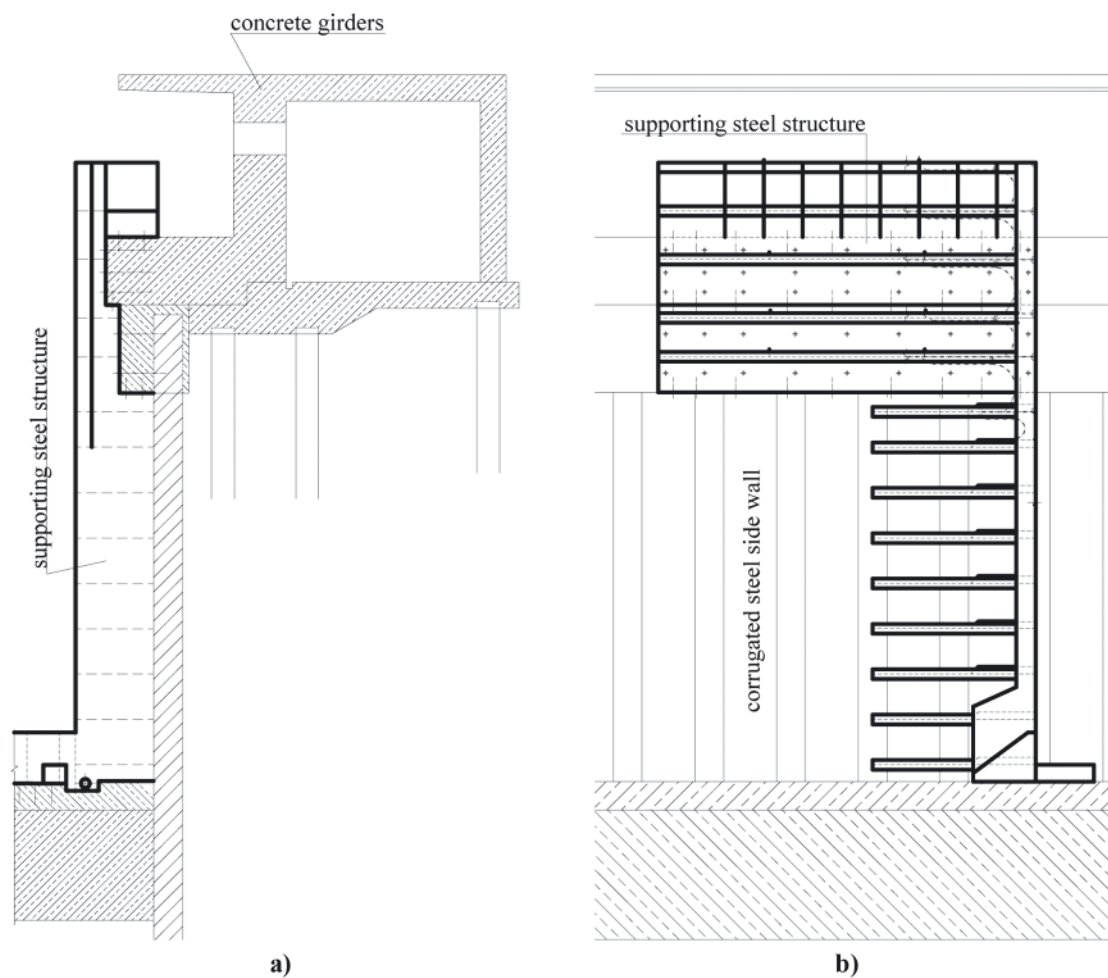*Fig. 2. Threshold structure and gasket system*

*Fig. 3. Supporting structure at the dock side walls: **a)** transverse cross-section, **b)** side view*

The box-type structure is supported at its ends by a special supporting structure connected to the dock sides (see Fig. 3). A simple assessment of reaction force values supporting the ends of the box-type structure gives result equal to 1/3 of the total force corresponding to the water pressure acting on the watertight wall. This was confirmed by FEM calculations described further in the paper.

This means that a reaction force equal approximately to 5 MN is developed at each end of the box-type structure for the water depth of 9.5 m. Such a great value of the reaction force requires applying a strong steel supporting structure connected to the concrete dock side walls at their upper regions. Moreover, high pressure values occur between the oak planks and the steel structure, close to the strength of the planks.

Another problem with supporting the box-type structure at its ends is related to its deflection caused by the water pressure. The structure is deflected between the end supports and twisted in relation to its longitudinal horizontal axis – as a result of supporting the gate at its lower edge by the threshold. Such type of deformation means that the reaction forces must be non-uniformly distributed along the height of the box-type structure. Much greater pressure values on the oak planks are expected at the level of the box deck than at the level of its bottom which causes some problems with the strength of the planks and keeping the gate watertight. This means that the end parts of the box-type structure should be fairly elastic while subjected to torsion – to minimize the difference between these pressure values at the deck and the bottom levels.

This quality of the box-type structure was obtained by a special construction of its ends. The closed rectangular transverse cross-section was replaced by an open type one, along the distance of 2.5 meters at each end. A part of the structure at one side of the watertight wall was removed and a strong flange was arranged there instead of a part of the box side wall. Furthermore, a platform was arranged at the level of the mid-height of the box. The platform is subjected to a shear force corresponding to the reaction force at the end of the box-type structure. Strong brackets connected to the platform and to the vertical watertight wall were arranged at the ends of the structure. Their vertical edges are loaded by pressure values developed at the oak planks.

The end regions of the box-type structure are schematically shown in Fig. 6 in the course of the paper, in the form of a FEM model developed to assess the gate structure strength.

The vertical watertight wall of the gate was placed near the middle of the box-type structure width to obtain as small values of displacements of its vertical end edges as possible. These displacements directed along the width of the dock are caused by considerable bending displacements of the box-type structure. Arranging this watertight wall at the plane of the side wall of the box-type structure would result in the value of these displacements up to 20 mm. Such considerable displacement values could cause the damage of the oak planks and the rubber gasket. The applied solution allowed to reduce the maximum value of the displacements to as little as 2 mm.
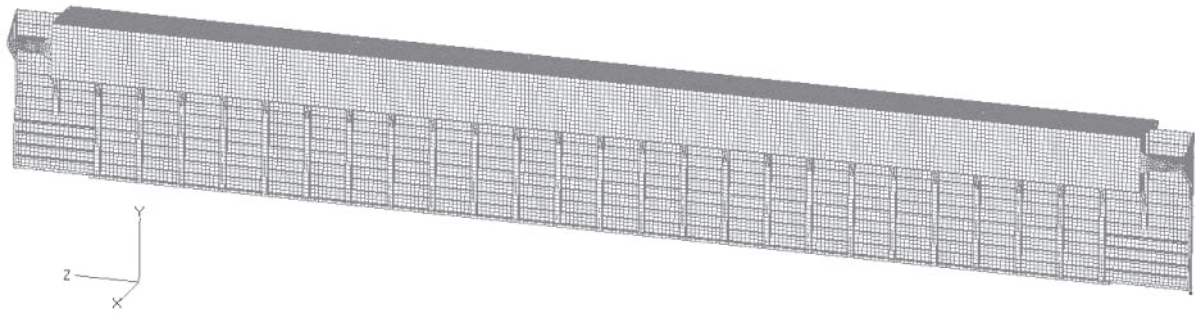
Fig. 4. *Gate steel structure mesh*

FEM STRENGTH ANALYSIS

A FEM strength analysis of the gate structure was performed to verify and correct its scantlings obtained through the initial simple calculations. The FEM model mesh is shown in Fig. 4.

4-node shell finite elements were used for the plating of sides and decks of the box-type structure, plating of the
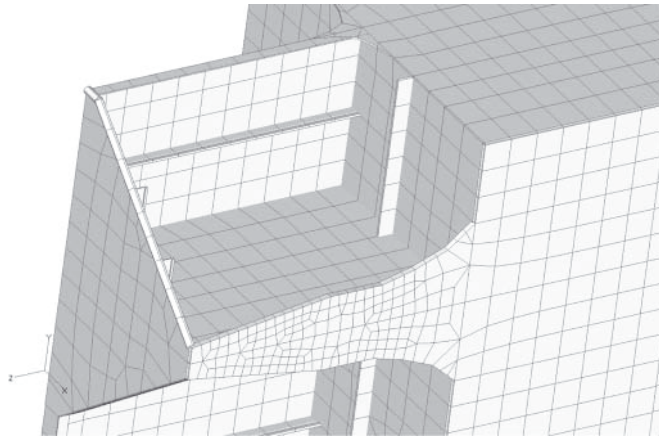

Fig. 5. *Deflection of the gate*

watertight wall as well as girder webs and plating stiffeners. Beam finite elements were used for both girder and stiffener flanges.

The FEM model was subjected to the pressure of water with the free surface at the level of 9.5 meters above the dock bottom. In the FEM model, this load was applied as a set of concentrated forces acting at the locations where the watertight wall horizontal stiffeners intersect the vertical girders shown in Fig. 1a.

A system of elastic rods was used to support the gate in the dock longitudinal direction. The rods approximately correspond to the elasticity of the rubber gasket.

Along the lower edge of the watertight wall, a similar set of vertical rods was used to support the structure in the vertical direction.

The deflection calculated with the FEM model is shown in Fig. 5.

Maximum deflection of the gate occurs at the upper deck level of the box-type structure, on the dock plane of the symmetry. Its value is 255 mm. The maximum value of normal stress due to bending of the box-type structure reaches the level of 150 MPa, in its side wall near its mid-length point.

The extreme level of Von Mises stress in the vertical girders (see Fig.1a) is of the order of 210 MPa. These stresses occur in central girder of the gate, near the bottom of the box.
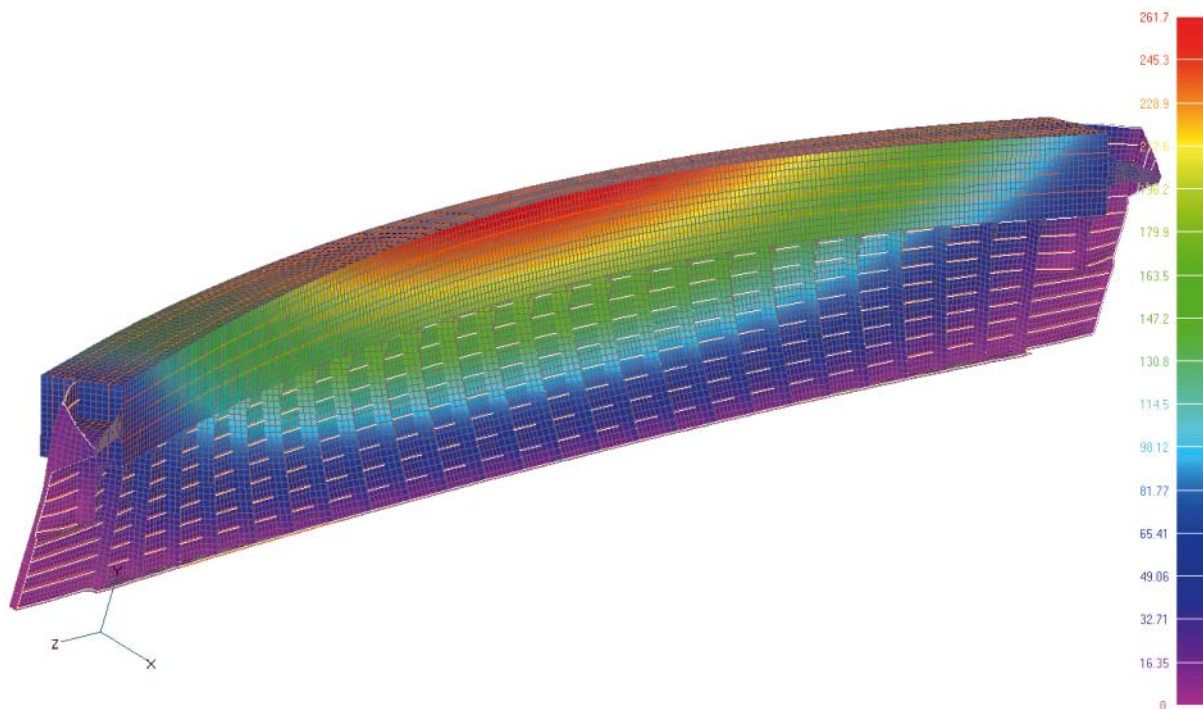

Fig. 6. *FEM model of the box end parts and stress values in the flange*

The results of FEM analysis showed that reaction forces along the lower edge of the gate are almost uniformly distributed while their distribution along the vertical edges is very far from a uniform one. The mean value of the continuous load on the oak planks, along the height of the box, measured in N/mm, is approximately 15 times greater than the mean value of such load along the remaining part of the vertical edge. In addition, the maximum value of this load occurring at the level of the box deck is 3 times greater than the minimum value occurring at the level of the box bottom.

2 meters below the bottom of the box, the value of the continuous load on the planks is approximately 5 times lesser than the mean value along the box height.

Such a distribution of load causes serious problems with the strength of the oak planks and the strength of the concrete side wall of the dock.

Many modifications of the structure were considered in the designing process to obtain a more even distribution of this load along the height of the box but it was impossible to obtain better results than those described above. This uneven distribution of the continuous reaction load along the vertical edges of the gate results from the box torsion. This reaction load must produce a torque value to counterbalance the torque induced by supporting the vertical girders of the watertight wall by the box. This torque is responsible for the complicated distribution of stress in the end parts of the box. The end parts should be fairly elastic to allow for a considerable angle of transverse cross-section rotation around the longitudinal axis of the box, over the distance of several meters only. On the other hand, the structure should be strong enough to withstand such a great torque. These two requirements are not easy to be fulfilled simulatneously.

After many attempts, an acceptable design of the box end parts in the form shown in Fig. 4 was found. An open type of box transverse cross-section was applied there, over the distance 2.5 meters.

The FEM model of these end parts and the calculated von Mises stress values in the strong flange installed in the plane of the box side wall are shown in Fig.6. The maximum value of the stress reaches 540 MPa there. The stress distribution in the flange domain is far from even and this is due to a simultaneous flange bending in both horizontal and vertical planes. It was necessary to apply the flange 60 mm thick which was made of steel with the yield point equal to 690 MPa while the whole gate steel structure is made of steel with the yield point 355 MPa.

SUMMARY

- The design of the gate appears quite simple except for the box-type structure end regions near the dock side walls. The structure should be strong and, simultaneously, it is to be rather elastic locally to allow for the rubber sealing compression throughout its length irrespective of the water level in the dock. It is a rather difficult task to fulfil both of the conditions simultaneously. A rather complicated construction of the gate at its ends was obtained by way of many modifications using a trial-and-error method to meet both of these conditions.
- The gate has been successfully used by the shipyard.

BIBLIOGRAPHY

1. Mazurkiewicz B. K.: *Design and Construction of Dry Docks*, Gulf Publishing Company Book Division, 1981.

CONTACT WITH THE AUTHORS

Marian Bogdaniuk, D. Sc., Eng.
Zenon Górecki, D. Sc., Eng.
Faculty of Ocean Engineering
and Ship Technology,
Gdańsk University of Technology
Narutowicza 11/12
80-233 Gdańsk, POLAND
e-mail: m.bogdaniuk@prs.pl
e-mail: zengor@pg.gda.pl

The Ship Handling Research and Training Centre at Ilawa is owned by the Foundation for Safety of Navigation and Environment Protection, which is a joint venture between the Gdynia Maritime University, the Gdansk University of Technology and the City of Ilawa.

Two main fields of activity of the Foundation are:

➲ Training on ship handling. Since 1980 more than 2500 ship masters and pilots from 35 countries were trained at Iława Centre. The Foundation for Safety of Navigation and Environment Protection, being non-profit organisation is reinvesting all spare funds in new facilities and each year to the existing facilities new models and new training areas were added. Existing training models each year are also modernised, that's why at present the Centre represents a modern facility perfectly capable to perform training on ship handling of shipmasters, pilots and tug masters.

➲ Research on ship's manoeuvrability. Many experimental and theoretical research programmes covering different problems of manoeuvrability (including human effect, harbour and waterway design) are successfully realised at the Centre.

The Foundation possesses ISO 9001 quality certificate.

Why training on ship handling?

The safe handling of ships depends on many factors - on ship's manoeuvring characteristics, human factor (operator experience and skill, his behaviour in stressed situation, etc.), actual environmental conditions, and degree of water area restriction.

Results of analysis of CRG (collisions, rammings and groundings) casualties show that in one third of all the human error is involved, and the same amount of CRG casualties is attributed to the poor controllability of ships. Training on ship handling is largely recommended by IMO as one of the most effective method for improving the safety at sea. The goal of the above training is to gain theoretical and practical knowledge on ship handling in a wide number of different situations met in practice at sea.

For further information please contact:
The Foundation for Safety of Navigation and Environment Protection

Head office:
36, Chrzanowskiego Street
80-278 GDAŃSK, POLAND
tel./fax: +48 (0) 58 341 59 19

Ship Handling Centre:
14-200 IŁAWA-KAMIONKA, POLAND
tel./fax: +48 (0) 89 648 74 90
e-mail: office@ilawashiphandling.com.pl
e-mail: office@portilawa.com

GDANSK UNIVERSITY OF TECHNOLOGY

is the oldest and largest scientific and technological academic institution in the Pomeranian region. The history of Gdansk University of Technology is marked by two basic dates, namely: October 6, 1904 and May 24, 1945.

The first date is connected with the beginning of the technical education at academic level in Gdansk. The second date is connected with establishing of Gdansk University of Technology, Polish state academic university. Gdansk University of Technology employ 2,500 staff, 1,200 whom are academics. The number of students approximates 20,000, most of them studying full-time. Their career choices vary from Architecture to Business and Management, from Mathematics and Computer Science to Biotechnology and Environmental Engineering, from Applied Chemistry to Geodesics and Transport, from Ocean Engineering to Mechanical Engineering and Ship Technology, from Civil Engineering to Telecommunication, Electrical and Control Engineering. Their life goals, however, are much the same - to meet the challenge of the changing world. The educational opportunities offered by our faculties are much wider than those of other Polish Technical universities, and the scientific research areas include all of 21st Century technology. We are one of the best schools in Poland and one of the best known schools in Europe – one that educates specialists excelling in the programming technology and computer methods used in solving complicated scientific, engineering, organizational and economic problems.

THE FACULTY OF OCEAN ENGINEERING AND SHIP TECHNOLOGY

The Faculty of Ocean Engineering and Ship Technology (FOEST) as the only faculty in Poland since the beginning of 1945 has continuously been educating engineers and doctors in the field of Naval Architecture and Marine Technology.

The educational and training activities of FOEST are supported by cooperation with Polish and foreign universities, membership in different international organizations and associations, as well as participation in scientific conferences and symposia. Hosting young scientists and students from different countries is also a usual practice in FOEST.

The activities of Faculty departments are related to: mechanics and strength of structures, hydromechanics, manufacturing, materials and system quality, power plants, equipment and systems of automatic control, mostly in shipbuilding, marine engineering and energetic systems.

FOEST is a member of such organizations like WEGEMT; The Association of Polish Maritime Industries and the co-operation between Nordic Maritime Universities and Det Norske Veritas. The intensive teaching is complemented and supported by extensive research activities, the core of which is performed in close collaboration between FOEST staff and industry. We take great care to ensure that the applied research meet both the long term and short term needs of Polish maritime industry. FOEST collaborates with almost all Polish shipyards. Close links are maintained with other research organizations and research institutions supporting the Polish maritime industry, such as Ship Design and Research Centre and Polish Register of Shipping, where several members of the Faculty are also members of the Technical Board.

The Faculty of Ocean Engineering and Ship Technology is a unique academic structure, which possesses numerous highly qualified and experienced staff in all above mentioned specific research areas. Moreover, the staff is used to effective co-operation and exchange of ideas between specialists of different detailed areas. This enables a more integrated and comprehensive treatment of research and practical problems encountered in such a complicated field of activity as naval architecture, shipbuilding and marine engineering.

The staff of the Faculty has strong international links worldwide, being members or cooperating with international organizations like International Maritime Organization IMO, International Towing Tank Conference ITTC, International Ship and Offshore Structures Congress ISSC, International Conference on Practical Design of Ship and other floating Structures PRADS just to name a few.

GDANSK UNIVERSITY OF TECHNOLOGY
Faculty of Ocean Engineering and Ship Technology
11/12 Narutowicza Street, 80-233 Gdansk, Poland
Tel (+48) 58 347 1548 ; Fax (+48) 58 341 4712
e-mail: sekoce@pg.gda.pl

www.oce.pg.gda.pl